

# **Forschungszentrum Karlsruhe**

Technik und Umwelt

Wissenschaftliche Berichte

FZKA 6197

Spreading with basal solidification

M. Bunk

Institut für Angewandte Thermo- und Fluidynamik  
Projekt Nukleare Sicherheitsforschung

Forschungszentrum Karlsruhe GmbH, Karlsruhe  
1999

## Abstract

In the present report an analytically based scheme is presented, which allows to capture the influence of basal solidification onto a spreading flow of liquid melt with poor thermal conductivity.

Based on an underlying lubrication theory we derive an approximation for the temperature field and, thus, for the s/l-interface. Solutions are found based on similarity transformations or numerical schemes using the method of lines. Effects due to capillarity or liberation of latent heat are negligible. Solidification occurs at a defined solidification temperature, no mushy solidification regime is presumed. For the temperature field we use a quasi-steady approximation, which leads with respect to reactor safety applications to a conservative result for the crust influence onto the spreading flow. Furthermore, we assume both thermal conductivity and density to be constant and equal in the liquid and solid phases.

The spreading flow is characterized in terms of Reynolds number  $Re$ , Froude number  $Fr$ , Prandtl number  $Pr$  and an aspect ratio  $\epsilon$ . For the spreading volume we allow for  $V \propto t^\alpha$ , which leads to a characterization of all possible spreading flows in terms of the exponent  $\alpha$ . Within the viscous/gravitational regime,  $\epsilon Re \ll 1$ , we find for melts with  $Pr \gg 1$  a weak influence of the bottom crust onto the spreading flow. With increasing crust thickness we find a slow down of the spreading, due to a reduction of the driving hydrostatic pressure head. For  $t \rightarrow \infty$  we find a complete stop of the spreading for  $\alpha < 7/4$ . For values  $\alpha \geq 7/4$  the influence of basal solidification, in contrast, will not lead to a stop of the spreading.

# Ausbreitung von Schmelzen bei gleichzeitiger Erstarrung auf der Bodenplatte

## Zusammenfassung

Gegenstand der vorliegenden Arbeit ist die Ausbreitung viskoser Schmelzen mit schlechter Temperaturleitfähigkeit unter dem Einfluß erstarrender Krusten auf der Bodenplatte.

Basierend auf einer nichtisothermen Dünnschichtapproximation wird eine Lösung für das Temperaturfeld und damit für die s/l-Grenzfläche hergeleitet. Zur Lösung werden Ähnlichkeitstransformationen und alternativ numerische Verfahren verwendet. Effekte durch Oberflächenspannung und Freisetzung von Latentwärme sind in Rahmen dieser Betrachtung vernachlässigbar. Innerhalb der Modellbildung erfolgt die Erstarrung bei einer festen Erstarrungstemperatur. Für das Temperaturfeld wird eine quasistationäre Näherung verwendet. Dies führt bei Reaktorsicherheitsfragen zu einer konservativen Abschätzung der nichtisothermen Einflüsse auf die Ausbreitung der Schmelze. Weiterhin werden für die Dichte und die Temperaturleitfähigkeit identische und konstante Werte in der festen und flüssigen Phase verwendet.

Charakterisiert wird das Problem der nichtisothermen Ausbreitung viskoser Schmelzen durch die Reynolds-Zahl  $Re$ , die Froude-Zahl  $Fr$ , die Prandtl-Zahl  $Pr$  und ein Längenverhältnis  $\epsilon$ . Für das Volumen der Schmelze wird das allgemeine Gesetz  $V \propto t^\alpha$  angenommen. Somit können anhand des Parameters  $\alpha$  typische Ausbreitungsprobleme klassifiziert werden. Für Schmelzen mit  $Pr \gg 1$  finden wir einen schwachen Einfluß der erstarrenden Krusten auf die Ausbreitung der darüberliegenden Schmelze. Mit wachsender Krustendicke wird die Ausbreitung durch eine Reduzierung der antreibenden hydrostatischen Druckdifferenz verlangsamt. Für  $t \rightarrow \infty$  ist lediglich für  $\alpha < 7/4$  mit einem Anhalten der Ausbreitung zu rechnen. Für  $\alpha \geq 7/4$  führt der Einfluß erstarrender Krusten auf der Bodenplatte hingegen nicht zu einem Stop der Ausbreitung.

# Contents

<b>1</b>	<b>Introduction</b>	<b>1</b>
<b>2</b>	<b>Theory</b>	<b>3</b>
2.1	Basic equations . . . . .	3
2.1.1	Dimensional formulation . . . . .	3
2.1.2	Nondimensional formulation . . . . .	3
2.2	Kinematic boundary conditions for spreading without solidification . . . . .	7
2.2.1	Dimensional formulation . . . . .	7
2.2.2	Nondimensional formulation . . . . .	8
2.3	Lubrication Theory . . . . .	9
<b>3</b>	<b>Isothermal spreading</b>	<b>11</b>
3.1	Velocity and pressure field . . . . .	11
3.2	Evolution equation for $H(X, \tau)$ . . . . .	13
3.2.1	Dependence of the conditions at $X = 0$ and $X \geq A(\tau)$ . . . . .	13
3.2.2	Similarity transformation . . . . .	15
3.2.2.1	Analytical solutions . . . . .	17
3.2.2.2	Numerical solutions . . . . .	19
3.2.2.3	Approximations . . . . .	20
3.2.3	Numerical solution of the evolution equation for $H(X, \tau)$ . . . . .	22
3.2.3.1	Transformation $(X, \tau) \rightarrow (\xi, \tau)$ . . . . .	23
3.2.3.2	Method of lines for the evolution equation of $H(\xi, \tau)$ . . . . .	23

3.2.3.3	Shooting method for $A(\tau)$ . . . . .	26
3.3	Results . . . . .	27
3.3.1	Position of the l/g-interface - $H(X, \tau)$ . . . . .	27
3.3.1.1	Similarity solution for $H(X, \tau)$ . . . . .	27
	Solution for $\tilde{H}$ . . . . .	27
	Solution for $H(X, \tau)$ . . . . .	29
3.3.1.2	Numerical solution for $H(X, \tau)$ . . . . .	31
3.3.2	Velocity fields . . . . .	36
<b>4</b>	<b>Nonisothermal spreading - without solidification</b>	<b>41</b>
4.1	Thermal boundary conditions . . . . .	42
4.1.1	Dimensional formulation . . . . .	42
4.1.2	Nondimensional formulation . . . . .	42
4.2	Matched asymptotic representation - heat losses at the substrate . . . . .	43
4.2.1	Outer solution . . . . .	44
4.2.2	Inner solution . . . . .	44
4.3	Numerical solution of the temperature field . . . . .	50
4.3.1	Transformation $(X, Z) \rightarrow (\xi, \zeta)$ . . . . .	50
4.3.2	Method of lines for the transformed energy equation . . . . .	51
4.3.3	Initial and boundary conditions - heat losses at the substrate . . . . .	52
4.4	Results . . . . .	53
4.4.1	Matched asymptotic solution . . . . .	53
4.4.2	Comparison matched asymptotic solution - numerical solution . . . . .	55
4.4.3	Estimation of the quasi-steady approximation . . . . .	57
<b>5</b>	<b>Modeling bottom crusting</b>	<b>59</b>
5.1	Basic idea . . . . .	59
5.2	Position of the s/l-interface . . . . .	60

<b>6</b>	<b>Isothermal spreading - solidified crust at the bottom</b>	<b>63</b>
6.1	Flow field with bottom crusting . . . . .	63
6.1.1	Boundary conditions . . . . .	63
6.1.2	Velocity and pressure field . . . . .	63
6.2	Evolution equation for $H(X, \tau)$ - general formulation . . . . .	64
6.3	Two strategies to formulate $S(X, \tau)$ - the weakly- and the fully-coupled problem	64
6.4	Evolution equation for $H(X, \tau)$ - the weakly-coupled problem . . . . .	65
6.4.1	Similarity transformation . . . . .	67
6.4.1.1	Numerical solution for the shape function $\tilde{H}_1$ . . . . .	68
6.4.2	Numerical solution of the nondimensional evolution equation for $H_1$	69
6.4.2.1	Transformation $(X, \tau) \rightarrow (\xi_1, \tau)$ . . . . .	69
6.5	Evolution equation for $H(X, \tau)$ - the fully-coupled problem . . . . .	70
6.5.1	Similarity transformation . . . . .	71
6.5.1.1	Numerical solution for the shape functions $\tilde{H}_1$ and $\tilde{G}_1$ . . . . .	72
6.5.2	Numerical solution of the nondimensional evolution equation for $H_1$	73
6.5.2.1	Transformation $(X, \tau) \rightarrow (\xi_1, \tau)$ . . . . .	73
6.5.2.2	Modified algorithm for numerical integration . . . . .	74
6.6	Results . . . . .	74
6.6.1	Position of the l/g-interface, $H_1(X, \tau)$ . . . . .	74
6.6.1.1	Similarity solution for $H_1(X, \tau)$ . . . . .	74
	Solution for $\tilde{H}_1(\xi)$ . . . . .	75
	Solution for $H(X, \tau)$ . . . . .	78
6.6.1.2	Numerical solution for $H_1(X, \tau)$ . . . . .	78
6.6.2	Velocity fields . . . . .	88
6.6.3	Convergence of the iterative scheme . . . . .	95
<b>7</b>	<b>Summary</b>	<b>96</b>

# Chapter 1

## Introduction

The process of spreading under the influence of heat losses and, hence, solidification has a wide range of applications in geology and engineering. A first example is the spreading of lava, following the eruption of a volcano. One important question here regards the safety of the population in the vicinity of the volcano. Thus, it has to be answered, whether the lava will reach the urban area, or whether solidification will prevent the flow of lava from intruding. Secondly, solidification of corium melts under the influence of heat losses may be critical for the coolability of the melt after a severe core melt down accident. In contrast to the lava problem, where a short spreading length is desirable, safety concepts rely on a large spreading length. If solidification leads to an accumulation of the corium melt, the removal of decay heat is more critical and erosion of the base material may be the consequence. Figure 1.1 shows a sketch of a reactor pressure vessel and the so-called core-catcher. After a severe core melt down accident, the melt is accumulated below the reactor pressure vessel. Due to the decay heat the melt is heated up, until the gate is eroded. After the gate opening the melt spreads onto the dry spreading area. Depending on the melt conditions (temperature, viscosity, constitution, . . .), three distinguishable spreading regimes occur:

- inertial/gravitational regime,
- viscous/gravitational regime,
- crust controlled regime.

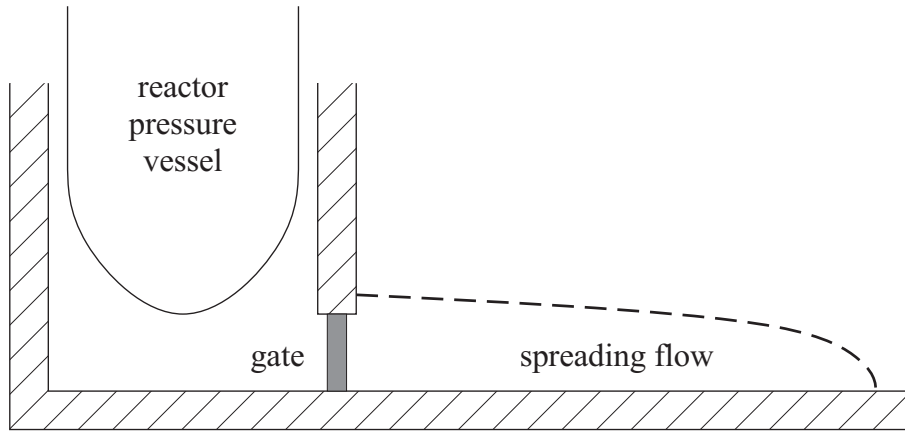


Figure 1.1: Sketch of a core-catcher.

The inertial/gravitational regime imposes no limiting conditions on the spreading process, whereas the viscous/gravitational regime and in particular the crust controlled regime lead to critical conditions for the spreading and the subsequent coolability of the corium melt. The isothermal spreading over a horizontal substrate within the viscous/gravitational regime is well studied. Huppert [3] found a similarity solution for the height profile of the spreading flow in a plane or axisymmetric geometry using lubrication theory.

The objective of this study is to investigate the spreading under the influence of solidification for fluids of poor thermal conductivity within the viscous/gravitational regime. We derive an analytically based scheme to describe the influence of solidification, whereby the process of solidification starts from the substrate. Solutions for both the velocity and the temperature field are derived in cartesian coordinates for the plane spreading. The influence of solidification on the spreading flow is discussed in terms of the spreading length history as it depends on various parameters, as e.g. inflow rate and solidification temperature.

# Chapter 2

## Theory

### 2.1 Basic equations

#### 2.1.1 Dimensional formulation

The basic conservation equations that describe the plane spreading process under the influence of gravity for incompressible Newtonian fluids in cartesian  $(x, z)$ -coordinates are the continuity equation

$$u_x + w_z = 0 \quad , \quad (2.1)$$

the Navier-Stokes equations

$$\rho (u_t + uu_x + wu_z) = -p_x + \mu (u_{xx} + u_{zz}) \quad , \quad (2.2)$$

$$\rho (w_t + uw_x + ww_z) = -p_z + \mu (w_{xx} + w_{zz}) - \rho g \quad , \quad (2.3)$$

and the energy equation

$$\rho c_p (T_t + uT_x + wT_z) = \lambda (T_{xx} + T_{zz}) \quad (2.4)$$

(cf. Schlichting [5]). This set of equations has to be solved with respect to the boundary conditions of the specific spreading problem.

#### 2.1.2 Nondimensional formulation

To estimate the order of magnitude of the terms in the basic equations (2.1-2.4) a nondimensional formulation will help to clarify. From figure 2.1, where a sketch of the plane

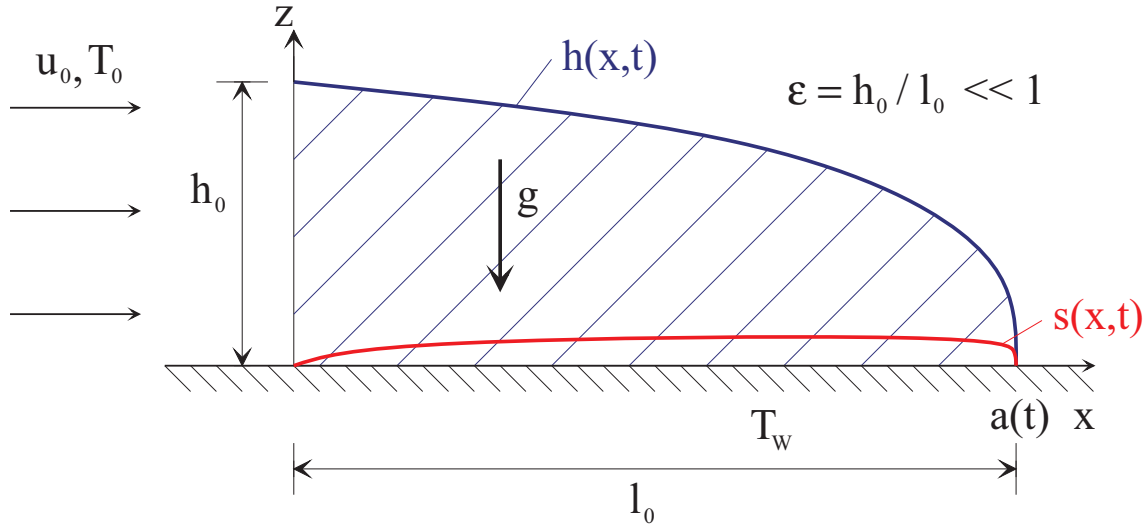


Figure 2.1: Sketch of a spreading flow.

spreading flow is shown, it is obvious that two different length scales are present within the problem. Introducing two separate length scales in the vertical and horizontal direction leads to

$$X = \frac{x}{l_0} \quad , \quad Z = \frac{z}{h_0} \quad .$$

The velocity is described by a typical horizontal inflow  $u_0$ . The vertical velocity scale  $w_0$  is unknown. The two dimensionless velocities are

$$U = \frac{u}{u_0} \quad , \quad W = \frac{w}{w_0} \quad .$$

A typical time scale within the problem is the horizontal transport time. Thus, we nondimensionalize the time by

$$\tau = \frac{t}{l_0/u_0} \quad .$$

To obtain a nondimensional pressure it is useful to introduce an unknown pressure scale  $p_0$ , which can be fixed during the calculation to obtain the pressure in an order of magnitude suitable to the spreading process, i.e. we use

$$P = \frac{p}{p_0} \quad .$$

The temperature scale includes the initial temperature  $T_0$  of the fluid and the ambient temperature  $T_\infty$ . The nondimensional temperature is

$$\Theta = \frac{T - T_\infty}{T_0 - T_\infty} \quad .$$

The nondimensional temperature varies in the range  $0 \leq \Theta \leq 1$ . Substituting the nondimensional variables into the continuity equation (2.1) yields

$$\frac{u_0}{l_0} U_X + \frac{w_0}{h_0} W_Z = 0 \quad .$$

In order to keep both terms in the same order of magnitude, to satisfy continuity, the following relationship holds

$$\frac{u_0}{l_0} \sim \frac{w_0}{h_0} \quad . \quad (2.5)$$

Thus, we fix the vertical velocity scale to be

$$w_0 = \frac{h_0}{l_0} u_0 = \epsilon u_0 \quad . \quad (2.6)$$

We obtain the nondimensional continuity equation

$$U_X + W_Z = 0 \quad .$$

For the horizontal momentum equation (2.2) we obtain

$$\rho \frac{u_0^2}{l_0} (U_\tau + UU_X + WU_Z) = -\frac{p_0}{l_0} P_X + \frac{\mu u_0}{h_0^2} (\epsilon^2 U_{XX} + U_{ZZ}) \quad .$$

To keep the pressure bounded we have to have

$$\frac{p_0}{l_0} \sim \frac{\mu u_0}{h_0^2} \quad . \quad (2.7)$$

We, therefore, set the pressure scale

$$p_0 = \frac{\mu u_0}{h_0} \frac{l_0}{h_0} = \frac{\mu u_0}{h_0} \frac{1}{\epsilon} \quad . \quad (2.8)$$

The pressure  $p_0$  is a viscous pressure scale which is appropriate to describe the viscous/gravitational regime of the spreading process. Introducing the nondimensional groups  $Re = (u_0 h_0)/\nu$  and  $Fr = u_0^2/(gh_0)$  with the kinematic viscosity  $\nu = \mu/\rho$ , we obtain the nondimensional horizontal momentum equation

$$\epsilon Re (U_\tau + UU_X + WU_Z) = -P_X + U_{ZZ} + \mathcal{O}(\epsilon^2) \quad .$$

For the vertical momentum equation (2.3) we obtain

$$\varrho \frac{\epsilon u_0^2}{l_0} (W_\tau + UW_X + WW_Z) = -\frac{\mu u_0}{h_0^2} \frac{1}{\epsilon} P_Z + \frac{\mu \epsilon u_0}{h_0^2} (\epsilon^2 W_{XX} + W_{ZZ}) - \varrho g \quad ,$$

which can be rewritten as

$$\epsilon^3 Re (W_\tau + UW_X + WW_Z) = -P_Z - \frac{\epsilon Re}{Fr} + \mathcal{O}(\epsilon^2) \quad .$$

For the energy equation (2.4) we obtain

$$\varrho c_p (T_0 - T_\infty) \frac{u_0}{l_0} (\Theta_\tau + U\Theta_X + W\Theta_Z) = \lambda (T_0 - T_\infty) \frac{1}{h_0^2} (\epsilon^2 \Theta_{XX} + \Theta_{ZZ}) \quad .$$

Introducing the nondimensional group  $Pr = \nu/\kappa$  with  $\kappa = \lambda/(\varrho c_p)$ , the final form writes

$$\epsilon Re Pr (\Theta_\tau + U\Theta_X + W\Theta_Z) = \Theta_{ZZ} + \mathcal{O}(\epsilon^2) \quad .$$

This leads to the following system of nondimensional equations

$$U_X + W_Z = 0 \quad , \quad (2.9)$$

$$\epsilon Re (U_\tau + UU_X + WU_Z) = -P_X + U_{ZZ} + \mathcal{O}(\epsilon^2) \quad , \quad (2.10)$$

$$\epsilon^3 Re (W_\tau + UW_X + WW_Z) = -P_Z - \frac{\epsilon Re}{Fr} + \mathcal{O}(\epsilon^2) \quad , \quad (2.11)$$

$$\epsilon Re Pr (\Theta_\tau + U\Theta_X + W\Theta_Z) = \Theta_{ZZ} + \mathcal{O}(\epsilon^2) \quad . \quad (2.12)$$

The nondimensional groups are

$$\epsilon = \frac{h_0}{l_0} \quad , \quad (2.13)$$

$$Re = \frac{u_0 h_0}{\nu} \quad , \quad (2.14)$$

$$Fr = \frac{u_0^2}{gh_0} \quad , \quad (2.15)$$

$$Pr = \frac{\nu}{\kappa} \quad . \quad (2.16)$$

The scaling is given by

$$X = \frac{x}{l_0} \quad , \quad (2.17)$$

$$Z = \frac{z}{h_0} \quad , \quad (2.18)$$

$$U = \frac{u}{u_0} \quad , \quad (2.19)$$

$$W = \frac{u}{\epsilon u_0} \quad , \quad (2.20)$$

$$P = \frac{p}{(\mu u_0)/(\epsilon h_0)} \quad , \quad (2.21)$$

$$\tau = \frac{t}{l_0/u_0} \quad , \quad (2.22)$$

$$\Theta = \frac{T - T_\infty}{T_0 - T_\infty} \quad . \quad (2.23)$$

## 2.2 Kinematic boundary conditions for spreading without solidification

### 2.2.1 Dimensional formulation

To describe the spreading flow, boundary conditions need to be fixed for both the flow field and the temperature field. In a first approach we focus on the flow field neglecting the influence of temperature ( $s(x, t) = 0$ ). The function  $h(x, t)$  yields the position of the unknown l/g-interface and  $a(t)$  is the position of the contact line, where the l/g-interface is in contact with the solid substrate, (cf. figure 2.1).

At the substrate the kinematic boundary conditions are

$$x, z = 0 : \quad u = w = 0 \quad , \quad (2.24)$$

at the l/g-interface  $h(x, t)$ , the shear stresses are continuous, so that

$$x, z = h : \quad \mu_l \frac{\partial |\vec{v}_l|}{\partial \vec{n}} = \mu_g \frac{\partial |\vec{v}_g|}{\partial \vec{n}} \quad ,$$

where  $l, g$  refer to liquid and ambient gas. A comparison of the viscosities

$$\frac{\mu_g}{\mu_l} \ll 1 \quad , \quad (2.25)$$

yields for the shear stress at the l/g-interface

$$x, z = h : \quad \frac{\partial |\vec{v}_l|}{\partial \vec{n}} = 0 \quad . \quad (2.26)$$

The kinematic boundary condition at the l/g-interface is

$$x, z = h : \quad h_x u = w - h_t \quad . \quad (2.27)$$

The pressure at the upper boundary  $h(x, t)$  writes

$$x, z = h : \quad p_l = p_g + \Delta p \quad .$$

The pressure difference  $\Delta p$  across the interface due to capillary forces is

$$\Delta p = \frac{-h_{xx}}{(1 + (h_x)^2)^{3/2}} \sigma \quad .$$

Neglecting pressure gradients in the ambient gas due to  $\varrho_l \gg \varrho_g$ , we obtain a constant pressure  $p_g \cong 0$  in the ambient gas. Thus, we have

$$x, z = h : \quad p_l \cong \Delta p \quad . \tag{2.28}$$

For the volume  $V(t)$  we have the integral conditions

$$V(t) = qt^\alpha = \int_0^{a(t)} h(x, t) dx \quad , \tag{2.29}$$

and

$$\dot{V}(t) = \alpha qt^{\alpha-1} = \int_0^{h(0,t)} u(x, z, t) dz \quad . \tag{2.30}$$

Finally, the height of the liquid has to be zero at the contact line and ahead of the contact line, i.e. we have the condition

$$x \geq a(t) : \quad h(x, t) = 0 \quad . \tag{2.31}$$

### 2.2.2 Nondimensional formulation

For more information about the significant terms in the boundary conditions it is necessary to have a nondimensional form. Formally, this is obtained by substituting the nondimensional variables (2.17-2.23) into the boundary conditions. The no-slip condition (2.24) at the substrate yields

$$X, Z = 0 : \quad U = W = 0 \quad . \tag{2.32}$$

The free-slip condition (2.26) at the l/g-interface together with

$$\vec{n} = \frac{1}{\sqrt{1 + (h_x)^2}} \begin{pmatrix} -h_x \\ 1 \end{pmatrix}$$

yields

$$X, Z = H : \frac{1}{\sqrt{1 + (\epsilon H_X)^2}} \cdot \frac{1}{\sqrt{U^2 + (\epsilon W)^2}} \cdot \left( (U^2 + (\epsilon W)^2)_Z - \epsilon^2 H_X (U^2 + (\epsilon W)^2)_X \right) = 0. \quad (2.33)$$

The kinematic boundary condition (2.27) at the l/g-interface yields

$$X, Z = H : \quad W = H_X U + H_\tau \quad . \quad (2.34)$$

From equation (2.28) we find that the liquid pressure  $P$  at the l/g-interface is

$$X, Z = H : \quad P = -\epsilon^3 \frac{1}{Ca} H_{XX} \frac{1}{\left(1 + (\epsilon H_X)^2\right)^{3/2}} \quad , \quad (2.35)$$

with the capillary number  $Ca = (\mu u_0)/\sigma$ . The integral condition (2.29) for the volume yields

$$\int_0^{A(\tau)} H(X, \tau) dX = C_V \tau^\alpha \quad \text{with} \quad C_V = \frac{q}{h_0 l_0} \left( \frac{l_0}{u_0} \right)^\alpha \quad . \quad (2.36)$$

From condition (2.30) for the volume flux we obtain

$$\int_0^{H(0, \tau)} U(X, Z, \tau) dZ = \alpha C_V \tau^{\alpha-1} \quad . \quad (2.37)$$

At the contact line condition (2.31) yields

$$X \geq A(\tau) : \quad H(X, \tau) = 0 \quad . \quad (2.38)$$

## 2.3 Lubrication Theory

The nondimensional equations involve several groups, which, under certain assumptions, allow to deduce a simplified description of the problem. Focusing on spreading flows which are dominated by viscous and gravitational forces we have

$$Re = \mathcal{O}(1) \quad \text{and} \quad \frac{\epsilon Re}{Fr} = \mathcal{O}(1) \quad .$$

Furthermore we have in a late stage of the spreading

$$\epsilon = \frac{h_0}{l_0} \ll 1 \quad .$$

This allows to simplify the original system of conservation equations (2.9-2.12) to

$$U_X + W_Z = 0 \quad , \quad (2.39)$$

$$0 = -P_X + U_{ZZ} \quad , \quad (2.40)$$

$$0 = -P_Z - \frac{\epsilon Re}{Fr} \quad , \quad (2.41)$$

$$\epsilon Re Pr (\Theta_\tau + U\Theta_X + W\Theta_Z) = \Theta_{ZZ} \quad . \quad (2.42)$$

The boundary conditions (2.32-2.35) can be simplified for  $\epsilon \ll 1$  to give

$$X, Z = 0 : \quad U = W = 0 \quad , \quad (2.43)$$

$$X, Z = H(X, \tau) : \quad U_Z = 0 \quad , \quad (2.44)$$

$$W = H_X U + H_\tau \quad , \quad (2.45)$$

$$P = 0 \quad (2.46)$$

for the flow field. The boundary condition (2.46) for the pressure at the l/g-interface is valid for capillary numbers

$$Ca = \frac{\mu u_0}{\sigma} > \epsilon^2 \quad .$$

Thermal boundary conditions will be inferred specifically in chapter 4.1 for nonisothermal spreading.

## Chapter 3

# Isothermal spreading

The isothermal spreading problem, based on lubrication theory, has been solved by Huppert [3]. His solution yields analytical expressions for the pressure  $P$  and for the velocities  $U$  and  $W$ , depending on the unknown position of the free l/g-interface  $H(X, \tau)$ . He obtains an evolution equation for  $H(X, \tau)$  to describe the l/g-interface. Using a similarity transformation, he finds for special cases analytical similarity solutions for  $H(X, \tau)$ , but generally the resulting ordinary differential equation has to be solved numerically. It is also possible to find approximations to the similarity solution. To get a more general approach we additionally solve the the evolution equation using a fully-numerical approach.

### 3.1 Velocity and pressure field

Integrating equation (2.41) with respect to  $Z$  gives

$$P = -\frac{\epsilon Re}{Fr}Z + P_1 \quad .$$

From (2.46) the constant of integration is

$$P_1 = \frac{\epsilon Re}{Fr}H(X, \tau) \quad .$$

The pressure field is given by

$$P = \frac{\epsilon Re}{Fr}(H - Z) \quad . \tag{3.1}$$

Substituting the pressure field (3.1) into the horizontal momentum equation (2.40) yields

$$U_{ZZ} = \frac{\epsilon Re}{Fr}H_X \quad .$$

Integration with respect to  $Z$  yields

$$U = \frac{1}{2} \frac{\epsilon Re}{Fr} H_X Z^2 + U_1 Z + U_2 \quad .$$

Based on the free-slip condition (2.44) and the no-slip condition (2.43) we obtain the constants of integration

$$U_1 = -\frac{\epsilon Re}{Fr} H_X H \quad , \quad U_2 = 0 \quad .$$

Thus, the horizontal velocity field is given by

$$U = \frac{\epsilon Re}{Fr} H_X \left( \frac{Z^2}{2} - H Z \right) \quad . \quad (3.2)$$

The vertical velocity  $W$  can be expressed from the continuity equation (2.39). Substituting (3.2) for  $U$  we obtain

$$W_Z = \frac{\epsilon Re}{Fr} \left( H_{XX} H Z + H_X^2 Z - H_{XX} \frac{Z^2}{2} \right) \quad .$$

Integration with respect to  $Z$  in conjunction with the no-slip condition (2.43) yields

$$W = \frac{1}{6} \frac{\epsilon Re}{Fr} Z^2 \left( 3H_X^2 + H_{XX}(3H - Z) \right) \quad . \quad (3.3)$$

It is useful to represent the flow field as a streamfunction. Therefore, we introduce a streamfunction  $\Psi$  which satisfies

$$U = \Psi_Z \quad , \quad W = -\Psi_X \quad .$$

Integrating both equations yields

$$\begin{aligned} \Psi &= \int U dZ + \Psi_1(X) \quad , \\ \Psi &= -\int W dX + \Psi_2(Z) \quad . \end{aligned}$$

Using equations (3.2-3.3) we obtain for the streamfunction

$$\Psi = \frac{\epsilon Re}{Fr} H_X \frac{Z^2}{6} (Z - 3H) \quad . \quad (3.4)$$

The streamfunction is normed to zero at the substrate ( $Z = 0$ ), since the substrate in all cases represents a line  $\Psi = \text{constant}$ .

## 3.2 Evolution equation for $H(X, \tau)$

Up to now we have analytical expressions for the flow and pressure field, involving the unknown position of the l/g-interface  $H(X, \tau)$ . Therefore, an equation for the evolution of the l/g-interface  $H(X, \tau)$  has to be found. Substituting the velocities (3.2, 3.3) into the kinematic boundary condition (2.45), we directly obtain

$$H_\tau - \frac{\epsilon Re}{3Fr} H^2 (3H_X^2 + HH_{XX}) = 0 \quad .$$

This simplifies to

$$H_\tau - \frac{\epsilon Re}{3Fr} (H^3 H_X)_X = 0 \quad .$$

This partial differential equation describes the position of the l/g-interface  $H(X, \tau)$  for the isothermal spreading problem. Substituting the velocity  $U$ , equation (3.2), into the integral condition (2.37) leads to

$$H_\tau - \frac{\epsilon Re}{3Fr} (H^3 H_X)_X = 0 \quad , \quad (3.5)$$

$$X = 0 : \quad -\frac{\epsilon Re}{3Fr} H^3 H_X = \alpha C_V \tau^{\alpha-1} \quad , \quad (3.6)$$

$$X \geq A(\tau) : \quad H = 0 \quad , \quad (3.7)$$

$$\text{volume constraint :} \quad \int_0^{A(\tau)} H dX = C_V \tau^\alpha \quad . \quad (3.8)$$

For the solution of this set of equations we can use either a similarity transformation to arrive at an ordinary differential equation, which has analytical solutions in some special cases. Alternatively, we can solve the problem numerically, which allows for a more general treatment of initial conditions. Both methods are described in the next sections.

### 3.2.1 Dependence of the conditions at $X = 0$ and $X \geq A(\tau)$

The conditions (3.6) and (3.7) are not independent. To show this we first integrate the evolution equation (3.5) in the following form

$$\int_0^{A(\tau)} H_\tau dX - \frac{1}{3} \frac{\epsilon Re}{Fr} \int_0^{A(\tau)} (H^3 H_X)_X dX = 0 \quad .$$

The second integral yields

$$\int_0^{A(\tau)} H_\tau dX - \frac{1}{3} \frac{\epsilon Re}{Fr} H^3 H_X \Big|_0^{A(\tau)} = 0 \quad .$$

In the limit  $X \rightarrow A(\tau)$ , we assume that  $H^3 H_X \rightarrow 0$ . This is valid if  $H^3$  is dominant in this limit, since  $H \rightarrow 0$ ,  $H_X \rightarrow -\infty$  may occur simultaneously. Thus, we have

$$\int_0^{A(\tau)} H_\tau dX + \frac{1}{3} \frac{\epsilon Re}{Fr} H^3(0, \tau) H_X(0, \tau) = 0 \quad . \quad (3.9)$$

The identity

$$\left( \int_0^{A(\tau)} H(X, \tau) dX \right)_\tau = \int_0^{A(\tau)} H_\tau(X, \tau) dX + H(A(\tau), \tau) A_\tau(\tau) \quad ,$$

together with condition (3.7) yields

$$\left( \int_0^{A(\tau)} H(X, \tau) dX \right)_\tau = \int_0^{A(\tau)} H_\tau(X, \tau) dX \quad .$$

From equation (3.9) we infer

$$\left( \int_0^{A(\tau)} H(X, \tau) dX \right)_\tau + \frac{1}{3} \frac{\epsilon Re}{Fr} H^3(0, \tau) H_X(0, \tau) = 0 \quad . \quad (3.10)$$

The condition for the volume flux (2.37) can be written as

$$\int_0^{H(0, \tau)} U(X, Z, \tau) dZ = \left( \int_0^{A(\tau)} H(X, \tau) dX \right)_\tau = \alpha C_V \tau^{\alpha-1} \quad . \quad (3.11)$$

Substituting (3.11) into (3.10) finally yields

$$\alpha C_V \tau^{\alpha-1} + \frac{1}{3} \frac{\epsilon Re}{Fr} H^3(0, \tau) H_X(0, \tau) = 0 \quad , \quad (3.12)$$

which is equivalent to condition (3.6). Hence, condition (3.7) and (3.6) are not independent (cf. Pert [4]).

### 3.2.2 Similarity transformation

To derive an analytical solution for the evolution equation (3.5) it is useful to employ a similarity transformation, which transforms the partial differential equation (3.5) into an ordinary differential equation.

Based on a similarity variable  $\eta$ , with  $0 \leq \eta \leq \eta_N$ , we can find solutions of the form

$$H(X, \tau) = C_1 \tau^n \tilde{H}(\eta/\eta_N) \quad . \quad (3.13)$$

We use

$$\eta = \frac{X}{C_0} \tau^{-m} \quad , \quad (3.14)$$

where

$$\eta_N = \frac{A(\tau)}{C_0} \tau^{-m} \quad (3.15)$$

describes the position of the contact line. Thus, a normalized variable  $\xi$  may be introduced as

$$\xi = \frac{\eta}{\eta_N} \quad , \quad 0 \leq \xi \leq 1 \quad . \quad (3.16)$$

Substituting (3.13) and (3.14) into the evolution equation (3.5) yields

$$C_1 \tau^{n-1} \left( n \tilde{H} - m \xi \tilde{H}_\xi \right) - \frac{1}{3} \frac{\epsilon R e}{Fr} \frac{C_1^4}{C_0^2} \tau^{4n-2m} \frac{1}{\eta_N^2} \left( \tilde{H}^3 \tilde{H}_\xi \right)_\xi = 0 \quad .$$

To transform this equation into an ordinary differential equation we set

$$4n - 2m = n - 1 \quad (3.17)$$

For the volume flux at  $\xi = 0$  we obtain with (3.6)

$$-\frac{1}{3} \frac{\epsilon R e}{Fr} \frac{C_1^4}{C_0} \tau^{4n-m} \frac{1}{\eta_N} \tilde{H}^3 \tilde{H}_\xi = \alpha C_V \tau^{\alpha-1} \quad . \quad (3.18)$$

At  $\xi = 1$  equation (3.7) yields

$$\tilde{H} = 0 \quad , \quad (3.19)$$

and the integral condition (3.8) yields

$$C_0 C_1 \tau^{m+n} \eta_N \int_0^1 \tilde{H} d\xi = C_V \tau^\alpha \quad . \quad (3.20)$$

The time dependency in (3.18, 3.20) cancels if equations

$$4n - m = \alpha - 1 \quad , \quad (3.21)$$

$$m + n = \alpha \quad (3.22)$$

hold. Solving the system (3.17, 3.21, 3.22), finally, yields

$$m = \frac{3\alpha + 1}{5} \quad , \quad (3.23)$$

$$n = \frac{2\alpha - 1}{5} \quad . \quad (3.24)$$

In similarity form we have the following system of ordinary differential equation, boundary and integral conditions

$$(\tilde{H}^3 \tilde{H}_\xi)_\xi - \frac{3Fr}{\epsilon Re} \frac{C_0^2}{C_1^3} \eta_N^2 \left( \frac{2\alpha - 1}{5} \tilde{H} - \frac{3\alpha + 1}{5} \xi \tilde{H}_\xi \right) = 0 \quad , \quad (3.25)$$

$$\xi = 0 : \quad \tilde{H}^3 \tilde{H}_\xi = -\alpha C_V \frac{3Fr}{\epsilon Re} \frac{C_0}{C_1^4} \eta_N \quad , \quad (3.26)$$

$$\xi = 1 : \quad \tilde{H} = 0 \quad , \quad (3.27)$$

$$\text{integral constraint} \quad \int_0^1 \tilde{H} d\xi = \frac{C_V}{C_0 C_1 \eta_N} \quad . \quad (3.28)$$

The constants  $C_0$  and  $C_1$  and the value of  $\eta_N$  remain to be determined. The values  $C_0$  and  $C_1$  define the length scales of  $\eta$  and  $\tilde{H}$ . Obeying the orders of magnitude in the system (3.25-3.28), the choice is largely free. The backward transformation from  $\eta$  to  $X, \tau$ -coordinates will cancel the influence of this arbitrary choice for  $C_0$  and  $C_1$ .

In equation (3.25) we choose

$$\frac{3Fr}{\epsilon Re} \frac{C_0^2}{C_1^3} \eta_N^2 = 1 \quad . \quad (3.29)$$

To determine the length scale for  $\eta_N$  we substitute the group of constants in (3.28) to be

$$\int_0^1 \tilde{H} d\xi = \frac{C_V}{C_0 C_1 \eta_N} = K \quad . \quad (3.30)$$

Evaluating condition (3.29) and (3.30) we find

$$C_0 = \left( \frac{\epsilon Re}{3Fr} \right)^{1/5} \left( \frac{C_V}{K} \right)^{3/5} \frac{1}{\eta_N} \quad ,$$

$$C_1 = \left( \frac{3Fr}{\epsilon Re} \right)^{1/5} \left( \frac{C_V}{K} \right)^{2/5} \quad .$$

From (3.15) it is obvious that  $C_0$  has to be independent of  $\eta_N$ . Thus,

$$K = (\eta_N)^{-5/3} \quad , \quad (3.31)$$

is readily inferred and the constants are

$$C_0 = \left( \frac{\epsilon Re}{3Fr} \right)^{1/5} C_V^{3/5} \quad , \quad (3.32)$$

$$C_1 = \left( \frac{3Fr}{\epsilon Re} \right)^{1/5} C_V^{2/5} \eta_N^{2/3} \quad . \quad (3.33)$$

$$\int_0^1 \tilde{H} d\xi = \eta_N^{-5/3} \quad . \quad (3.34)$$

In summary we obtain for the evolution equation

$$(\tilde{H}^3 \tilde{H}_\xi)_\xi + \frac{3\alpha + 1}{5} \xi \tilde{H}_\xi - \frac{2\alpha - 1}{5} \tilde{H} = 0 \quad , \quad (3.35)$$

together with the boundary conditions

$$\xi = 0 : \quad \tilde{H}^3 \tilde{H}_\xi = -\frac{\alpha}{\eta_N^{5/3}} \quad , \quad (3.36)$$

$$\xi = 1 : \quad \tilde{H} = 0 \quad . \quad (3.37)$$

The complete set of equations and the similarity transformation is summarized in table 3.1. The solution of the resulting ordinary differential equation (3.35) can generally be found by means of a numerical integration algorithm, or for the special case of  $\alpha = 0$  in an analytical form.

### 3.2.2.1 Analytical solutions

For the analytical solution of the transformed evolution equation (3.35) we assume solutions of the form

$$\tilde{H}(\xi) = c(1 - \xi^a)^b \quad . \quad (3.38)$$

This form automatically fulfills the boundary condition (3.37). Substituting (3.38) into (3.35) yields

$$-\frac{1}{5\xi^2} \left\{ c(1 - \xi^a)^{b-2} \left( 5abc^3 \xi^a (1 - \xi^a)^{3b} (1 - \xi^a + a(4b\xi^a - 1)) \right) - \xi^2 (1 - \xi^a) (2\alpha - 1 + \xi^a (1 - 2\alpha + a(b + 3b\alpha))) \right\} = 0 \quad .$$

$H(X, \tau) = \left( \frac{3Fr}{\epsilon Re} \right)^{1/5} C_V^{2/5} \tau^{(2\alpha-1)/5} \eta_N^{2/3} \tilde{H}(\eta/\eta_N)$ $A(\tau) = \left( \frac{\epsilon Re}{3Fr} \right)^{1/5} C_V^{3/5} \tau^{(3\alpha+1)/5} \eta_N$ <p style="text-align: center;">with</p> $\eta = \left( \frac{\epsilon Re}{3Fr} \right)^{-1/5} C_V^{-3/5} X \tau^{-(3\alpha+1)/5} \quad 0 \leq \eta \leq \eta_N$ $\xi = \frac{\eta}{\eta_N} \quad 0 \leq \xi \leq 1$	
$(\tilde{H}^3 \tilde{H}_\xi)_\xi + \frac{3\alpha+1}{5} \xi \tilde{H}_\xi - \frac{2\alpha-1}{5} \tilde{H} = 0$	
$\xi = 0 :$	$\tilde{H}^3 \tilde{H}_\xi = -\frac{\alpha}{\eta_N^{5/3}}$
$\xi = 1 :$	$\tilde{H} = 0$
volume constraint	$\int_0^1 \tilde{H}(\xi) d\xi = \eta_N^{-5/3}$

Table 3.1: Similarity transformation and system of ordinary differential equation, boundary and integral conditions for  $H(X, \tau)$ .

For

$$\begin{aligned} a &= 2 \quad , \\ b &= 1/3 \quad , \end{aligned}$$

the above equation simplifies to

$$\frac{c}{45(1-\xi^2)^{2/3}} \left( 10c^3(5\xi^2-3) - 3(5\xi^2+6\alpha-3) \right) = 0 \quad .$$

This equation is identically fulfilled if the bracket evaluates to zero. We immediately find

$$\alpha = 0 \quad . \tag{3.39}$$

The above equation reads

$$\frac{c(10c^3-3)(5\xi^2-3)}{45(1-\xi^2)^{2/3}} = 0 \quad .$$

We neglect complex and trivial solutions for  $c$  and obtain

$$c = \left( \frac{3}{10} \right)^{1/3} \quad . \tag{3.40}$$

Thus, we have for  $\alpha = 0$

$$\tilde{H}(\xi) = \left( \frac{3}{10} \right)^{1/3} (1-\xi^2)^{1/3} \quad , \tag{3.41}$$

as a special analytical solution of the evolution equation (3.35).

### 3.2.2.2 Numerical solutions

As shown in the previous section it is possible to find an analytical solution for  $\alpha = 0$ . For the general case  $\alpha \neq 0$  we have to integrate equation (3.35) numerically. Two difficulties are encountered using a numerical method. Firstly, standard integration routines solve an initial value problem by forward (or backward) integration. Here, boundary conditions are given on both sides of the integration interval. Secondly, the singularity at  $\xi = 1$  can hardly be resolved by a numerical routine. To resolve both problems we will seek a solution within the interval  $\xi \in [0, \xi_{max}]$  with  $\xi_{max} \rightarrow 1$ . The boundary conditions at  $\xi = \xi_{max}$  are approximated in the form

$$\tilde{H}(\xi) = c(1-\xi)^{1/3} \quad .$$

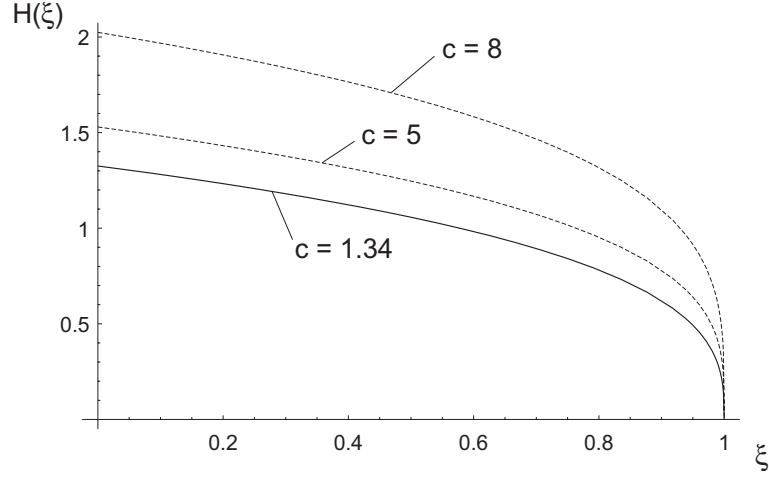


Figure 3.1: Shooting parameter for the numerical solution of  $\tilde{H}(\xi)$ .

The parameter  $c$  is found by iteration from a shooting method. For the shooting method we use

$$(\tilde{H}^3 \tilde{H}_\xi)_\xi + \frac{3\alpha + 1}{5} \xi \tilde{H}_\xi - \frac{2\alpha - 1}{5} \tilde{H} = 0 \quad , \quad (3.42)$$

$$\tilde{H}(\xi_{max}) = c(1 - \xi_{max})^{1/3} \quad , \quad (3.43)$$

$$\tilde{H}_\xi(\xi_{max}) = -\frac{c}{3} (1 - \xi_{max})^{-2/3} \quad . \quad (3.44)$$

We start with an initial guess for the value  $c$  and verify after the numerical integration whether the condition

$$\tilde{H}(0)^3 \tilde{H}_\xi(0) = -\alpha \int_0^1 \tilde{H} d\xi \quad (3.45)$$

is satisfied. In figure 3.1 the development of the solution for different values of  $c$  is shown. Starting with  $c = 8$  we find that the shooting condition (3.45) is satisfied for  $c = 1.34$  to a given accuracy.

### 3.2.2.3 Approximations

It is useful to have also an analytical approximation of the exact numerical solution  $\tilde{H}(\xi)$ . Two different methods are employed to find an approximation for  $\tilde{H}(\xi)$ . This simplifies the subsequent calculations of the temperature field.

### Expansion for $\xi \rightarrow 1$

An expansion of the form

$$\tilde{H}_{exp}(\xi) = c(1 - \xi)^{1/3} \left( 1 + c_1(1 - \xi) + c_2(1 - \xi)^2 + \dots \right) \quad , \quad (3.46)$$

yields an approximation for  $\xi \rightarrow 1$ . Furthermore, we can verify from equation (3.46) the shooting parameter  $c$  in section 3.2.2.2. Substituting (3.46) into (3.35) yields

$$\begin{aligned} \mathcal{O}(1) : \quad & c \left( \frac{c^3}{9} - \frac{1}{5} \left( \alpha + \frac{1}{3} \right) \right) = 0 \quad , \\ \mathcal{O}((1 - \xi)^1) : \quad & c_1 \left( \frac{28}{9}c^4 - \frac{4c}{5} \left( \alpha + \frac{1}{3} \right) \right) + \frac{c}{5} \left( \frac{4}{3} - \alpha \right) = 0 \quad , \\ \mathcal{O}((1 - \xi)^2) : \quad & 7c_2 \left( \frac{10}{9}c^4 - \frac{c}{5} \left( \alpha + \frac{1}{3} \right) \right) + \frac{35}{3}c^4c_1^2 + \frac{1}{5}cc_1 \left( 2\alpha + \frac{7}{3} \right) = 0 \quad . \end{aligned}$$

For the constants  $c, c_1, c_2$  we obtain

$$\begin{aligned} c &= \left( \frac{3}{5} \right)^{1/3} (1 + 3\alpha)^{1/3} \quad , \\ c_1 &= \frac{3\alpha - 4}{24(3\alpha + 1)} \quad , \\ c_2 &= -\frac{153\alpha^2 - 288\alpha + 112}{4032(3\alpha + 1)^2} \quad . \end{aligned}$$

Thus, the approximation (3.46) is summarized to the leading order by

$$\tilde{H}_{exp}(\xi) = \left( \frac{3}{5}(1 + 3\alpha) \right)^{1/3} (1 - \xi)^{1/3} \left( 1 + \frac{3\alpha - 4}{24(3\alpha + 1)}(1 - \xi) + \mathcal{O}((1 - \xi)^2) \right) \quad . \quad (3.47)$$

### Weighted residual method

A more general approximation, which is valid in the interval  $\xi \in [0, 1]$ , can be found by a weighted residual method. We use as a trial solution

$$\tilde{H}_{WRM}(\xi) = c(1 - \xi)^b \quad , \quad (3.48)$$

which yields for the residual of equation (3.35)

$$R = b(4b - 1)c^4(1 - \xi)^{4b-2} - \frac{c}{5}(1 - \xi)^{b-1}(-1 + \xi(1 + b) + \alpha(2 + (3b - 2)\xi)) \quad . \quad (3.49)$$

Using two weighting functions  $w_1(\xi)$  and  $w_2(\xi)$  we can formulate two equations

$$\int_0^1 (Rw_i) d\xi = 0 \quad , \quad i = 1, 2 \quad .$$

Thus, we have two conditions to infer the unknown parameters  $b, c$ . For two sets of weighting functions we obtain

- $w_1(\xi) = 1, w_2(\xi) = \xi$ :

$$\begin{aligned}\tilde{H}_{WRM1}(\xi) &= c(1 - \xi)^b \quad , & (3.50) \\ b &= \frac{10\alpha}{4 + 27\alpha} \quad , \\ c &= \left( \frac{(4 + 27\alpha)^2}{40 + 370\alpha} \right)^{1/3} \quad .\end{aligned}$$

- $w_1(\xi) = 1, w_2(\xi) = c(1 - \xi)^b$ :

$$\begin{aligned}\tilde{H}_{WRM2}(\xi) &= c(1 - \xi)^b \quad , & (3.51) \\ b &= \frac{4\alpha - 2 + \sqrt{9 + \alpha(44 + 151\alpha)}}{5 + 45\alpha} \quad , \\ c &= \left( \frac{-347\alpha^2 + 42\alpha - 3 + (1 + 53\alpha)\sqrt{9 + \alpha(44 + 151\alpha)}}{50(1 + 3\alpha)} \right)^{1/3} \quad .\end{aligned}$$

### 3.2.3 Numerical solution of the evolution equation for $H(X, \tau)$

To solve equation (3.5) numerically we have to address to the problem of the moving contact line  $A(\tau)$ , which is shown in figure 3.2. We need a very fine numerical grid in the vicinity of  $A(\tau)$  to resolve the singular behaviour of  $H(X, \tau)$ . The similarity solution shows close to the contact line the following behaviour

$$\begin{aligned}X \rightarrow A(\tau) : \quad H &\rightarrow 0 \quad , \\ H_X &\rightarrow -\infty \quad .\end{aligned}$$

To solve the problem in  $X, \tau$ -coordinates we need an adaptive mesh moving with the contact line  $A(\tau)$ . Hereby,  $A(\tau)$  is part of the solution of the spreading problem. Alternatively, we may resolve the complete  $X, \tau$ -domain with a suitable fine grid, which inflicts a large number of nodes. A more efficient method to obtain a numerical solution defines a new variable

$$\xi = \frac{X}{A(\tau)} \quad , \quad (3.52)$$

in order to transform the spreading problem onto a fixed domain. In a fixed domain we are free to resolve the region around the contact line in particular with a very fine grid to obtain an adequate numerical approximation of  $H(X, \tau)$  for  $X \rightarrow A(\tau)$ .

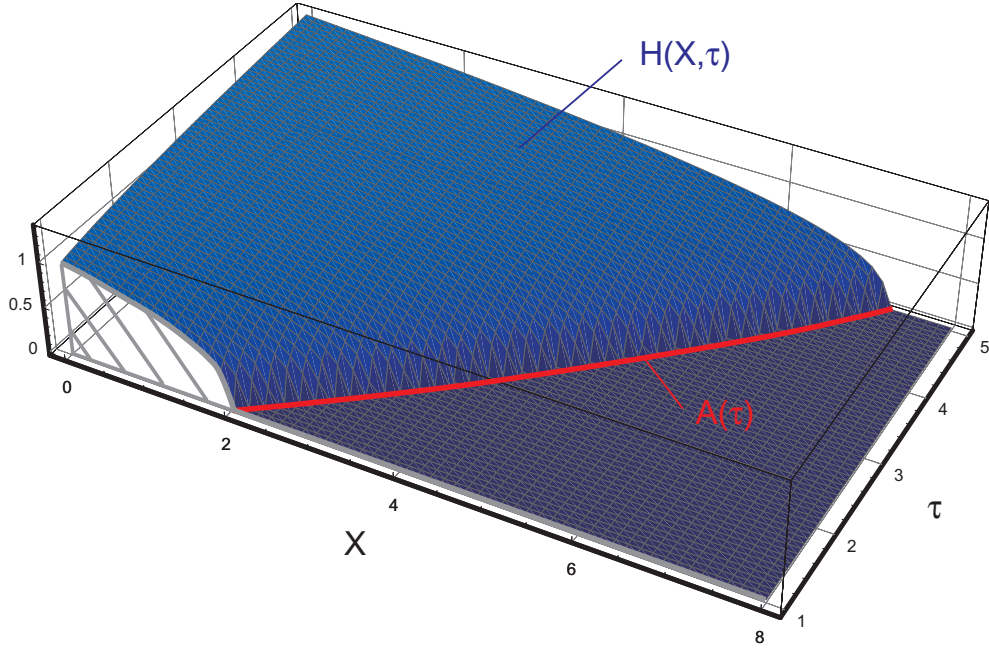


Figure 3.2: Sketch of the numerical solution of  $H(X, \tau)$ .

### 3.2.3.1 Transformation $(X, \tau) \rightarrow (\xi, \tau)$

Substituting equation (3.52) into the equations (3.5-3.8) yields

$$H_\tau - \xi \frac{A_\tau}{A} H_\xi - \frac{1}{3} \frac{\epsilon Re}{Fr} \frac{1}{A^2} (H^3 H_\xi)_\xi = 0 \quad , \quad (3.53)$$

$$\xi = 0 : \quad -\frac{1}{3} \frac{\epsilon Re}{Fr} \frac{1}{A} H^3 H_\xi = \alpha C_V \tau^{\alpha-1} \quad , \quad (3.54)$$

$$\xi = 1 : \quad H = 0 \quad , \quad (3.55)$$

$$\text{integral constraint :} \quad \int_0^1 H d\xi = \frac{C_V \tau^\alpha}{A} \quad . \quad (3.56)$$

The transformation allows to formulated the spreading problem on a rectangular domain, as shown in figure 3.3.

### 3.2.3.2 Method of lines for the evolution equation of $H(\xi, \tau)$

Equation (3.53) is a nonlinear diffusion equation, first order in time and second order in space. As equation (3.53) is nonlinear we use the method of lines to change the partial differential equation into a system of ordinary differential equations, which can be integrated

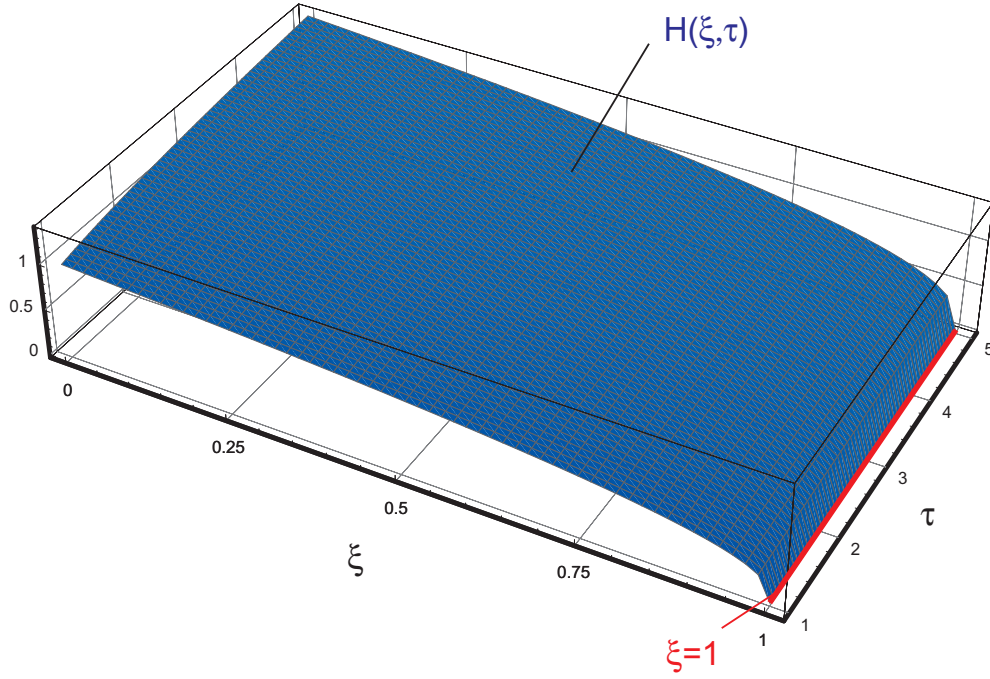


Figure 3.3: Sketch of the numerical solution of  $H(\xi, \tau)$ .

numerically using a standard scheme like Adams or Gear (cf. [7]), depending on the stiffness of the resulting system. We replace the derivatives with respect to  $\xi$  by a finite difference approximation and obtain a system of  $(i_{max} - 1)$  ordinary differential equations in time  $\tau$ . We use non-uniform spacing

$$\Delta\xi_i = \xi_i - \xi_{i-1} \quad , \quad i = 1, \dots, i_{max} \quad , \quad (3.57)$$

as shown in figure 3.4. Thus, we have a discrete representation of

$$H_i(\tau) \simeq H(\xi_i, \tau) \quad , \quad (3.58)$$

at discrete values  $\xi = \xi_i$  within an interval  $\tau_0 \leq \tau \leq \tau_{max}$ .

We employ central differences for both the first derivatives, i.e.

$$H_{\xi}(\xi_i, \tau) \approx \frac{H_{i+1} - H_{i-1}}{\Delta\xi_{i+1} + \Delta\xi_i} \quad , \quad i = 1, \dots, i_{max} - 1 \quad (3.59)$$

and the second derivatives, i.e.

$$H_{\xi\xi}(\xi_i, \tau) \approx 2 \frac{\Delta\xi_i H_{i+1} - (\Delta\xi_{i+1} + \Delta\xi_i) H_i + \Delta\xi_{i+1} H_{i-1}}{\Delta\xi_{i+1} \Delta\xi_i (\Delta\xi_{i+1} + \Delta\xi_i)} \quad , \quad i = 1, \dots, i_{max} - 1 \quad , \quad (3.60)$$

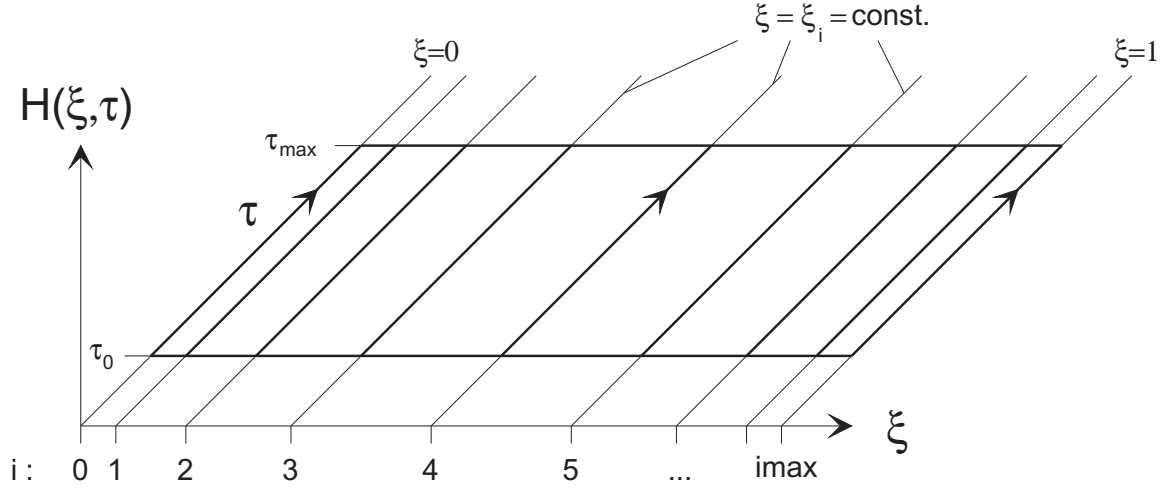


Figure 3.4: Sketch of the method of lines for  $H(\xi, \tau)$ .

in equation (3.53). Around  $\xi = 1$  we, employ a fifth order backward difference to increase accuracy around this singular point.

For a discretized formulation of equation (3.54) we use the forward difference for the derivative  $H_\xi$ , i.e.

$$H_\xi(0, \tau) \approx \frac{-\Delta\xi_2(2\Delta\xi_1 + \Delta\xi_2)H_0 + (\Delta\xi_1 + \Delta\xi_2)^2 H_1 - \Delta\xi_1^2 H_2}{\Delta\xi_1 \Delta\xi_2 (\Delta\xi_1 + \Delta\xi_2)} . \quad (3.61)$$

To avoid multiple solutions we introduce for  $H$

$$H(0, \tau) \approx H_1(\tau) + \frac{\Delta\xi_1(\Delta\xi_3(2\Delta\xi_2 + \Delta\xi_3)H_1 - (\Delta\xi_2 + \Delta\xi_3)^2 H_2 + \Delta\xi_2^2 H_3)}{\Delta\xi_2 \Delta\xi_3 (\Delta\xi_2 + \Delta\xi_3)} . \quad (3.62)$$

Expression (3.62) results from a Taylor-expansion around  $\xi = \xi_1$  and a forward difference approximation of the respective derivatives.

The discrete formulation of the evolution equation and the boundary conditions represents now a system of  $(i_{max} - 1)$  coupled ordinary differential equations together with two boundary conditions at  $\xi_0$  and  $\xi_{imax}$ .

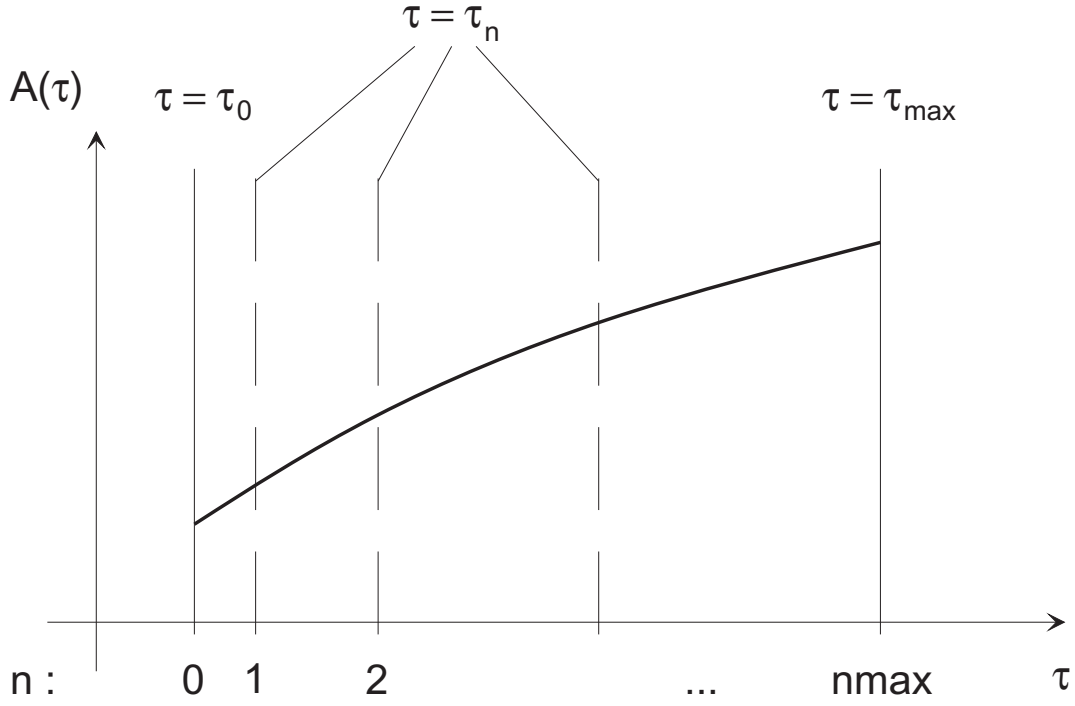


Figure 3.5: Subdomains for the shooting method for  $A(\tau)$ .

### 3.2.3.3 Shooting method for $A(\tau)$

The position of the contact line  $A(\tau)$  is unknown and cannot be calculated from  $H(\xi, \tau)$ . Therefore, we use a shooting method together with the integral constraint (3.56) to calculate  $A(\tau)$ . The performance during the calculation can be improved, if we split the interval  $\tau_0 \leq \tau \leq \tau_{max}$  into  $n_{max}$  subdomains as shown in figure 3.5. Within each interval we assume for  $A(\tau)$  a Taylor-expansion

$$A_n(\tau) = A_{n-1} + c_n \cdot (\tau - \tau_{n-1}) \quad , \quad \begin{array}{l} n = 1, \dots, n_{max} \quad , \\ \tau_{n-1} \leq \tau \leq \tau_n \quad . \end{array} \quad (3.63)$$

For the calculation of the coefficient  $c_n$  we use equation (3.56) at  $\tau = \tau_n$ . This yields

$$\tau = \tau_n : \quad \int_0^1 H d\xi = \frac{C_V \tau^\alpha}{A} \quad . \quad (3.64)$$

### 3.3 Results

As shown in the previous section it is possible to find either similarity solutions or numerical solutions for  $H(X, \tau)$ . Based on these solutions we can determine the pressure  $P$ , the velocities  $U$ ,  $W$  and the streamfunction  $\Psi$  using equations (3.1-3.4).

#### 3.3.1 Position of the l/g-interface - $H(X, \tau)$

##### 3.3.1.1 Similarity solution for $H(X, \tau)$

The similarity transformation of equation (3.5) reduces the partial differential equation to an ordinary differential equation. The coefficients in equation (3.35) no longer depend on the nondimensional groups  $\epsilon$ ,  $Re$ ,  $Fr$ , but only on the parameter  $\alpha$ . We solve for  $\tilde{H}$  depending on the characteristic of the flow. Having solved equation (3.35) for the shape function  $\tilde{H}(\xi)$  we can determine a solution for specific  $\epsilon$ ,  $Re$ ,  $Fr$  using equations (3.13-3.14).

**Solution for  $\tilde{H}$**  Figure 3.6 shows the results for  $\tilde{H}$  using the numerical method described in section 3.2.2.2. We can see the significant influence of the parameter  $\alpha$ . For  $\alpha = 0$  we get the spreading of a constant volume, i.e. a drop. With increasing  $\alpha$  the shape becomes steeper due to an increased inflow (cf. equation (3.36)).

Figure 3.7 shows the analytical solution (3.41) for  $\alpha = 0$  together with the numerical result (cf. also figure 3.6). The good agreement demonstrates that the numerical method is suitable for this type of problem.

As shown in section 3.2.2.3 it is possible to find analytical approximations for  $\tilde{H}(\xi)$ . Figure 3.8 shows results for  $\tilde{H}$  based on either the expansion  $\tilde{H}_{exp}$ , equation (3.47), or the numerical solution. The agreement for  $\alpha > 0$  is good. For  $\alpha = 0$  there is a slight discrepancy as  $\xi \rightarrow 0$ . From the analytical solution (3.41) we infer for  $\alpha = 0$

$$\tilde{H} \propto (1 - \xi^2)^{1/3} \quad .$$

In contrast, the expansion yields the form

$$\tilde{H} \propto (1 - \xi)^{1/3} \quad .$$

Thus, we may expect some discrepancy for this case.

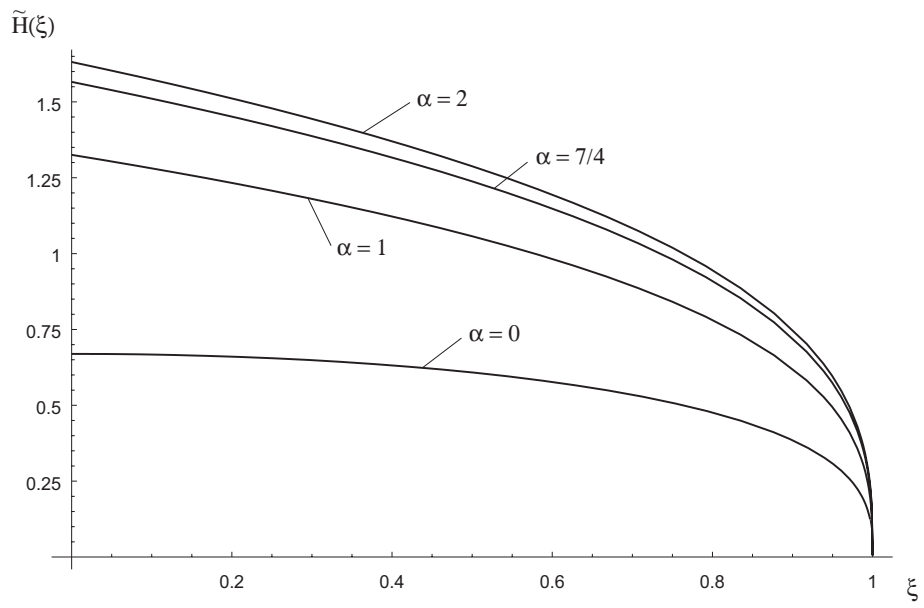


Figure 3.6: Numerical solution for  $\tilde{H}$ ,  $\alpha = 0, 1, 7/4, 2$ .

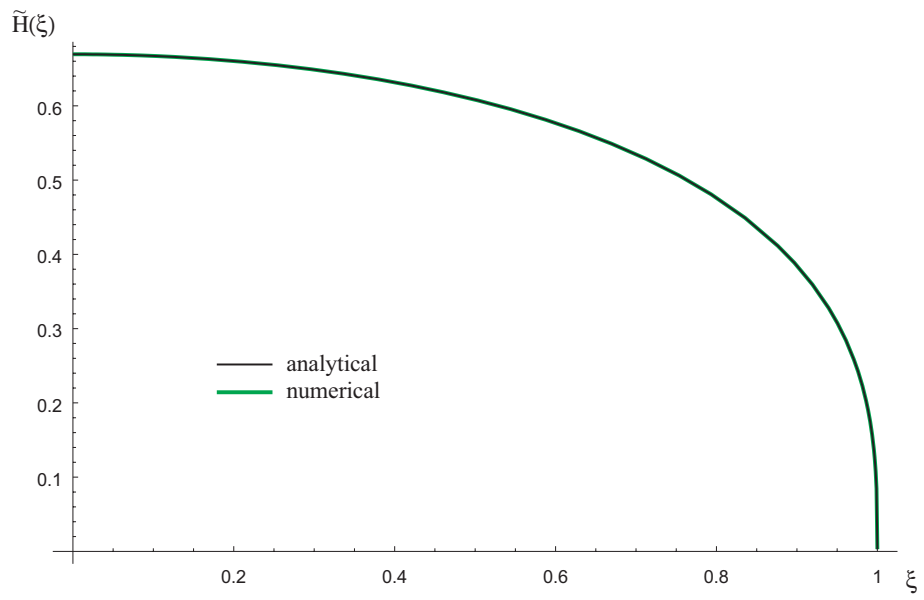


Figure 3.7: Analytical and numerical solution for  $\tilde{H}$ ,  $\alpha = 0$ .

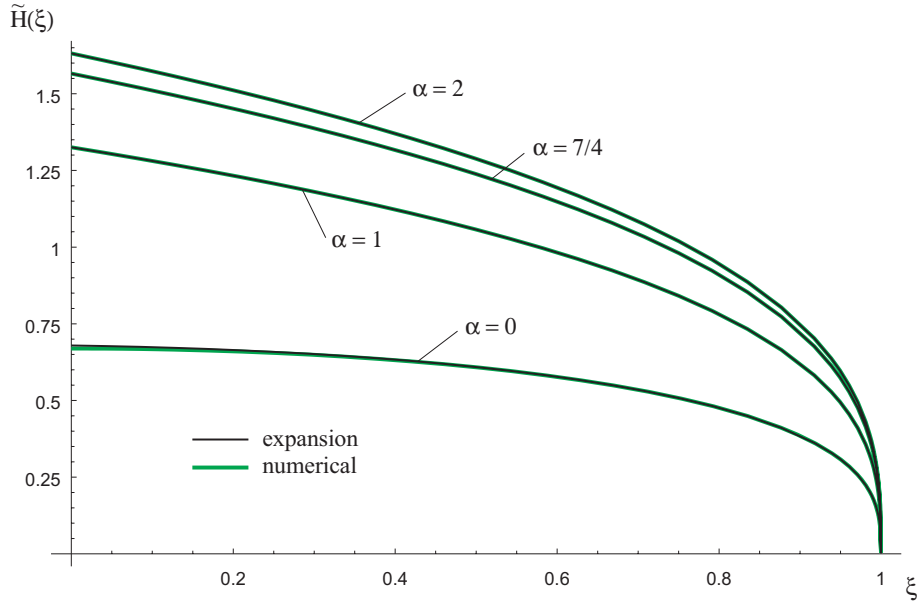


Figure 3.8: Expansion  $\tilde{H}_{exp}$ , equation (3.47), and the numerical solution for  $\tilde{H}$ ,  $\alpha = 0, 1, 7/4, 2$ .

Using a weighted residual method for the approximation of  $\tilde{H}(\xi)$  yields again good agreement for  $\alpha > 0$ , as shown in figure 3.9 and 3.10. Only for  $\alpha = 0$  the weighted residual method fails due to inappropriate trial functions. The accuracy of the different approximations can be estimated, based on the value  $\eta_N$ , equation (3.34). In figure 3.11  $\eta_N$  is plotted versus  $\alpha$ . For  $\tilde{H}_{exp}$ , equation (3.47), the agreement is good and the discrepancy for all values of  $\alpha > 0$  is of the order  $10^{-5}$ . The maximum error occurs around  $\alpha = 0$ , where the approximation  $\tilde{H}_{exp}$  yields values for  $\eta_N$ , which are 0.2% lower than the numerical values. Both solutions  $\tilde{H}_{WRM1}$  and  $\tilde{H}_{WRM2}$ , equation (3.50) and (3.51), give good approximations for  $\alpha \geq 1$ . The discrepancy is lower than 0.4% in this range. However, the error is two orders of magnitude larger if compared to the approximation  $\tilde{H}_{exp}$ , equation (3.47). On the other hand  $\tilde{H}_{WRM1}$  and  $\tilde{H}_{WRM2}$  allow for a simpler mathematical formulation.

**Solution for  $H(X, \tau)$**  We have seen in the previous section, that the solution of  $\tilde{H}$  depends only on the spatial coordinate  $\xi$  and the parameter  $\alpha$ , which captures the volume history. The nondimensional groups have no influence on  $\tilde{H}$ . The influence of the nondimensional groups is encoded in the backward transformation from the similarity variable  $\xi$  to the

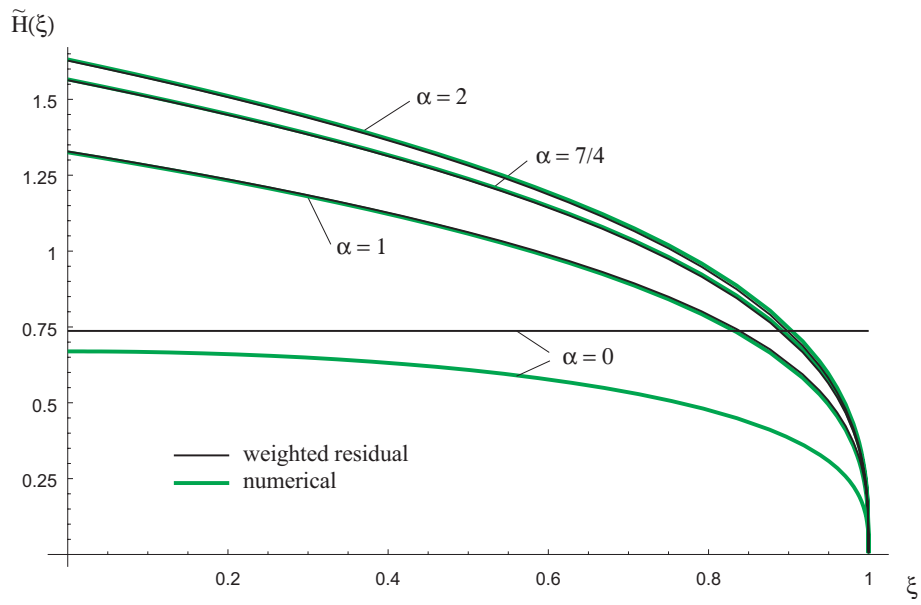


Figure 3.9: Weighted residual solution  $\tilde{H}_{WRM1}$ , equation (3.50), and the numerical solution for  $\tilde{H}$ ,  $\alpha = 0, 1, 7/4, 2$ .

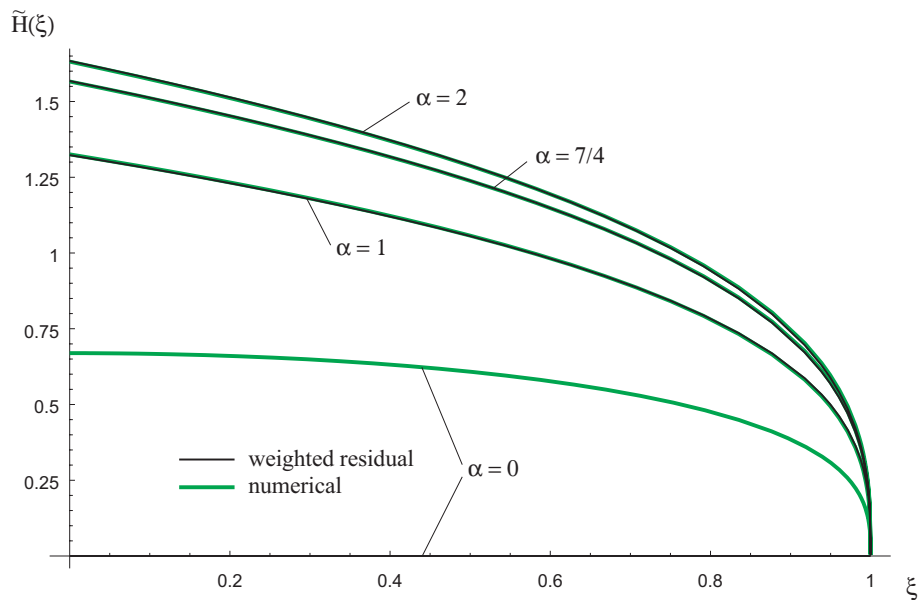


Figure 3.10: Weighted residual solution  $\tilde{H}_{WRM2}$ , equation (3.51), and the numerical solution for  $\tilde{H}$ ,  $\alpha = 0, 1, 7/4, 2$ .

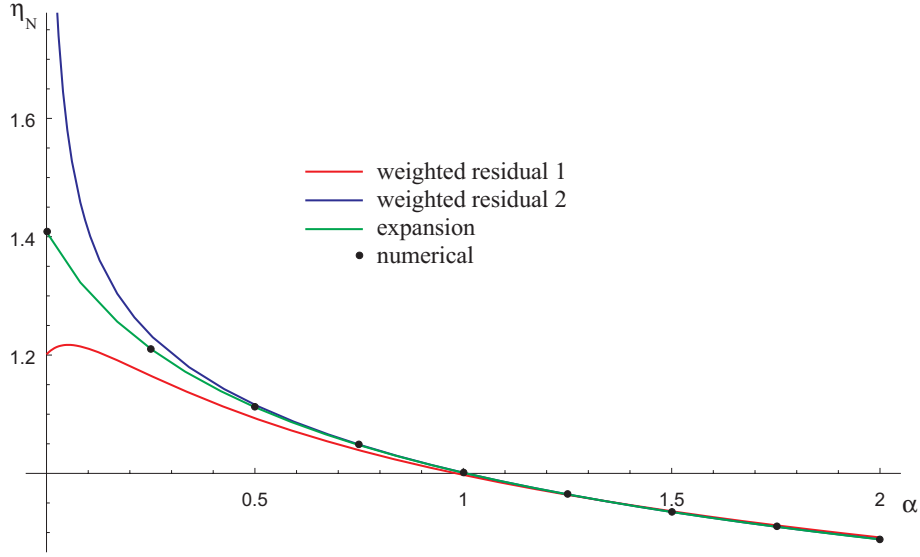


Figure 3.11: Approximate and numerical solutions for  $\eta_N$ .

$X, \tau$ -coordinates.

Substituting the coefficients  $m, n$ , equations (3.23, 3.24), the length scales  $C_0, C_1$ , equations (3.32, 3.33), into equation (3.13), together with the similarity variable  $\eta$ , equation (3.14), and  $\eta_N$ , equation (3.15), we obtain for the interface

$$H(X, \tau) = \left(\frac{3Fr}{\epsilon Re}\right)^{1/5} C_V^{2/5} \eta_N^{2/3} \tau^{(2\alpha-1)/5} \tilde{H} \left( \left(\frac{3Fr}{\epsilon Re}\right)^{1/5} \frac{X}{\tau^{(3\alpha+1)/5} C_V^{3/5} \eta_N} \right), \quad (3.65)$$

and for the contact line

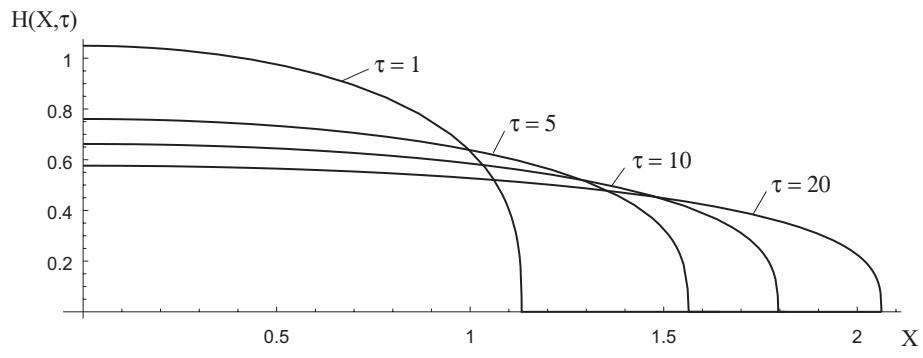
$$A(\tau) = \left(\frac{\epsilon Re}{3Fr}\right)^{1/5} C_V^{3/5} \eta_N \tau^{(3\alpha+1)/5}. \quad (3.66)$$

Depending on the required accuracy one of the approximations for  $\tilde{H}$  (cf. equations (3.47, 3.50, 3.51)) may be used to express  $H(X, \tau)$ . In figures 3.12, 3.13 the solution for  $H(X, \tau)$ , approximated by the numerical solution for  $\tilde{H}$ , is shown for different values of  $\alpha$ .

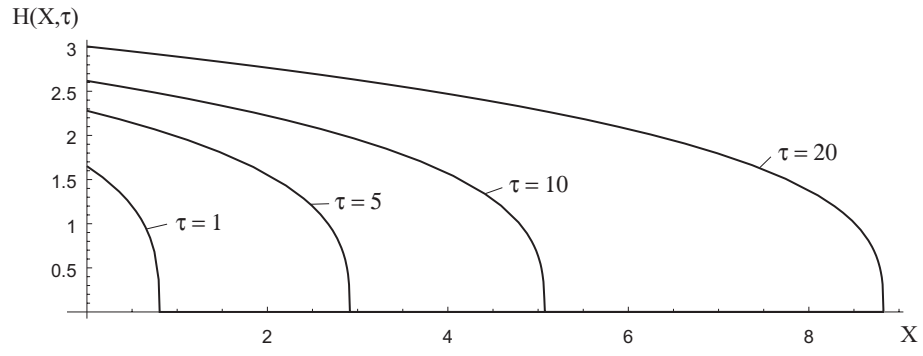
### 3.3.1.2 Numerical solution for $H(X, \tau)$

Solving the evolution equation (3.5) via a similarity transformation yields the long time solution for  $H$ , see Smyth [6]. In this case it is not necessary to formulate an initial condition at a time  $\tau = \tau_0$ . The volume constraint (3.8) guarantees a unique solution.

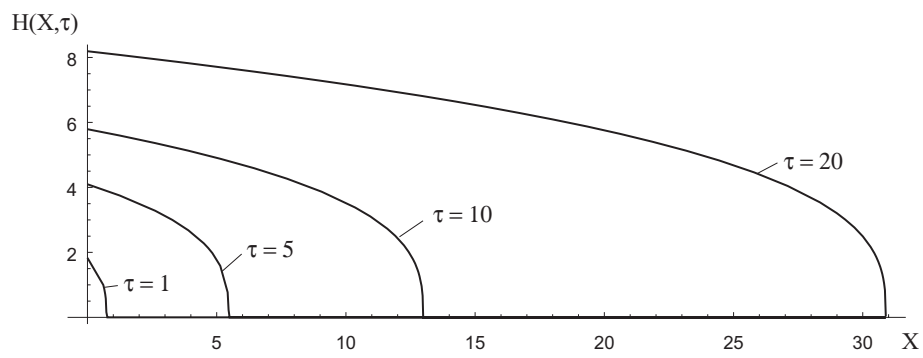
$\alpha = 0$



$\alpha = 1$



$\alpha = 7/4$



$\alpha = 2$

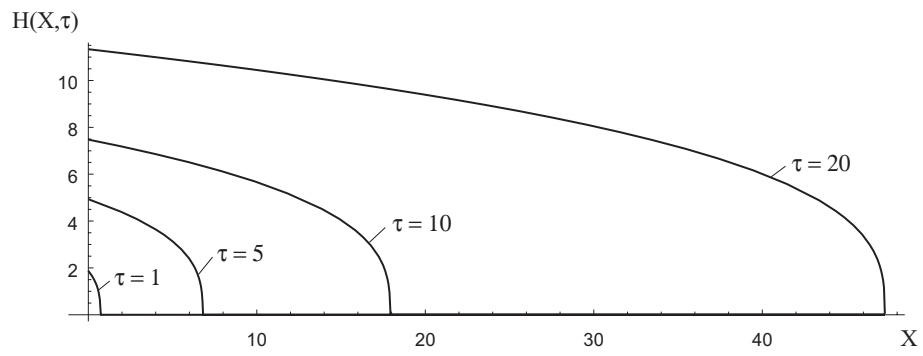


Figure 3.12:  $H(X, \tau)$ , similarity transformation,  $\alpha = 0, 1, 7/4, 2$ .

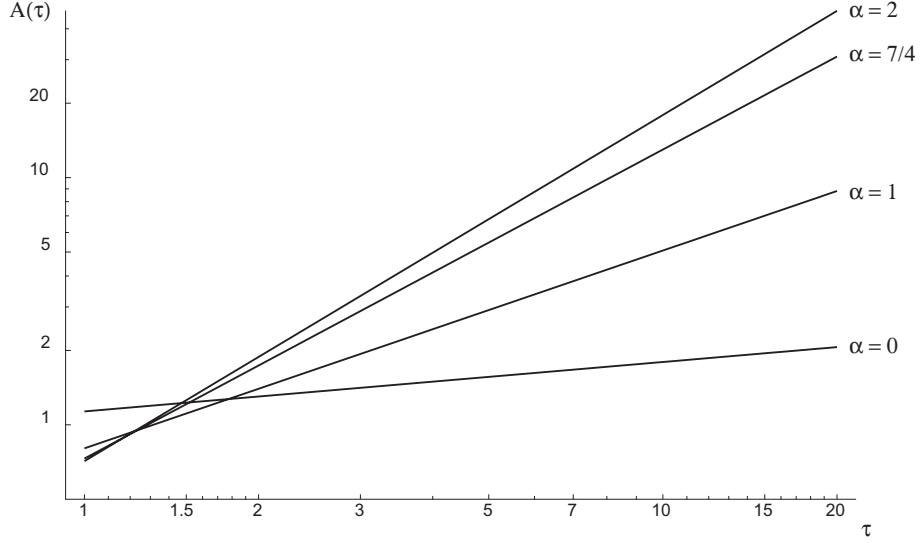


Figure 3.13: Position of the contact line  $A(\tau)$ , similarity transformation,  $\alpha = 0, 1, 7/4, 2$ .

For the numerical integration of equation (3.53) we have to specify initial conditions at  $\tau = \tau_0$ . To fulfill the boundary conditions (3.54, 3.55) and the volume constraint (3.56) we use the initial shapes

$$H(\xi, \tau_0) = c(1 - \xi^2) \quad , \quad \alpha = 0 \quad , \quad (3.67)$$

$$H(\xi, \tau_0) = c(1 - \xi) \quad , \quad \alpha > 0 \quad . \quad (3.68)$$

Substituting (3.67) and (3.68) into the boundary conditions (3.54) and (3.56) for  $\alpha = 0$  yields

$$c = \frac{3C_V}{2A(\tau_0)} \quad , \quad A(\tau_0) \rightarrow \text{arbitrary} \quad .$$

For  $\alpha > 0$  we obtain

$$c = \left( \frac{6Fr\alpha}{\epsilon Re} \right)^{1/5} C_V^{2/5} \tau_0^{(2\alpha-1)/5} \quad , \quad A(\tau_0) = \left( \frac{16\epsilon Re}{3Fr\alpha} \right)^{1/5} C_V^{3/5} \tau_0^{(3\alpha-1)/5} \quad .$$

For the following calculations the parameters are chosen as

$$\begin{aligned} Re &= 1 \quad , \quad Fr = 0.01 \quad , \\ \epsilon &= 0.01 \quad , \quad C_V = 1 \quad . \end{aligned}$$

The initial conditions for  $\tau_0 = 0.5$  are summarized in table 3.2. Figures 3.14-3.17 show

$\alpha$	$H(\xi, \tau_0)$	$A(\tau_0)$
0	$3/2(1 - \xi^2)$	1
1	$1.246(1 - \xi)$	0.803
7/4	$1.132(1 - \xi)$	0.525
2	$1.084(1 - \xi)$	0.461

Table 3.2: Initial conditions for the numerical integration of  $H(\xi, \tau)$ .

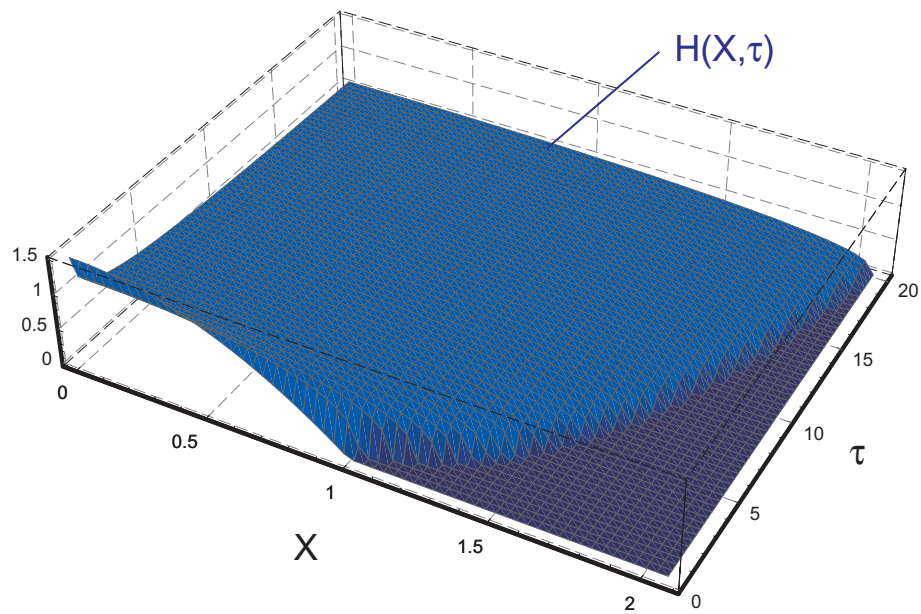


Figure 3.14: Numerical solution of  $H(\xi, \tau)$ ,  $\alpha = 0$ .

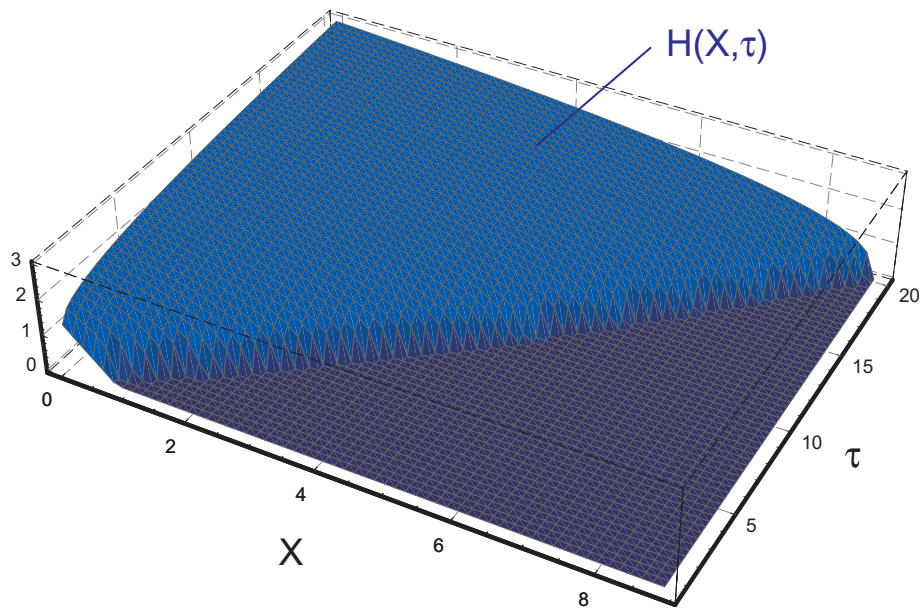


Figure 3.15: Numerical solution of  $H(\xi, \tau)$ ,  $\alpha = 1$ .

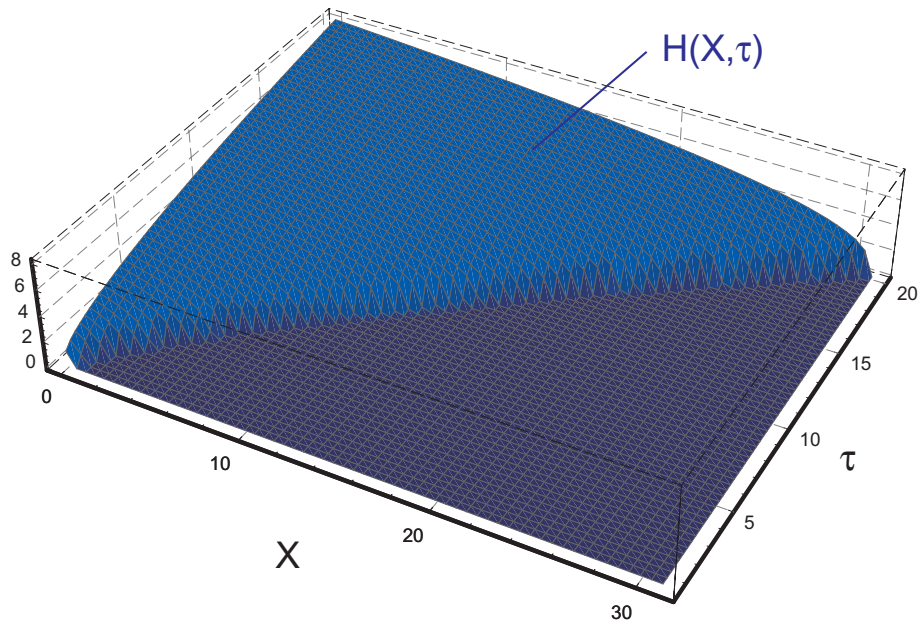


Figure 3.16: Numerical solution of  $H(\xi, \tau)$ ,  $\alpha = 7/4$ .

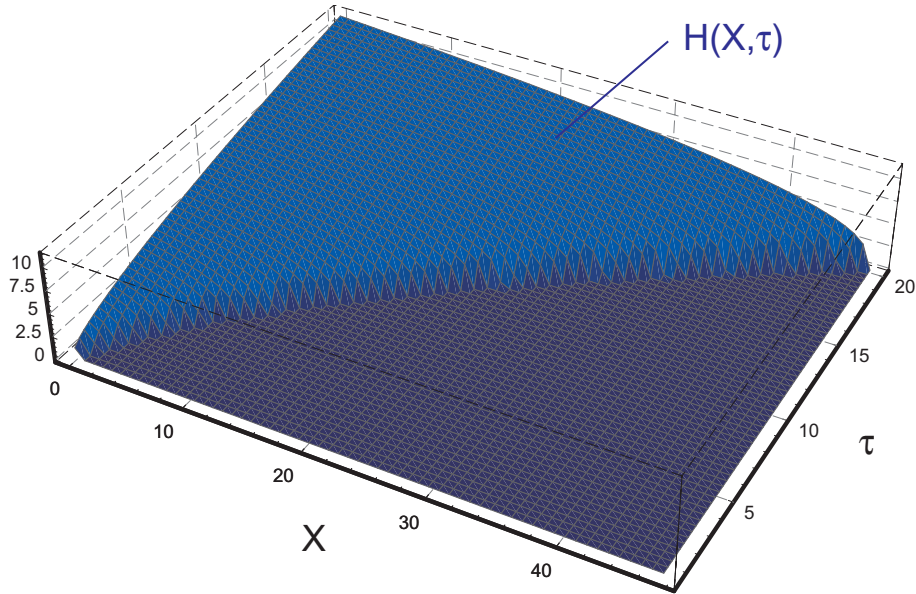


Figure 3.17: Numerical solution of  $H(\xi, \tau)$ ,  $\alpha = 2$ .

the solution for  $H(X, \tau)$  using the numerical method discussed in section 3.2.3 for  $\alpha = 0, 1, 7/4, 2$ .

As expected the initial conditions have only an influence for small times  $\tau \simeq \tau_0$ . For long times we obtain good agreement between the numerical and the similarity solution as shown in figure 3.18, which shows both solutions in normalized coordinates  $\xi = X/A(\tau)$ . The history of the contact line  $A(\tau)$  is shown in figure 3.19. Again good agreement is achieved, which verifies the numerical method.

### 3.3.2 Velocity fields

In section 3.1 we have inferred that the pressure  $P$ , which drives the spreading flow, the velocities  $U$ ,  $W$  and the streamfunction  $\Psi$  all depend on the function  $H(X, \tau)$ . Based on either the similarity solution or the numerical solution for  $H$  we can compute these quantities. Figure 3.20 shows streamlines for  $\alpha = 0, 1, 7/4, 2$ . For  $\alpha = 0$  we have the spreading of a constant volume, i.e. of a drop. Due to symmetry there is no horizontal velocity component  $U$  at  $X = 0$ . The boundary condition (3.6) yields  $H_X = 0$  and from equation (3.2) we have  $U(0, Z, \tau) = 0$ . For all other cases,  $\alpha > 0$ , we have an inflow at  $X = 0$ , i.e. almost parallel streamlines. Thus, we expect a mainly horizontal flow for

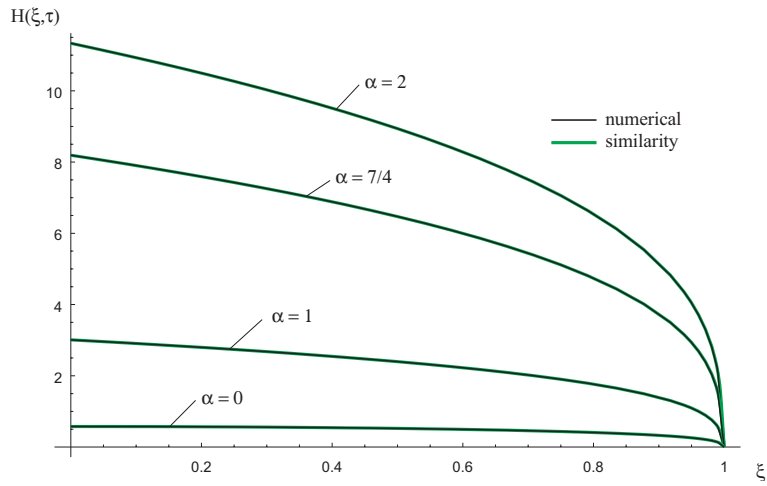


Figure 3.18: Comparison of the similarity transformation and the numerical solution for  $H(\xi, \tau)$ .  $\alpha = 0, 1, 7/4, 2$ ,  $\tau = 20$ .

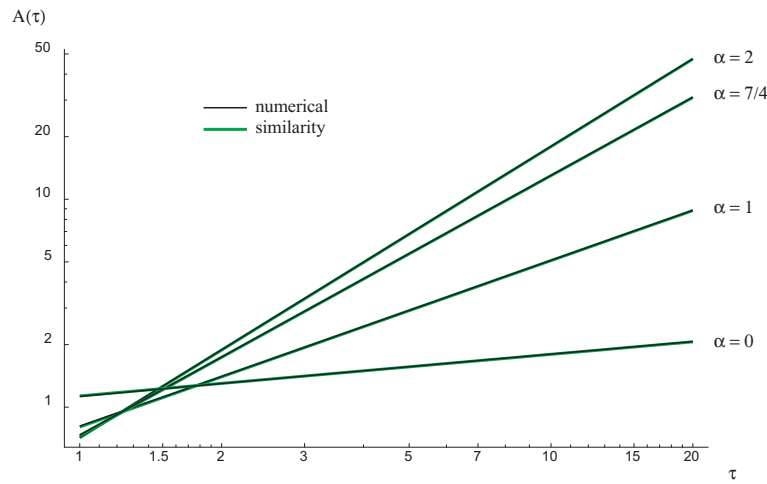
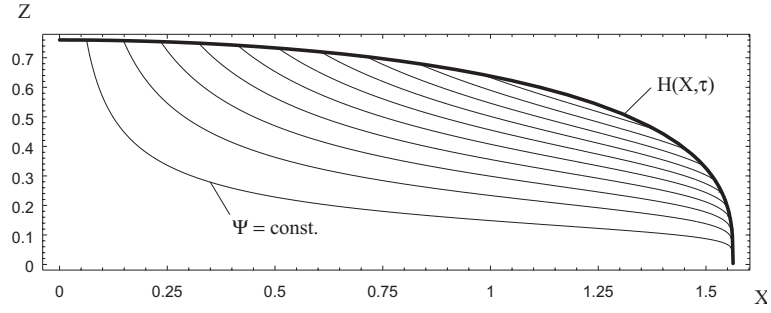


Figure 3.19: Comparison of the similarity transformation and the numerical solution for  $A(\tau)$ .  $\alpha = 0, 1, 7/4, 2$ .

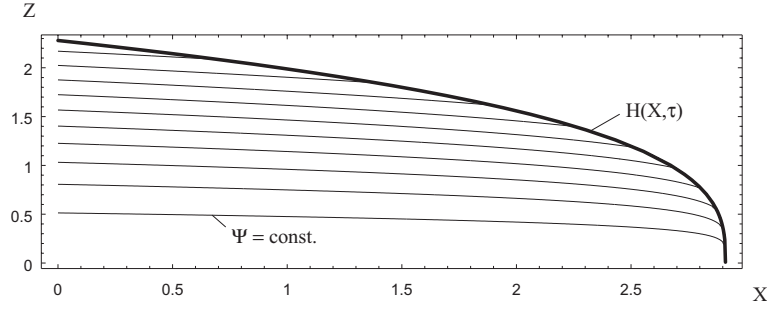
$\alpha > 0$ . In contrast, for  $\alpha = 0$ , vertical velocities are dominant. For  $Z \rightarrow 0$  streamlines are parallel to the substrate, which represents the streamline  $\Psi = 0$ . At the l/g-interface we get streamlines ending at  $H(X, \tau)$ . This is a result of the time dependent l/g-interface.

Figure 3.21 shows the velocity components  $U$  and  $W$  at  $X = 0$  and  $X = 0.9A(\tau)$ . The velocity plots confirm the different behavior for  $\alpha = 0$  and  $\alpha > 0$  at  $X = 0$ . For  $X \rightarrow A(\tau)$  the balance between  $U$  and  $W$  obviously is independent of  $\alpha$ . However, the amplitudes of  $U, W$  increase with increasing  $\alpha$ .

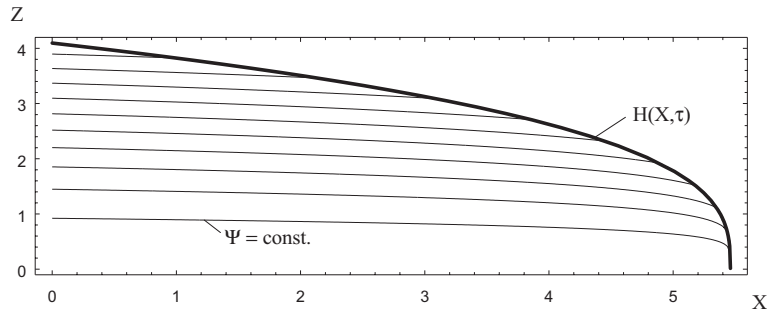
$\alpha = 0$ :



$\alpha = 1$ :



$\alpha = 7/4$ :



$\alpha = 2$ :

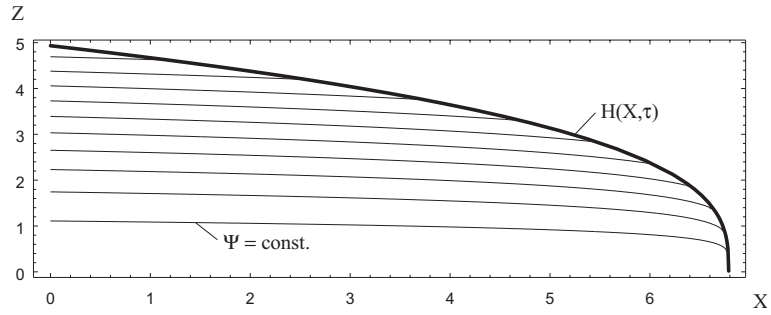


Figure 3.20: Streamlines for isothermal spreading without crusting,  $\tau = 5$ .

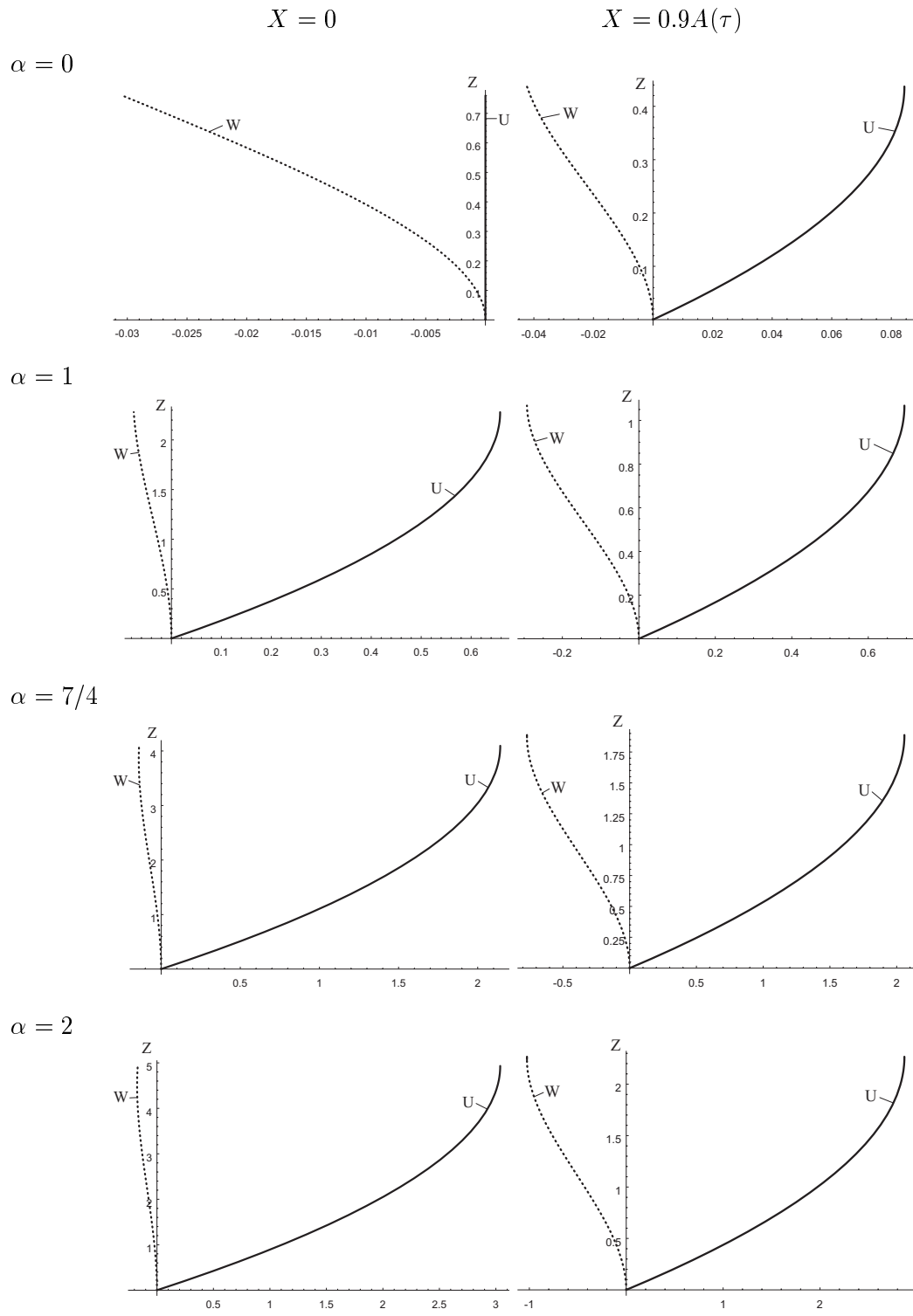


Figure 3.21: Velocity components at  $X = 0$  and  $X = 0.9A(\tau)$ ,  $\tau = 5$ .

## Chapter 4

# Nonisothermal spreading - without solidification

The energy equation (2.12) yields

$$\epsilon RePr (\Theta_\tau + U\Theta_X + W\Theta_Z) = \Theta_{ZZ} \quad .$$

We shall focus onto melts with large Prandtl numbers, such that

$$\epsilon RePr \gg 1 \tag{4.1}$$

holds. This assumption allows a matched-asymptotic formulation of the thermal field. Furthermore, we restrict to the quasi-steady problem, thus

$$\Theta_\tau = 0 \quad . \tag{4.2}$$

The quasi-steady approximation will give the thickest possible thermal boundary layer and, therefore, a 'worst-case approximation' for the influence of nonisothermal effects on the spreading process. A weighted residual method will give an estimation of  $\Theta$  using the transient energy equation (2.12).

With respect to the quasi-steady problem we restrict our calculations to spreading problems with  $\alpha > 0$ . Figure 3.21 shows that  $U(0, Z) = 0$  for  $\alpha = 0$ . The convective heat transport in the horizontal direction vanishes and the remaining terms in the energy equation describe only heat transport in the vertical direction. This will lead to unphysical results. For spreading with  $\alpha = 0$  it seems not to be possible to calculate a quasi-steady solution for  $\Theta$  with an underlying lubrication approximation.

## 4.1 Thermal boundary conditions

To solve the nonisothermal problem we have additionally to fix thermal boundary conditions.

### 4.1.1 Dimensional formulation

For the analytical solution for the nonisothermal problem we will use  $T = T_0$  as inflow condition and two boundary conditions of the third kind (see Carslaw & Jaeger [1]). At the inflow, the substrate and the l/g-interface we have

$$x = 0, z : \quad T = T_0 \quad , \quad (4.3)$$

$$x, z = 0 : \quad -h_l(T - T_\infty) = \lambda \frac{\partial T}{\partial \vec{n}} \quad , \quad (4.4)$$

$$x, z = h(x, t) : \quad -h_u(T - T_\infty) = \lambda \frac{\partial T}{\partial \vec{n}} \quad . \quad (4.5)$$

Here  $h_l$  and  $h_u$  are the heat transfer coefficients at the substrate and at the l/g-interface. The boundary conditions (4.4, 4.5) are fairly general and include through variable  $h_i$  both, the isothermal and the adiabatic case.

### 4.1.2 Nondimensional formulation

It is useful to derive a nondimensional formulation of the thermal boundary conditions to recognize which terms are important and which terms can be neglected for simplicity. For the normal derivative

$$\frac{\partial T}{\partial \vec{n}} = \vec{n} \text{ grad } T \quad ,$$

we obtain

$$x, z = 0 : \quad \frac{\partial T}{\partial \vec{n}} = -T_z \quad , \quad (4.6)$$

$$x, z = h(x, t) : \quad \frac{\partial T}{\partial \vec{n}} = \frac{1}{\sqrt{1 + h_x^2}} (T_z - h_x T_x) \quad . \quad (4.7)$$

Substituting (4.6) and (4.7) in the boundary conditions (4.3-4.5) together with the scaling (2.17, 2.23) yields in the nondimensional formulation

$$X = 0, Z : \quad \Theta = 1 \quad , \quad (4.8)$$

$$X, Z = 0 : \quad \Theta = \frac{1}{Bi_l} \Theta_Z \quad , \quad (4.9)$$

$$X, Z = H(X, \tau) : \quad \Theta = -\frac{1}{Bi_u} \frac{1}{\sqrt{1 + \epsilon^2 H_X^2}} (\Theta_Z - \epsilon^2 H_X \Theta_X) \quad . \quad (4.10)$$

In nondimensional form the heat transfer at both interfaces is encoded in the Biot numbers

$$Bi_l = \frac{h_l h_0}{\lambda} \quad , \quad (4.11)$$

$$Bi_u = \frac{h_u h_0}{\lambda} \quad . \quad (4.12)$$

Using equation (2.13),

$$\epsilon = \frac{h_0}{l_0} \ll 1 \quad ,$$

we find in a leading order

$$X = 0, Z : \quad \Theta = 1 \quad , \quad (4.13)$$

$$X, Z = 0 : \quad \Theta = \frac{1}{Bi_l} \Theta_Z \quad , \quad (4.14)$$

$$X, Z = H(X, \tau) : \quad \Theta = -\frac{1}{Bi_u} \Theta_Z \quad . \quad (4.15)$$

This is the approximated form of the thermal boundary conditions, valid within the lubrication approximation ( $\epsilon \ll 1$ ).

## 4.2 Matched asymptotic representation - heat losses at the substrate

Figure 4.1 shows typical profiles for the velocity  $U$  and the temperature  $\Theta$  for the spreading of a melt with a high Prandtl number. We have a outer region where  $\Theta$  is equal to the initial temperature  $\Theta_0 = 1$ . Only within a thin thermal boundary layer  $\delta_{th} \ll h_0$  we have a balance between heat transport due to convection and conduction.

Given the quasi-steady state approximation (4.2), the energy equation (2.12) reads

$$\epsilon RePr (U \Theta_X + W \Theta_Z) = \Theta_{ZZ} \quad ,$$

$$\epsilon RePr \gg 1 \quad .$$

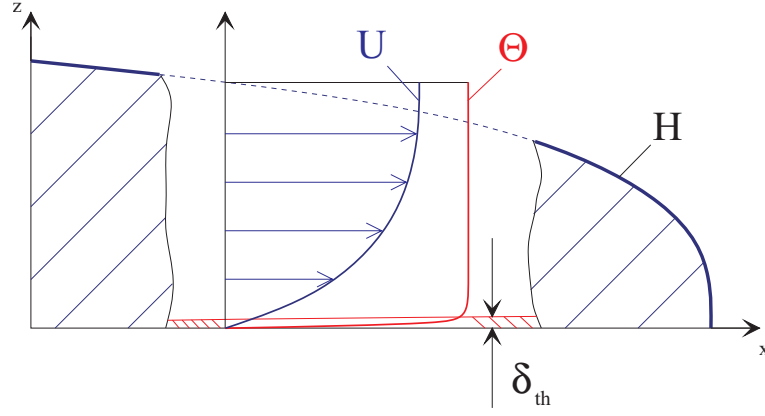


Figure 4.1: Sketch for spreading flows of high Prandtl number melts.

For the problem with heat losses at the perfectly conducting substrate and an adiabatic  $l/g$ -interface we have  $Bi_l \rightarrow \infty$ ,  $Bi_u \rightarrow 0$  and, thus, the thermal boundary conditions (4.13-4.15) simplify to

$$X = 0, Z : \quad \Theta = 1 \quad , \quad (4.16)$$

$$X, Z = 0 : \quad \Theta = 0, \quad , \quad (4.17)$$

$$X, Z = H(X, \tau) : \quad \Theta_Z = 0 \quad . \quad (4.18)$$

#### 4.2.1 Outer solution

Within the outer region we have

$$U\Theta_X + W\Theta_Z = 0 \quad .$$

Together with the boundary conditions (4.16) and (4.18) we obtain the outer solution

$$\Theta = \Theta_0 = 1 \quad . \quad (4.19)$$

#### 4.2.2 Inner solution

Inside the thermal boundary layer we have to keep the conductive term, i.e. we have

$$\epsilon Re Pr (U\Theta_X + W\Theta_Z) = \Theta_{ZZ} \quad . \quad (4.20)$$

As we expect a balance between convection and conduction, the scaling of equation (4.20) cannot be suitable. In particular,  $h_0$  is not the adequate length scale to describe the processes within the thermal boundary layer. We introduce rescaled coordinates  $\hat{X}, \hat{Z}$  to obtain a correct description of the physics close to the substrate. We introduce the modified length scales

$$\hat{X} = X \quad , \quad \hat{Z} = \frac{h_0}{\delta_{th}} Z \quad ,$$

where  $\delta_{th}$  is the thermal boundary layer thickness. For the velocities we introduce formally

$$\hat{U} = \frac{U}{U_0} \quad , \quad \hat{W} = \frac{W}{W_0} \quad .$$

From the continuity equation (2.39) we obtain

$$U_0 \hat{U}_{\hat{X}} + \frac{W_0}{\delta_{th}/h_0} \hat{W}_{\hat{Z}} = 0 \quad .$$

Assuming that  $U$  is a linear function in  $Z$  across the thermal boundary layer we take  $U_0 = \delta_{th}/h_0$  as a horizontal velocity scale. From the continuity equation we infer  $W_0 = (\delta_{th}/h_0)^2$  and summarize the rescaling to be

$$\hat{X} = X \quad , \quad (4.21)$$

$$\hat{Z} = \frac{h_0}{\delta_{th}} Z \quad , \quad (4.22)$$

$$\hat{U} = \frac{h_0}{\delta_{th}} U \quad , \quad (4.23)$$

$$\hat{W} = \left( \frac{h_0}{\delta_{th}} \right)^2 W \quad . \quad (4.24)$$

Substituting the new variables (4.21-4.24) into the energy equation (4.20) yields

$$\epsilon RePr \frac{\delta_{th}}{h_0} \left( \hat{U} \hat{\Theta}_{\hat{X}} + \hat{W} \hat{\Theta}_{\hat{Z}} \right) = \left( \frac{h_0}{\delta_{th}} \right)^2 \hat{\Theta}_{\hat{Z}\hat{Z}} \quad . \quad (4.25)$$

From equation (4.25), if a balance of convective and conductive transport is to be maintained, the factors have to be of the same order of magnitude, i.e.

$$\epsilon RePr \frac{\delta_{th}}{h_0} \sim \left( \frac{h_0}{\delta_{th}} \right)^2 \quad . \quad (4.26)$$

Thus, the thermal boundary layer thickness  $\delta_{th}$  can be estimated to be

$$\delta_{th} \sim \frac{h_0}{(\epsilon RePr)^{1/3}} \quad . \quad (4.27)$$

Equation (4.27) yields a first idea for the influence of nonisothermal effects within spreading problems of high Prandtl number melts. We choose  $\delta_{th} = h_0/(\epsilon Re Pr)^{1/3}$  and obtain

$$\hat{U}\hat{\Theta}_{\hat{X}} + \hat{W}\hat{\Theta}_{\hat{Z}} = \hat{\Theta}_{\hat{Z}\hat{Z}} \quad . \quad (4.28)$$

The boundary conditions are

$$\hat{X} = 0, \hat{Z} : \quad \hat{\Theta} = 1 \quad , \quad (4.29)$$

$$\hat{X}, \hat{Z} = 0 : \quad \hat{\Theta} = 0 \quad , \quad (4.30)$$

$$\hat{X}, \hat{Z} \rightarrow \infty : \quad \hat{\Theta} = 1 \quad . \quad (4.31)$$

For the streamfunction in rescaled coordinates we obtain,

$$\hat{\Psi} = \frac{\epsilon Re}{6 Fr} \left( \frac{\delta_{th}}{h_0} \right)^2 \hat{H}_{\hat{X}} \hat{Z}^2 (\hat{Z} - 3\hat{H}) \quad . \quad (4.32)$$

As we have a thin thermal boundary layer, we can simplify the convective terms within the heat transport equation by a Taylor-expansion of  $\hat{\Psi}$  around  $Z = 0$ . The streamfunction, thus, can be approximated by

$$\hat{\Psi} \simeq \hat{\Psi}|_{\hat{Z}=0} + \hat{Z} \cdot \hat{\Psi}_{\hat{Z}}|_{\hat{Z}=0} + \frac{\hat{Z}^2}{2} \cdot \hat{\Psi}_{\hat{Z}\hat{Z}}|_{\hat{Z}=0} \quad .$$

With

$$\hat{U} = \hat{\Psi}_{\hat{Z}} \quad , \quad \hat{W} = -\hat{\Psi}_{\hat{X}} \quad ,$$

the approximations for the velocities  $\hat{U}, \hat{W}$  are

$$\hat{U} \simeq -\frac{\epsilon Re}{Fr} \left( \frac{\delta_{th}}{h_0} \right)^2 \hat{H} \hat{H}_{\hat{X}} \hat{Z} \quad , \quad (4.33)$$

$$\hat{W} \simeq \frac{\epsilon Re}{Fr} \left( \frac{\delta_{th}}{h_0} \right)^2 \frac{\hat{Z}^2}{2} (\hat{H}_{\hat{X}}^2 + \hat{H} \hat{H}_{\hat{X}\hat{X}}) \quad . \quad (4.34)$$

Substituting the velocities (4.33) and (4.34) into the energy equation (4.28) yields

$$\frac{\epsilon Re}{Fr} \left( \frac{\delta_{th}}{h_0} \right)^2 \hat{Z} \left( -\hat{H} \hat{H}_{\hat{X}} \hat{\Theta}_{\hat{X}} + \frac{1}{2} (\hat{H} \hat{H}_{\hat{X}})_{\hat{X}} \hat{Z} \hat{\Theta}_{\hat{Z}} \right) = \hat{\Theta}_{\hat{Z}\hat{Z}} \quad . \quad (4.35)$$

We introduce a new function

$$f(\hat{X}, \tau) = -\hat{H} \hat{H}_{\hat{X}} \quad , \quad (4.36)$$

which allows to simplify the energy equation (4.35), i.e. we have

$$\frac{\epsilon Re}{Fr} \left( \frac{\delta_{th}}{h_0} \right)^2 \hat{Z} \left( f \hat{\Theta}_{\hat{X}} - \frac{1}{2} f_{\hat{X}} \hat{Z} \hat{\Theta}_{\hat{Z}} \right) = \hat{\Theta}_{\hat{Z}\hat{Z}} \quad . \quad (4.37)$$

We assume a solution in similarity form. Thus, a similarity variable

$$\eta = \frac{\hat{Z}}{k(\hat{X})} \quad (4.38)$$

and a shape function

$$\hat{\Theta} = F(\eta) \quad (4.39)$$

is introduced to yield

$$F_{\eta\eta} + \underbrace{\frac{\epsilon Re}{Fr} \left(\frac{\delta_{th}}{h_0}\right)^2 \left(\frac{1}{2}k^3 f_{\hat{X}} + f k^2 k_{\hat{X}}\right)}_{C_F} \eta^2 F_{\eta} = 0 \quad . \quad (4.40)$$

The boundary conditions (4.30, 4.31) in similarity form are given by

$$\eta = 0 : F = 0 \quad , \quad (4.41)$$

$$\eta \rightarrow \infty : F = 1 \quad . \quad (4.42)$$

The reduction to an ordinary differential equation is only possible if the bracket is a constant.

With the choice

$$C_F = 1 \quad ,$$

we use

$$\frac{\epsilon Re}{Fr} \left(\frac{\delta_{th}}{h_0}\right)^2 \left(\frac{1}{2}k^3 f_{\hat{X}} + f k^2 k_{\hat{X}}\right) = 1 \quad , \quad (4.43)$$

to determine the function  $k$ . The solution is

$$k(\hat{X}, \tau) = \left(\frac{3Fr}{\epsilon Re} \left(\frac{h_0}{\delta_{th}}\right)^2\right)^{1/3} \left(\frac{C + \int \sqrt{f} d\hat{X}}{f^{3/2}}\right)^{1/3} \quad . \quad (4.44)$$

To fulfill boundary condition (4.29), we impose

$$\hat{X} = 0 : k = 0 \quad .$$

This inflow condition allows to fix the constant  $C$  in equation (4.44) and, thus, we have

$$k(\hat{X}, \tau) = \left(\frac{3Fr}{\epsilon Re} \left(\frac{h_0}{\delta_{th}}\right)^2\right)^{1/3} \left(\frac{\int_0^{\hat{X}} \sqrt{f(\hat{X}^*)} d\hat{X}^*}{f^{3/2}}\right)^{1/3} \quad . \quad (4.45)$$

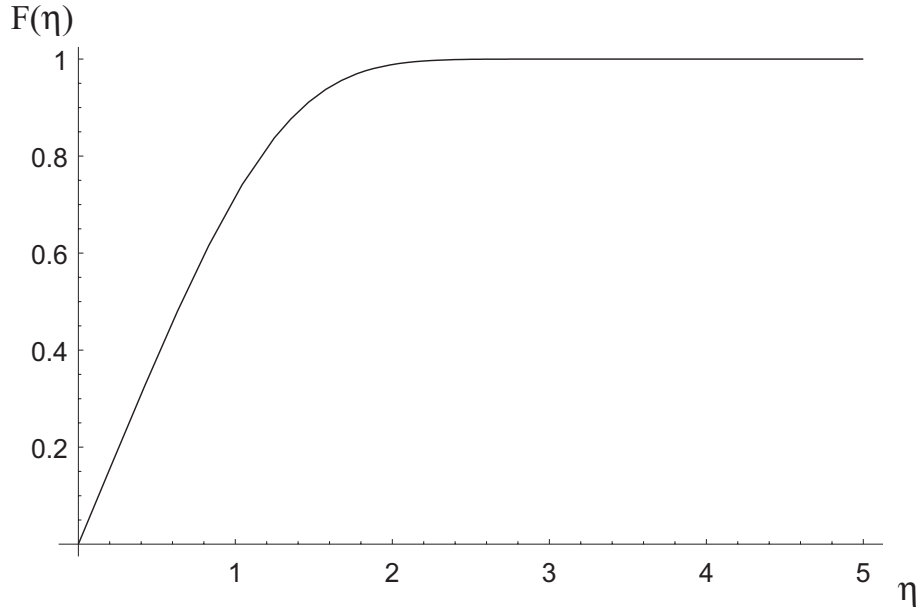


Figure 4.2: Solution for  $F(\eta)$ .

Substituting (4.45) into (4.38) yields for the similarity variable

$$\eta = \left( \frac{\epsilon Re}{3Fr} \left( \frac{\delta_{th}}{h_0} \right)^2 \right)^{1/3} \hat{Z} \left( \frac{\int_0^{\hat{X}} \sqrt{f(\hat{X}^*)} d\hat{X}^*}{f^{3/2}} \right)^{-1/3}. \quad (4.46)$$

The energy equation (4.37) now simplifies due to the similarity transformation. We obtain

$$F_{\eta\eta} + \eta^2 F_\eta = 0$$

and, applying the boundary conditions (4.41, 4.42), the solution is

$$F(\eta) = 1 - \frac{(1/3, \eta^3/3)}{(1/3)}. \quad (4.47)$$

The solution (4.47) is plotted in figure 4.2. Table 4.1 summarizes the similarity transformation.

energy equation:

$$\frac{\epsilon Re}{Fr} \left( \frac{\delta_{th}}{h_0} \right)^2 \hat{Z} \left( -\hat{H} \hat{H}_{\hat{X}} \hat{\Theta}_{\hat{X}} + \frac{1}{2} (\hat{H} \hat{H}_{\hat{X}})_{\hat{X}} \hat{Z} \hat{\Theta}_{\hat{Z}} \right) = \hat{\Theta}_{\hat{Z} \hat{Z}}$$

simplified energy equation:

$$\frac{\epsilon Re}{Fr} \left( \frac{\delta_{th}}{h_0} \right)^2 \hat{Z} \left( f \hat{\Theta}_{\hat{X}} - \frac{1}{2} f_{\hat{X}} \hat{Z} \hat{\Theta}_{\hat{Z}} \right) = \hat{\Theta}_{\hat{Z} \hat{Z}}$$

with

$$f = -\hat{H} \hat{H}_{\hat{X}}$$

similarity variable:

$$\eta = \left( \frac{\epsilon Re}{3Fr} \left( \frac{\delta_{th}}{h_0} \right)^2 \right)^{1/3} \hat{Z} \left( \frac{\int_0^{\hat{x}} \sqrt{f(\hat{x}^*)} d\hat{x}^*}{f^{3/2}} \right)^{-1/3}$$

solution:

$$\hat{\Theta} = F(\eta) = 1 - \frac{(1/3, \eta^3/3)}{(1/3)}$$

Table 4.1: Summary of the similarity transformation - heat losses at the substrate.

### 4.3 Numerical solution of the temperature field

The asymptotic solution of the energy equation (2.12) is restricted to cases, where  $\epsilon RePr \gg 1$  is valid, i.e. for spreading flows with thin thermal boundary layers. A more general solution can be obtained via a numerical solution. The energy equation (2.12) together with the quasi-steady approximation (4.2) yields

$$\epsilon RePr(U\Theta_X + W\Theta_Z) = \Theta_{ZZ} \quad . \quad (4.48)$$

Furthermore, a numerical solution allows the treatment of more general boundary conditions at the l/g-interface and at the substrate. The quasi-steady approximation reduces the independent variables to  $X$  and  $Z$ . Thus, we have to solve a two dimensional problem.

#### 4.3.1 Transformation $(X, Z) \rightarrow (\xi, \zeta)$

Similar to the numerical solution of  $H(X, \tau)$  in section 3.2.3, the moving contact line  $A(\tau)$  requires a moving mesh for the numerical solution of  $\Theta$  in  $X, Z$ -coordinates. Furthermore, the upper boundary at  $Z = H(X, \tau)$  varies in time and space. Thus, we introduce new variables

$$\xi = \frac{X}{A(\tau)} \quad , \quad (4.49)$$

$$\zeta = \frac{Z}{H(X, \tau)} \quad . \quad (4.50)$$

The transformation is valid for  $\tau > 0$  and  $X < A(\tau)$ , as  $A(0) \rightarrow 0$  and  $H(A, \tau) = 0$ . This allows a solution on a rectangular domain as shown in figure 4.3. The spatial derivatives can be expressed using the new variables,

$$\begin{aligned} \frac{\partial}{\partial X} &= \frac{1}{A} \frac{\partial}{\partial \xi} - \zeta \frac{H_\xi}{AH} \frac{\partial}{\partial \zeta} \quad , \\ \frac{\partial}{\partial Z} &= \frac{1}{H} \frac{\partial}{\partial \zeta} \quad . \end{aligned}$$

Substituting the velocities (3.2, 3.3) and the new variables (4.49, 4.50) into the energy equation (4.48) yields

$$\frac{(\epsilon Re)^2 Pr}{Fr A^2} \left\{ H^4 H_\xi \left( \frac{\zeta^2}{2} - \zeta \right) \Theta_\xi + \frac{1}{6} H^3 \zeta^2 (3 - \zeta) \left( 3H_\xi^2 + HH_{\xi\xi} \right) \Theta_\zeta \right\} = \Theta_{\zeta\zeta} \quad . \quad (4.51)$$

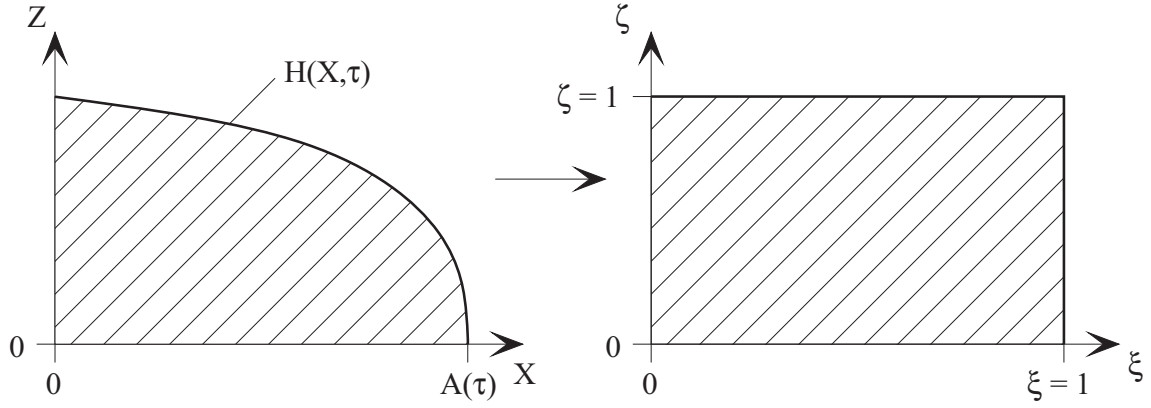


Figure 4.3: Transformation of coordinates  $(X, Z) \rightarrow (\xi, \zeta)$ .

### 4.3.2 Method of lines for the transformed energy equation

As shown in section 3.2.3.2 the method of lines can be used to discretize the equations. Thus, standard methods for the numerical integration may be employed. To resolve the thin thermal boundary layer,  $\epsilon RePr \gg 1$ , we employ a non-uniform spacing

$$\Delta\zeta_j = \zeta_j - \zeta_{j-1} \quad , \quad j = 1, \dots, j_{max} \quad , \quad (4.52)$$

as shown in figure 4.4.

This yields an approximation

$$\Theta_j \simeq \Theta(\xi, \zeta_j) \quad , \quad (4.53)$$

at discrete values of  $\zeta = \zeta_j$ . Due to a singularity at  $\xi = 1$ , where  $\zeta$  is not defined, we restrict the integration to the semi open interval  $\xi \in [0, 1[$ . We employ central differences for both the first derivative

$$\Theta_\zeta(\xi, \zeta_i) \simeq \frac{\Theta_{j+1} - \Theta_{j-1}}{\Delta\zeta_{j+1} + \Delta\zeta_j} \quad , \quad j = 1, \dots, j_{max} - 1 \quad (4.54)$$

and the second derivative

$$\Theta_{\zeta\zeta}(\xi, \zeta_i) \simeq 2 \frac{\Delta\zeta_j \Theta_{j+1} - (\Delta\zeta_{j+1} + \Delta\zeta_j) \Theta_j + \Delta\zeta_{j+1} \Theta_{j-1}}{\Delta\zeta_{j+1} \Delta\zeta_j (\Delta\zeta_{j+1} + \Delta\zeta_j)} \quad , \quad j = 1, \dots, j_{max} - 1 \quad , \quad (4.55)$$

in equation (4.51). The discrete formulation of the energy equation consists of a system of  $(j_{max} - 1)$  coupled ordinary differential equations at discrete values  $\zeta_j$ , subject to boundary conditions at  $\zeta_0$  and  $\zeta_{j_{max}}$ . The boundary conditions depend on the heat transfer conditions at the l/g-interface and at the substrate.

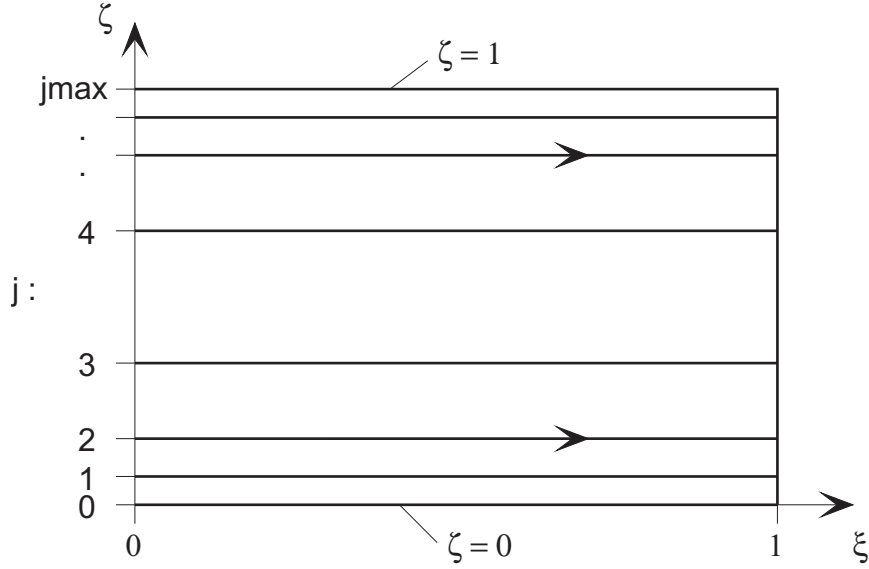


Figure 4.4: Sketch of the method of lines for  $\Theta(\xi, \zeta)$ .

### 4.3.3 Initial and boundary conditions - heat losses at the substrate

For the case of an adiabatic l/g-interface we have the thermal boundary conditions similar to those in section 4.2. Introducing the new variables (4.49-4.50) into the boundary conditions (4.16-4.18) yields

$$\xi = 0, \zeta : \quad \Theta = 1 \quad , \quad (4.56)$$

$$\xi, \zeta = 0 : \quad \Theta = 0, \quad , \quad (4.57)$$

$$\xi, \zeta = 1 : \quad \Theta_{\zeta} = 0 \quad . \quad (4.58)$$

Using a backward difference for  $j = j_{max}$

$$\Theta_{\xi}(\xi, 1) \simeq \frac{\Delta\zeta_j^2 \Theta_{j-2} - (\Delta\zeta_j + \Delta\zeta_{j-1})^2 \Theta_{j-1} + \Delta\zeta_{j-1} (2\Delta\zeta_j + \Delta\zeta_{j-1}) \Theta_j}{\Delta\zeta_j \Delta\zeta_{j-1} (\Delta\zeta_j + \Delta\zeta_{j-1})} \quad ,$$

results in conjunction with equation (4.58)

$$\Theta(\xi, 1) \simeq \frac{(\Delta\zeta_j + \Delta\zeta_{j-1})^2 \Theta_{j-1} - \Delta\zeta_j^2 \Theta_{j-2}}{\Delta\zeta_{j-1} (2\Delta\zeta_j + \Delta\zeta_{j-1})} \quad , \quad j = j_{max} \quad . \quad (4.59)$$

## 4.4 Results

### 4.4.1 Matched asymptotic solution

In section 4.2 we have obtained the similarity solution

$$F(\eta) = 1 - \frac{(1/3, \eta^3/3)}{(1/3)}$$

for the temperature field within the thermal boundary layer. Using the backward transformation (4.21, 4.22) yields the temperature field in  $X, Z, \tau$ -coordinates. For the similarity variable we obtain

$$\eta = \left( \frac{(\epsilon Re)^2 Pr}{3Fr} \frac{(-HH_X)^{3/2} Z^3}{\int_0^X \sqrt{-HH_X} dX^*} \right)^{1/3} .$$

At this point we can make use of an approximation for  $H(X, \tau)$  (cf. section 3.2.2.3). Using  $\xi = X/A(\tau)$  yields

$$\eta = \left( \frac{(\epsilon Re)^2 Pr}{3FrA^2} \frac{(-HH_\xi)^{3/2} Z^3}{\int_0^\xi \sqrt{-HH_\xi} d\xi^*} \right)^{1/3} .$$

Solutions of the form

$$H = C_1 \tau^{(2\alpha-1)/5} \underbrace{c(1-\xi)^b}_{\tilde{H}} ,$$

allow to evaluate the integral. Thus, we find the analytical expression

$$\eta = \left( \frac{(\epsilon Re)^2 Pr}{3FrA^2} \frac{b(1+2b)c^2 C_1^2 (1-\xi)^{3(b-1/2)} \tau^{6/15(2\alpha-1)} Z^3}{1 - (1-\xi)^{1/2+b}} \right)^{1/3} . \quad (4.60)$$

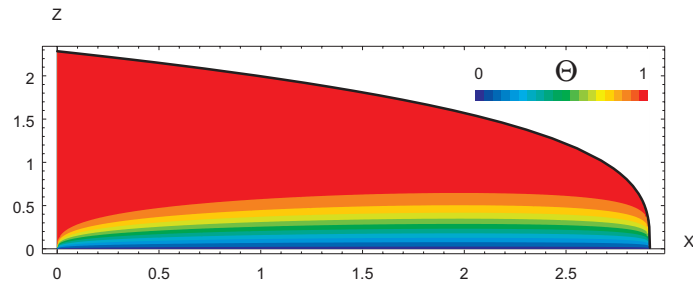
For general functions  $H$  we have to evaluate the integral numerically. Thus, we have only a numerical representation of  $\eta$  and cannot obtain an analytical solution. For the subsequent results we use the approximation from the weighted residual method (3.51) for  $\tilde{H}$ , whereas the constants  $b, c$  are given by

$$b = \frac{4\alpha - 2 + \sqrt{9 + \alpha(44 + 151\alpha)}}{5 + 45\alpha} ,$$

$$c = \left( \frac{-347\alpha^2 + 42\alpha - 3 + (1 + 53\alpha)\sqrt{9 + \alpha(44 + 151\alpha)}}{50(1 + 3\alpha)} \right)^{1/3}$$

Figures 4.5-4.7 show temperature fields for  $\alpha = 1, 7/4, 2$  at  $\tau = 5$  and  $\tau = 20$  computed based on equation (4.60).

$\tau = 5$



$\tau = 20$

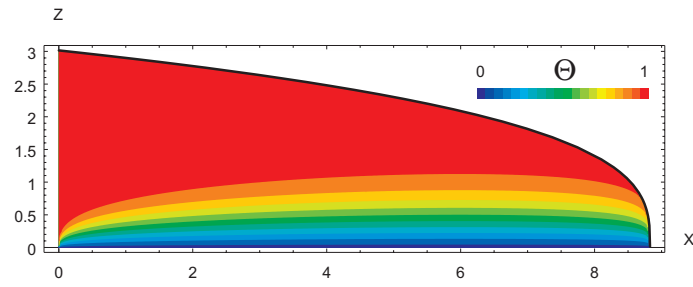
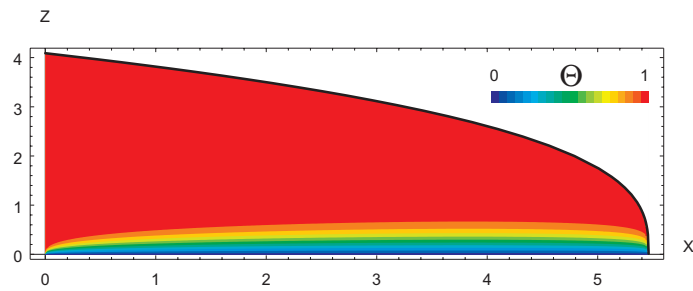


Figure 4.5: Temperature field - similarity solution,  $\alpha = 1$ ,  $\epsilon = 0.01$ ,  $Re = 1$ ,  $Fr = 0.01$ ,  $C_V = 1$ ,  $Pr = 10000$ .

$\tau = 5$



$\tau = 20$

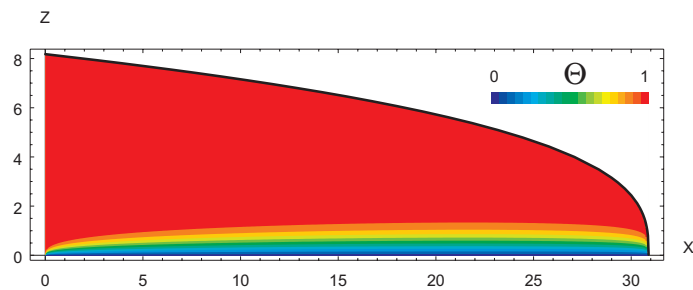
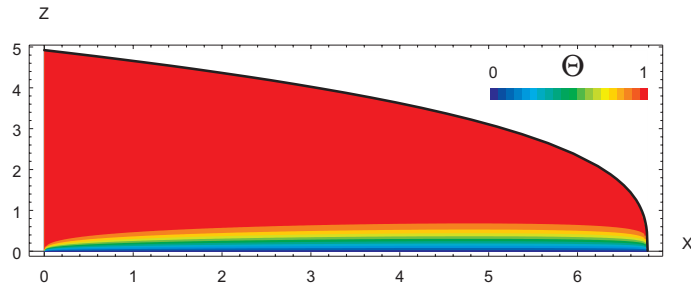


Figure 4.6: Temperature field - similarity solution,  $\alpha = 7/4$ ,  $\epsilon = 0.01$ ,  $Re = 1$ ,  $Fr = 0.01$ ,  $C_V = 1$ ,  $Pr = 10000$ .

$$\tau = 5$$



$$\tau = 20$$

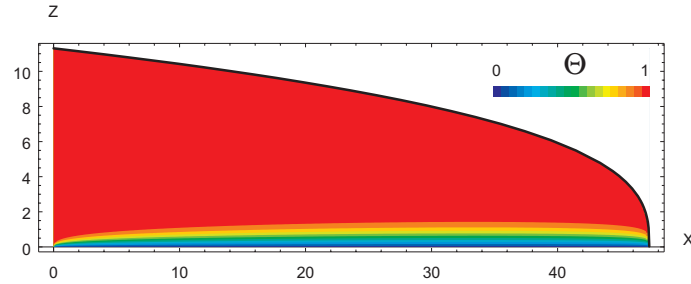
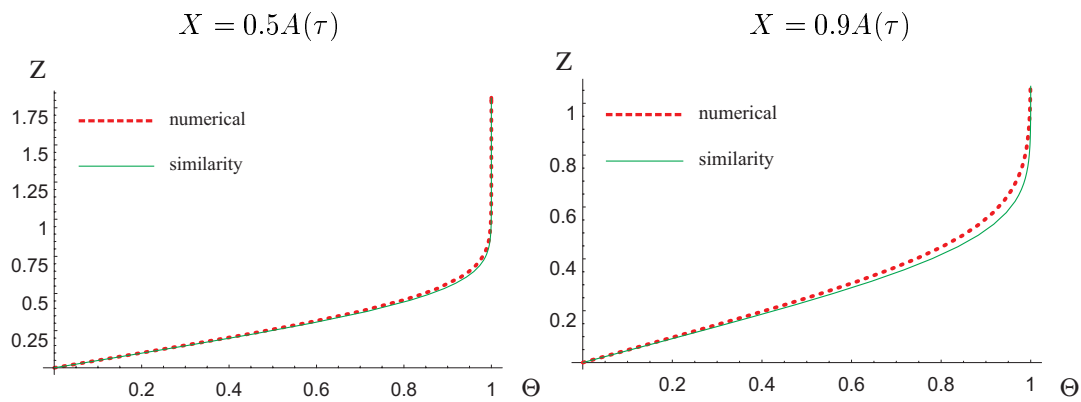


Figure 4.7: Temperature field - similarity solution,  $\alpha = 2$ ,  $\epsilon = 0.01$ ,  $Re = 1$ ,  $Fr = 0.01$ ,  $C_V = 1$ ,  $Pr = 10000$ .

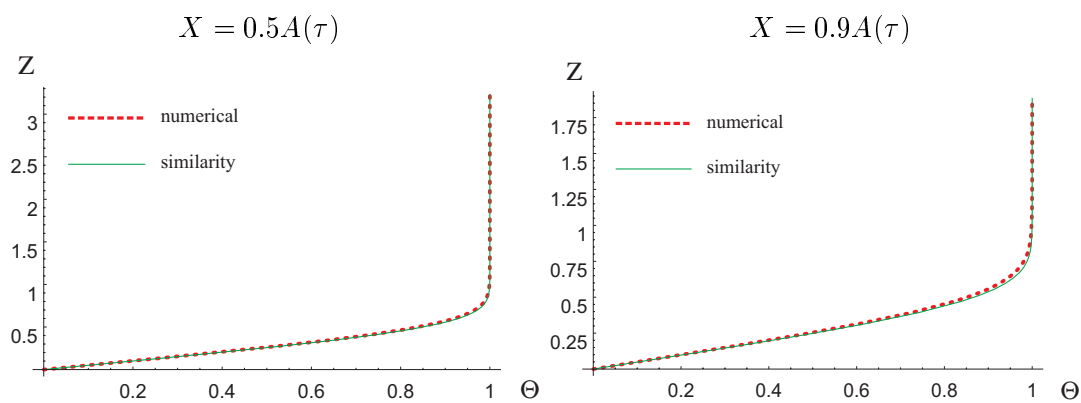
#### 4.4.2 Comparison matched asymptotic solution - numerical solution

Figure 4.8 shows vertical temperature profiles for  $\alpha = 1, 7/4, 2$  at  $\tau = 5$  calculated either by the similarity transformation (section 4.2), or by numerical integration (section 4.3). The agreement of both solutions is good. The similarity solution in all cases underpredicts slightly the thickness of the thermal boundary layer. Due to the Taylor-expansion of the velocities, equation (4.33, 4.34), we overestimate the convective heat transport with increasing boundary layer thickness. As shown in figure 4.8 this deviation is small and the model will improve for increasing Prandtl numbers  $Pr$ . Close to the contact line at  $X = 0.9A(\tau)$  the influence of the boundary condition  $\Theta_Z = 0$  at the upper boundary  $Z = H(X, \tau)$  leads to small differences. For the similarity solution we locate the upper boundary at  $\eta \rightarrow \infty$ , i.e. we match the inner solution to the semi-infinite outer region. At the contact line the thickness of the liquid, and thus of the outer region tends to zero. As the semi-infinite assumption is violated, the thermal boundary condition  $\Theta_Z = 0$  at the l/g-interface is not fulfilled in this case.

$\alpha = 1$



$\alpha = 7/4$



$\alpha = 2$

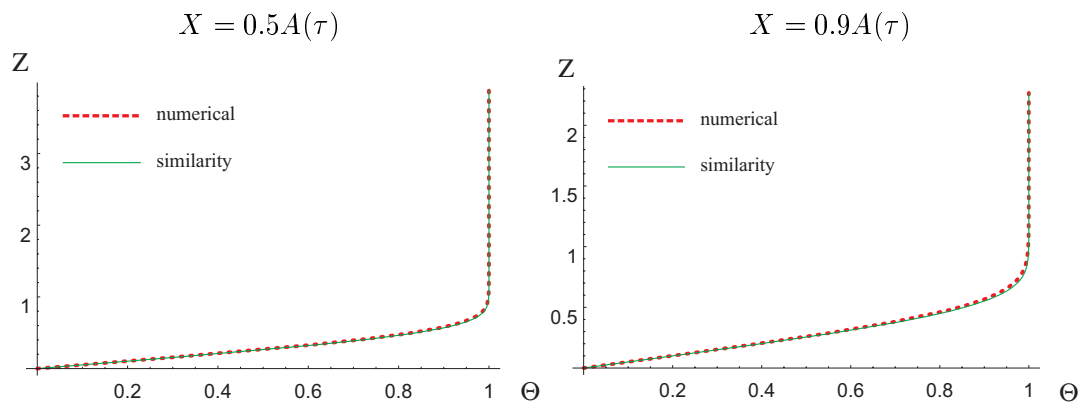


Figure 4.8: Comparison of the similarity solution and the numerical solution for  $\Theta$ ,  $\epsilon = 0.01$ ,  $Re = 1$ ,  $Fr = 0.01$ ,  $C_V = 1$ ,  $Pr = 10000$ ,  $\tau = 5$ .

### 4.4.3 Estimation of the quasi-steady approximation

For nuclear safety purposes the quasi-steady approximation (4.2) will be 'conservative' in that way that it leads to a 'worst-case approximation', i.e. we expect the strongest possible influence of the temperature field onto the spreading process. To evaluate this approximation, we try to find an estimation for the importance of the transient term  $\Theta_\tau$ .

For a more accurate description of the thermal field we introduce a modified similarity variable

$$\eta_t = C_{m\eta} \eta_{qs} \quad . \quad (4.61)$$

Substituting the similarity solution (4.47)

$$\Theta = F(\eta_t) \quad , \quad (4.62)$$

into the transient energy equation (2.12) in conjunction with a weighted residual method allows to minimize the integral error. This procedure will not give the correct solution for the temperature field, but we obtain an estimation of the transient effects onto the thickness of the thermal boundary layer.

For the calculation of  $C_{m\eta}$  we use

$$\int_0^A \int_0^H R dZ dX = 0 \quad , \quad (4.63)$$

together with the residuum of equation (2.12), i.e.

$$R = \epsilon Re Pr (\Theta_\tau + U\Theta_X + W\Theta_Z) - \Theta_{ZZ} \quad . \quad (4.64)$$

Figure 4.9 shows the residuum profile  $R/R_0$  for different values of  $C_{m\eta}$ . For  $C_{m\eta} \simeq 1.2$  the amplitude of  $R$  is about 40% of the amplitude of the quasi-steady solution ( $C_{m\eta} = 1$ ). Moreover, it is obvious, that the integral of  $R$  is zero for  $C_{m\eta} \simeq 1.2$ . The values of  $C_{m\eta}$ , which minimize the integral error of the residuum (cf. equation (4.63)) are plotted in figure 4.10. For all values  $\alpha$ ,  $C_{m\eta}$  approaches a constant value for  $\tau \gg 1$ . For  $\alpha = 1$  the necessary correction of the quasi-steady solution is less than 20%. Thus, the quasi-steady description of the temperature field remains a reasonable approximation.

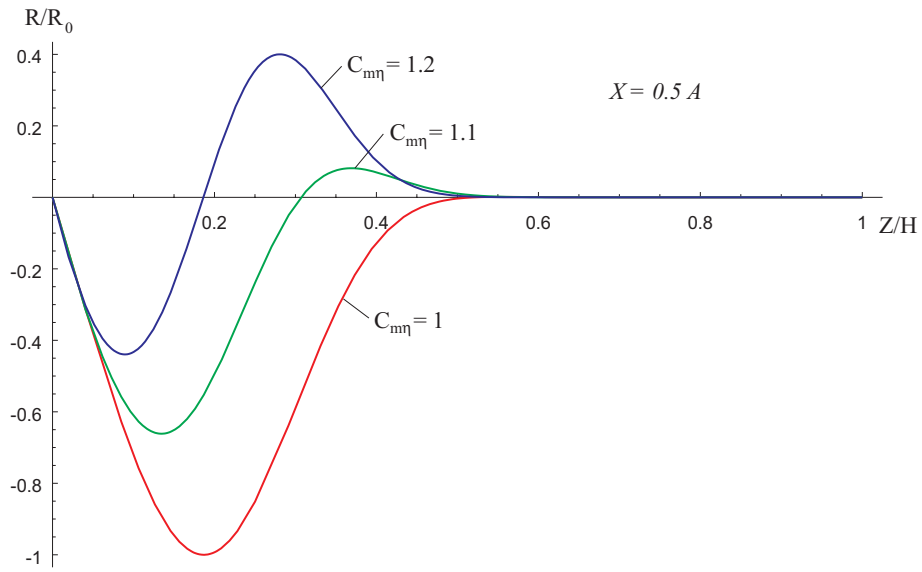


Figure 4.9: Residuum  $R/R_0$  at  $X = 0.5A(\tau)$ ,  $\alpha = 1$ ,  $\tau = 5$ ,  $Pr = 10000$ .

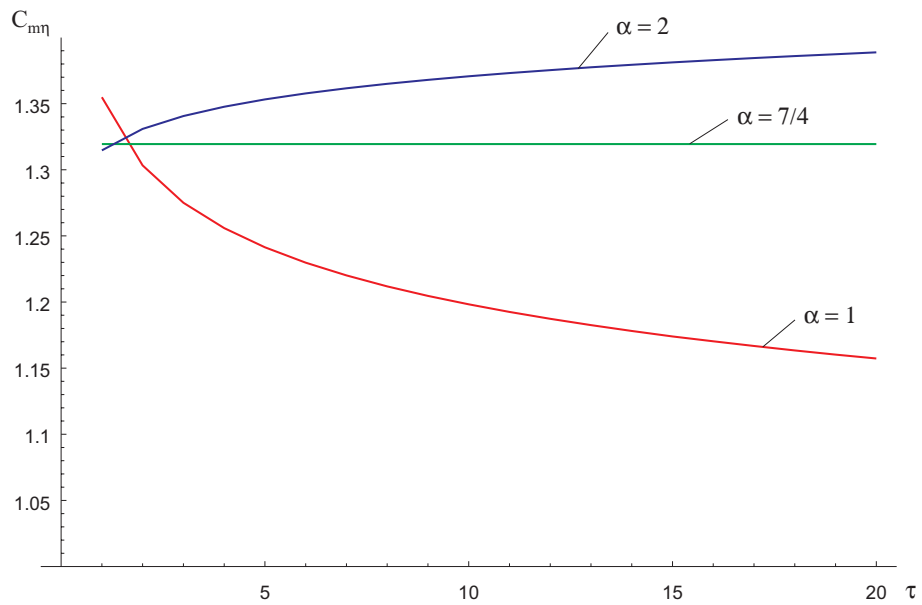


Figure 4.10: Value of  $C_{m\eta}$ ,  $\alpha = 1, 7/4, 2$ ,  $Pr = 10000$ .

# Chapter 5

## Modeling bottom crusting

### 5.1 Basic idea

For melts with a high Prandtl number we can expect thin thermal boundary layers and, therefore, thin solidified regions. Thus, solidification should have a weak influence onto the spreading process. Given thin bottom crusts, we attempt to solve for the flow and temperature field successively to avoid the fully-coupled problem, which mathematically appears much more difficult. Such a method should be adequate as long as the coupling between the kinematics and the thermal field is weak. This is the case for  $Pr \gg 1$ .

The influence of the bottom crust onto the spreading flow can be captured by successively performing the following steps:

1. We infer a solution for the flow field of the isothermal spreading problem. Here no influence of solidification occurs. This problem has been solved previously by Huppert [3].
2. Based on the above flow field we solve for the temperature field, employing a similarity transformation.
3. Given the thermal field, we determine the position of the s/l-interface  $S(X, \tau)$ . Here, we use the condition  $\Theta = \Theta_S$ , where  $\Theta_S$  is the dimensionless solidification temperature, to find  $S(X, \tau)$ . As the s/l-interface follows the solidification isotherm, we neglect the liberation of latent heat. This is a reasonable approximation for low solidification speed or fluids which solidify without crystallization (cf. Fink & Griffiths [2]).

4. We impose the no-slip condition at the s/l-interface  $S(X, \tau)$  and solve again the spreading problem on top of the crust. Thus, we obtain a first approximation for the kinematic influence of the bottom crust.
5. We infer an improved temperature field, which includes both, the flow field in presence of the crust and heat conduction within the crust.
6. Based on this improved temperature field, we infer an improved crust  $S_2(X, \tau)$  at the solidification isotherm  $\Theta = \Theta_S$ . From

$$E = \frac{S_2(X, \tau)}{S_1(X, \tau)} \quad (5.1)$$

we judge the quality of the model.

## 5.2 Position of the s/l-interface

Using the similarity solution for the thermal field, section 4.4.1, we have for the similarity variable

$$\eta = \eta_S = \left( \frac{(\epsilon Re)^2 Pr}{3Fr} \frac{(-HH_X)^{3/2} Z^3}{\int_0^X \sqrt{-HH_X} dX^*} \right)^{1/3} \quad (5.2)$$

to define the isotherm  $\Theta = \Theta_S$ .  $\eta_S$  corresponds to the value of the inverse solution of  $\Theta_S = F(\eta_S)$  (cf. equation (4.47)). Solving equation (5.2) for  $Z$  yields for the bottom crust

$$S(X, \tau) = \eta_S \left( \frac{3Fr}{(\epsilon Re)^2 Pr} \frac{\int_0^X \sqrt{-HH_X} dX^*}{(-HH_X)^{3/2}} \right)^{1/3}. \quad (5.3)$$

We shall see that the velocity field depends on both the function  $S$  and the derivative  $S_X$ . From equation (5.3) the derivative evaluates to

$$S_X(X, \tau) = \eta_S \left( \frac{3Fr}{(\epsilon Re)^2 Pr} \right)^{1/3} \frac{\left( 2 - \frac{3 \int_0^X \sqrt{-HH_X} dX^* (-H_X^2 - HH_{XX})}{(-HH_X)^{3/2}} \right)}{6 \left( \int_0^X \sqrt{-HH_X} dX^* \right)^{2/3}}.$$

Due to the lubrication approximation (cf. section 2.3)  $S_X$  exhibits a singularity as  $X \rightarrow 0$ . Thus, at  $X = 0$  we have  $S = 0$  and the fluid hits a solidified crust with a slope  $S_X \rightarrow \infty$ . This will lead to high velocities in the vertical direction which are unphysical. Based on the lubrication theory we have a balance of viscous and inertial forces. Hereby, the contribution from the vertical velocity  $W$  is neglected against the contribution from the

horizontal velocity  $U$ . To overcome this difficulty, we smooth the function  $S(X, \tau)$  at  $X = 0$ . Thus, we use

$$S(X, \tau) = \eta_S (1 - e^{-C_{mS} X/A(\tau)}) \left( \frac{3Fr}{(\epsilon Re)^2 Pr} \frac{\int_0^X \sqrt{-HH_X} dX^*}{(-HH_X)^{3/2}} \right)^{1/3}, \quad (5.4)$$

with  $C_{mS} \gg 1$ . The properties of this approach can be demonstrated by means of test-functions

$$H = (1 - X)^{1/3}, \quad A = 1,$$

which are typical for isothermal spreading flows (cf. section 3.3.1). Furthermore, we set

$$\eta_S \left( \frac{3Fr}{(\epsilon Re)^2 Pr} \right)^{1/3} = 1.$$

From definition (5.3), a Taylor series expansion yields the leading order approximation

$$X \rightarrow 0: \quad S \propto X^{1/3}, \quad S_X \propto X^{-2/3}.$$

The modified definition results in

$$X \rightarrow 0: \quad S \propto X^{4/3}, \quad S_X \propto X^{1/3}.$$

Thus, we have removed the singularity at  $X = 0$ .

In figure 5.1 the modification of the crust profile is shown for different values of  $C_{mS}$  close to  $X = 0$ . For  $C_{mS} \geq 500$  the influence is limited to a region  $0 \leq X \leq 0.01A(\tau)$ . In the limit  $C_{mS} \rightarrow \infty$  we recover the original, singular, crust profile based on equation (5.3). As the influence of the smoothing is present only in a narrow region, the main effect of the crust onto the spreading flow should be unaffected.

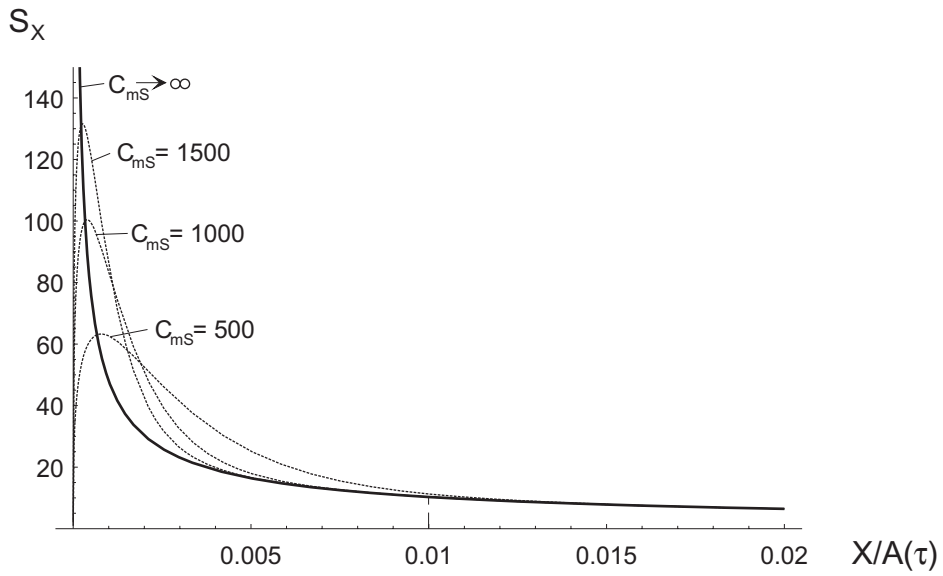
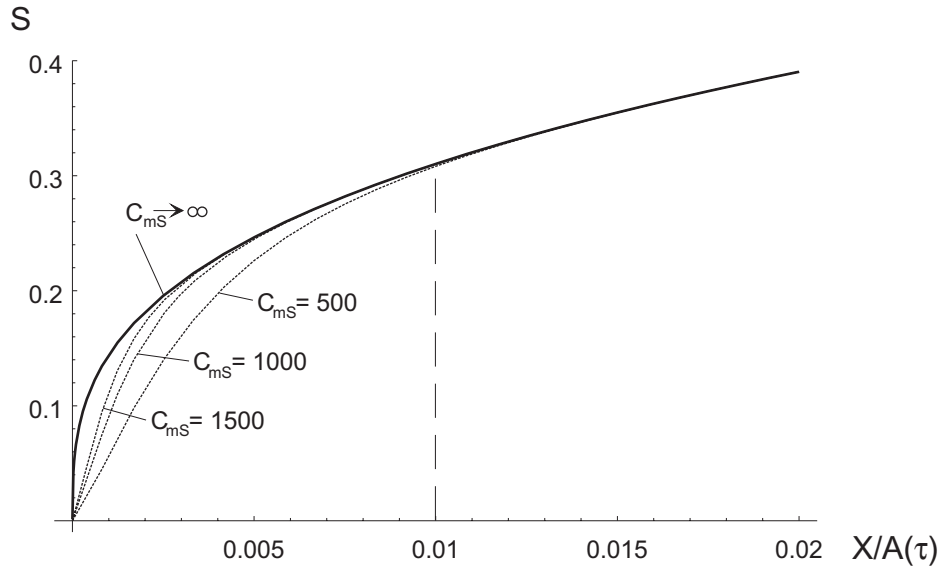


Figure 5.1: Crust  $S$  and derivative  $S_X$  based on equation (5.4), for different values of  $C_{mS}$  in the region  $0 \leq X \leq 0.02A(\tau)$ .

## Chapter 6

# Isothermal spreading - solidified crust at the bottom

### 6.1 Flow field with bottom crusting

#### 6.1.1 Boundary conditions

In section 2.3 we have formulated the boundary conditions for the spreading flow at  $S(X, \tau) = 0$  and  $H(X, \tau)$ . Due to solidification, we now have the no-slip condition at  $S(X, \tau)$ . Kinetically, the boundary conditions are

$$X, Z = S(X, \tau) : \quad U = W = 0 \quad , \quad (6.1)$$

$$X, Z = H(X, \tau) : \quad U_Z = 0 \quad , \quad (6.2)$$

$$W = H_X U + H_\tau \quad , \quad (6.3)$$

$$P = 0 \quad . \quad (6.4)$$

#### 6.1.2 Velocity and pressure field

The calculation of  $P$ ,  $U$ ,  $W$  and  $\Psi$  follows the course of section 3.1. The main difference is the no-slip condition (6.1) at  $S(X, \tau)$ . For the pressure  $P$  we obtain from equation (3.1)

$$P = \frac{\epsilon Re}{Fr} (H - Z) \quad . \quad (6.5)$$

Substituting  $P$  into equation (2.40) and integration with respect to  $Z$  yields

$$U = \frac{\epsilon Re}{2Fr}(Z - S)H_X (Z - 2H + S) \quad . \quad (6.6)$$

where the boundary conditions (6.1, 6.2) have been applied.

The continuity equation (2.39) together with the no-slip condition (6.1) results in the vertical velocity

$$W = -\frac{\epsilon Re}{6Fr}(Z - S) \left( 6(H - S)H_X S_X + (Z - S)(Z - 3H + 2S)H_{XX} - 3(Z - S)H_X^2 \right). \quad (6.7)$$

For the streamfunction we obtain

$$\Psi = \frac{\epsilon Re}{6Fr}(Z - S)^2(Z - 3H + 2S)H_X \quad . \quad (6.8)$$

## 6.2 Evolution equation for $H(X, \tau)$ - general formulation

Similar to section 3.2 we substitute the velocities  $U$  and  $W$  into the kinematic boundary condition (6.3) at the l/g-interface to derive an evolution equation for  $H$ , namely

$$H_\tau - \frac{\epsilon Re}{3Fr} \left( (H - S)^3 H_X \right)_X = 0 \quad . \quad (6.9)$$

As shown in section 3.2 it is possible to infer solutions to this nonlinear diffusion equation (6.9) either by a similarity transformation or by using numerical methods. The above evolution equation now includes the kinematic influence of the bottom crust  $S(X, \tau)$  onto the spreading flow.

## 6.3 Two strategies to formulate $S(X, \tau)$ - the weakly- and the fully-coupled problem

As shown in section 5.2 the bottom crust is a function of the l/g-interface position  $H(X, \tau)$ . Following our iterative scheme (cf. section 5.1) to model the influence of bottom crusting, we may express  $S(X, \tau)$  in two ways, based on two different degrees of approximation, namely  $H_0, H_1$ . Thus we have

### 1. the weakly-coupled problem

$$S_1(X, \tau) = f(H_0(X, \tau)) \quad . \quad (6.10)$$

### 2. the fully-coupled problem

$$S_1(X, \tau) = f(H_1(X, \tau)) \quad , \quad (6.11)$$

Figure 6.1 illustrates the characteristics of both approximations. While the fully-coupled problem takes into account that the crust depends on the unknown l/g-interface  $H_1(X, \tau)$ , which results from spreading with bottom crusting, the weakly-coupled problem uses as a first approximation  $H_0(X, \tau)$ , the l/g-interface from the isothermal spreading problem. A major difference arises in the mathematical formulation of both problems. For the fully-coupled problem we have to solve a differential-integral equation. For the weakly-coupled problem we can make use of approximations (cf. section 3.3.1.1) to express  $H_0(X, \tau)$ . This allows to find an analytical solution for  $S_1(X, \tau)$ . The solution of the evolution equation in this case occurs straight forward compared to the fully-coupled problem.

## 6.4 Evolution equation for $H(X, \tau)$ - the weakly-coupled problem

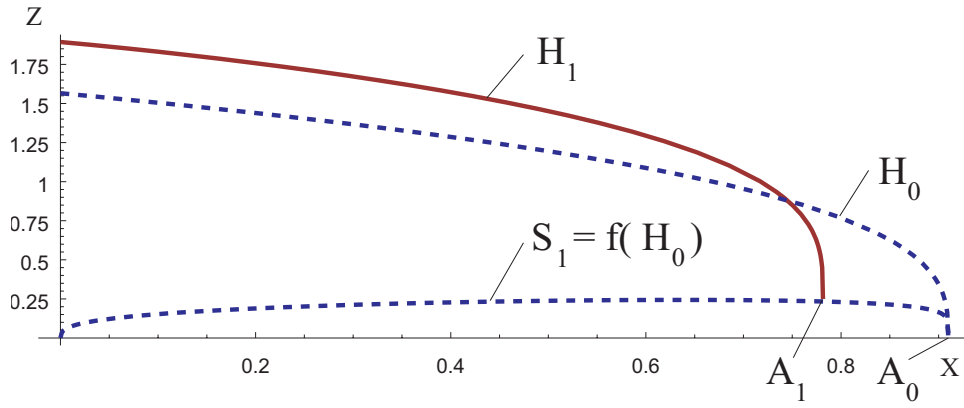
As mentioned in the previous section, we use  $H_0(X, \tau)$  based on a weighted residual approximation to express  $S_1(X, \tau)$ . To distinguish solutions from the zeroth and first approximation for spreading under influence of a bottom crust, we use the subscripts 0 for quantities from zeroth and 1 for quantities from the first approximation. Equation (3.65) together with equation (3.50) or (3.51) yields

$$H_0(X, \tau) = cC_{1,0}\tau^{(2\alpha-1)/5} \left( 1 - \frac{X\tau^{-(3\alpha+1)/5}}{C_{0,0}\eta_{N,0}} \right)^b \quad . \quad (6.12)$$

Equation (5.4) for  $S_1(X, \tau)$  yields

$$\begin{aligned} S_1(X, \tau) = & \eta_S \left( 1 - e^{-\frac{C_{mS} X \tau^{-(3\alpha+1)/5}}{C_{0,0}\eta_{N,0}}} \right) \left( \frac{6Fr}{(\epsilon Re)^2 Pr} \frac{(C_{0,0}\eta_{N,0})^2 \tau^{2(2+\alpha)/15}}{b(1+2b)(cC_{1,0})^2} \right)^{1/3} \\ & \left( 1 - \frac{X\tau^{-(3\alpha+1)/5}}{C_{0,0}\eta_{N,0}} \right)^{1/2-b} \left( 1 - \left( 1 - \frac{X\tau^{-(3\alpha+1)/5}}{C_{0,0}\eta_{N,0}} \right)^{1/2+b} \right)^{1/3} \quad . \quad (6.13) \end{aligned}$$

weakly-coupled problem:



fully-coupled problem:

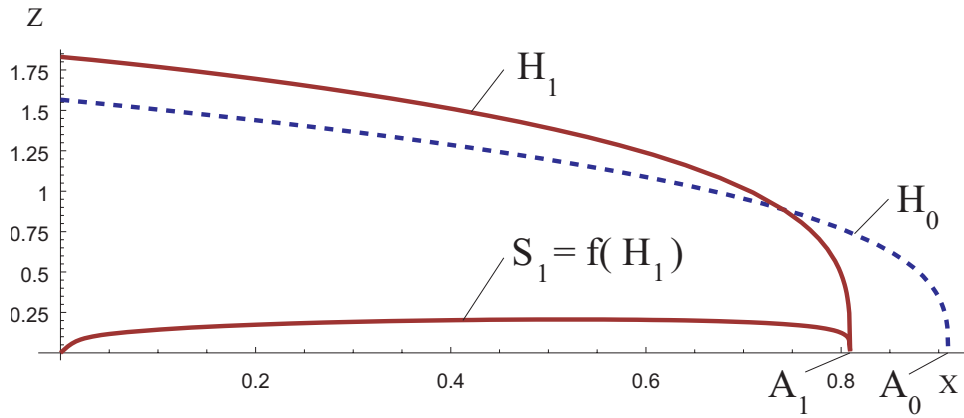


Figure 6.1: Two strategies to model  $S(X, \tau)$  - the weakly- and the fully-coupled problem.

The resulting set of the evolution equation, the boundary and integral conditions is

$$H_{1,\tau} - \frac{\epsilon Re}{3Fr} \left( (H_1 - S_1)^3 H_{1,X} \right)_X = 0 \quad . \quad (6.14)$$

$$X = 0 : -\frac{\epsilon Re}{3Fr} H_1^3 H_{1,X} = \alpha C_V \tau^{\alpha-1} \quad , \quad (6.15)$$

$$X = A(\tau) : H_1 = S_1 \quad , \quad (6.16)$$

$$\text{volume constraint : } \int_0^{A(\tau)} H_1 dX = C_V \tau^\alpha \quad . \quad (6.17)$$

Compared to the isothermal problem (cf. equation (3.7)) we obtain a modified boundary condition at the contact line  $X = A(\tau)$ . This is a result of the decreasing spreading velocity due to the influence of the bottom crust which reduces the driving pressure head.

#### 6.4.1 Similarity transformation

For the similarity transformation of the weakly-coupled problem we have to be careful with respect to the scales  $C_0$  and  $C_1$ . From figure 6.1 it is obvious that  $H_0$  and  $H_1$  do not have the same contact line. To distinguish both cases we use

$$H_i(X, \tau) = C_{1,i} \tau^n \tilde{H}_i(\eta/\eta_{N,i}) \quad , \quad (6.18)$$

$$\eta = \frac{X}{C_{0,0}} \tau^{-m} \quad . \quad (6.19)$$

Thus, we employ a single similarity variable  $\eta$ , i.e.  $C_{0,0} = C_{0,1}$  (cf. equation (3.32)), but allow different positions of the contact lines  $\eta_{N,1} \neq \eta_{N,0}$ . For the normalized variable  $\xi_i$  we obtain

$$\xi_i = \frac{\eta}{\eta_{N,i}} \quad , \quad 0 \leq \xi_i \leq 1 \quad .$$

Substituting (6.18, 6.19) into equation (6.13) yields

$$S_1 = \left( \frac{3Fr}{\epsilon Re} \right)^{1/5} C_V^{2/5} P \tau^{2(2+\alpha)/15} \hat{S}(\xi_1) \quad , \quad (6.20)$$

with

$$\hat{S} = \left( 1 - e^{-C_{mS} \frac{\eta_{N,1}}{\eta_{N,0}} \xi_1} \right) \left( 1 - \frac{\eta_{N,1}}{\eta_{N,0}} \xi_1 \right)^{1/2-b} \left( 1 - \left( 1 - \frac{\eta_{N,1}}{\eta_{N,0}} \xi_1 \right)^{1/2+b} \right)^{1/3} \quad , \quad (6.21)$$

$$P = \eta_S \left( \frac{2\eta_{N,0}}{b(1+2b)c^2 Pr} \right)^{1/3} \left( \frac{1}{9C_V^4 Fr^2 \epsilon Re} \right)^{1/5} . \quad (6.22)$$

The quantities  $b$ ,  $c$ , and  $\eta_{N,0}$  are part of the solution  $H_0(X, \tau)$  (cf. equations (3.50,3.51))  
From the evolution equation (6.14) we infer

$$m = \frac{5}{4} \quad , \quad n = \frac{1}{2} \quad , \quad \alpha = \frac{7}{4} \quad ,$$

$$\left( \left( \tilde{H}_1 - \frac{P}{\eta_{N,1}^{2/3}} \hat{S} \right)_{\xi_1}^3 \tilde{H}_{1,\xi_1} \right)_{\xi_1} + \frac{5}{4} \xi_1 \tilde{H}_{1,\xi_1} - \frac{1}{2} \tilde{H}_1 = 0 \quad , \quad (6.23)$$

and for the length scale

$$C_{1,1} = \left( \frac{3Fr}{\epsilon Re} \right)^{1/5} C_V^{2/5} \eta_{N,1}^{2/3} . \quad (6.24)$$

The boundary and integral conditions are

$$\xi_1 = 0 : \quad \tilde{H}_1^3 \tilde{H}_{1,\xi_1} = -\frac{7}{4} \eta_{N,1}^{-5/3} \quad , \quad (6.25)$$

$$\xi_1 = 1 : \quad \tilde{H}_1 = \frac{P}{\eta_{N,1}^{2/3}} \hat{S} \quad , \quad (6.26)$$

$$\text{integral constraint :} \quad \int_0^1 \tilde{H}_1 d\xi_1 = \eta_{N,1}^{-5/3} . \quad (6.27)$$

As we additionally introduce the time behavior of the crust, we can expect only similarity transformations for which both, the thermal boundary layer and the height of the fluid behave in a consistent manner. This is the case for  $\alpha = 7/4$  only.

#### 6.4.1.1 Numerical solution for the shape function $\tilde{H}_1$

It was possible to find an analytical solution for the transformed evolution equation without solidification, (cf. section 3.2.2.1). However, for the present problem it is reasonable to search only for numerical solutions in the case of spreading with solidification. Similar to section 3.2.2.2, we seek a numerical solution to the transformed evolution equation (6.23). For the integration we use the same algorithm as in section 3.2.2.2. In the weakly-coupled problem we have two shooting parameters and two shooting conditions. A further shooting parameter is  $\eta_{N,1}$ , the position of the contact line which results from the coupling between  $\eta_{N,1}$  and  $\tilde{H}_1$ . For the spreading process without solidification  $\eta_N$  has been directly calculated from the solution of  $\tilde{H}$ , (cf. equation (3.34)). In summary we have the initial value problem

$$\left( \left( \tilde{H}_1 - \frac{P}{\eta_{N,1}^{2/3}} \hat{S} \right)^3 \tilde{H}_{1,\xi_1} \right)_{\xi_1} + \frac{5}{4} \xi_1 \tilde{H}_{1,\xi_1} - \frac{1}{2} \tilde{H}_1 = 0 \quad , \quad (6.28)$$

with

$$\hat{S} = \left( 1 - e^{-C_{mS} \frac{\eta_{N,1}}{\eta_{N,0}} \xi_1} \right) \left( 1 - \frac{\eta_{N,1}}{\eta_{N,0}} \xi_1 \right)^{1/2-b} \left( 1 - \left( 1 - \frac{\eta_{N,1}}{\eta_{N,0}} \xi_1 \right)^{1/2+b} \right)^{1/3} \quad , \quad (6.29)$$

$$P = \eta_S \left( \frac{2\eta_{N,0}}{b(1+2b)c^2 Pr} \right)^{1/3} \left( \frac{1}{9C_V^4 Fr^2 \epsilon Re} \right)^{1/5} \quad , \quad (6.30)$$

$$\xi_1 = \xi_{1,max} : \quad \tilde{H}_1 = \frac{P}{\eta_{N,1}^{2/3}} \hat{S}(1) + c(1 - \xi_1)^{1/3} \quad , \quad (6.31)$$

$$\tilde{H}_{1,\xi_1} = -\frac{c}{3}(1 - \xi_1)^{-2/3} \quad . \quad (6.32)$$

The shooting conditions to determine  $c$  and  $\eta_{N,1}$  are

$$c : \quad \tilde{H}_1(0)^3 \tilde{H}_{1,\xi_1}(0) = -\frac{7}{4} \int_0^{\xi_{1,max}} \tilde{H}_1 d\xi_1 \quad , \quad (6.33)$$

$$\eta_{N,1} : \quad \eta_{N,1}^{-5/3} = \int_0^{\xi_{1,max}} \tilde{H}_1 d\xi_1 \quad . \quad (6.34)$$

## 6.4.2 Numerical solution of the nondimensional evolution equation for $H_1(X, \tau)$

After introducing transformation (3.52)

$$\xi_1 = \frac{X}{A_1(\tau)} \quad ,$$

we use the same algorithm as described in section 3.2.3.

### 6.4.2.1 Transformation $(X, \tau) \rightarrow (\xi_1, \tau)$

We substitute the transformation (3.52) into the evolution equation (6.14), the boundary and integral conditions (6.15-6.17) and obtain the system

$$H_{1,\tau} - \xi_1 \frac{A_{1,\tau}}{A_1} H_{1,\xi_1} - \frac{\epsilon Re}{3Fr} \frac{1}{A_1^2} \left( (H_1 - S_1)^3 H_{1,\xi_1} \right)_{\xi_1} = 0 \quad . \quad (6.35)$$

with

$$\xi_1 = 0 : -\frac{1}{3} \frac{\epsilon Re}{Fr} \frac{1}{A_1} H_1^3 H_{1,\xi_1} = \alpha C_V \tau^{\alpha-1} \quad , \quad (6.36)$$

$$\xi_1 = 1 : H_1 = S_1 \quad , \quad (6.37)$$

$$\text{integral constraint : } \int_0^1 H_1 d\xi_1 = \frac{C_V \tau^\alpha}{A_1} \quad . \quad (6.38)$$

We use the method of lines to solve for  $H_1$  and a shooting method to solve for  $A_1$ . Both methods have been used in sections 3.2.3.2, 3.2.3.3 and are described there in more detail.

## 6.5 Evolution equation for $H(X, \tau)$ - the fully-coupled problem

A solution to the fully-coupled problem may be found by substituting (5.4) into the evolution equation (6.9), which yields

$$H_{1,\tau} - \frac{\epsilon Re}{3Fr} \left( \left( H_1 - \eta_S (1 - e^{-\frac{C_{mS} X}{A_1(\tau)}}) \left( \frac{3Fr}{(\epsilon Re)^2 Pr} \frac{\int_0^X \sqrt{-H_1 H_{1,X}} dX^*}{(-H_1 H_{1,X})^{3/2}} \right)^{1/3} \right)^3 H_{1,X} \right)_X = 0 \quad .$$

With

$$G_1 = \int_0^X \sqrt{-H_1 H_{1,X}} dX^* \quad (6.39)$$

we arrive at a system of two coupled differential equations

$$H_{1,\tau} - \frac{\epsilon Re}{3Fr} \left( \left( H_1 - \eta_S (1 - e^{-\frac{C_{mS} X}{A_1(\tau)}}) \left( \frac{3Fr}{(\epsilon Re)^2 Pr} \frac{G_1}{(-H_1 H_{1,X})^{3/2}} \right)^{1/3} \right)^3 H_{1,X} \right)_X = 0 \quad , \quad (6.40)$$

$$G_{1,X} = \sqrt{-H_1 H_{1,X}} \quad . \quad (6.41)$$

The boundary and integral conditions for  $H_1$  are similar to (3.6-3.8) as  $S_1$  is zero at both  $X = 0$  and  $X \geq A_1(\tau)$ . We have

$$X = 0 : -\frac{\epsilon Re}{3Fr} H_1^3 H_{1,X} = \alpha C_V \tau^{\alpha-1} \quad , \quad (6.42)$$

$$G_1 = 0 \quad , \quad (6.43)$$

$$X \geq A_1(\tau) : H_1 = 0 \quad , \quad (6.44)$$

$$\text{volume constraint : } \int_0^{A_1(\tau)} H_1 dX = C_V \tau^\alpha \quad . \quad (6.45)$$

### 6.5.1 Similarity transformation

As we use the fully-coupled description for  $S_1(X, \tau)$ , we avoid a coupling between the zeroth and first approximation. We employ the similarity transformation from section 3.2.2 to obtain

$$H_1(X, \tau) = C_1 \tau^n \tilde{H}_1(\eta/\eta_{N,1}) \quad , \quad (6.46)$$

$$\eta = \frac{X}{C_0} \tau^{-m} \quad . \quad (6.47)$$

With the normalized variable

$$\xi_1 = \frac{\eta}{\eta_{N,1}} \quad , \quad 0 \leq \xi_1 \leq 1 \quad , \quad (6.48)$$

we obtain for the function  $G_1$

$$G_1 = (C_0 \eta_N)^{1/2} C_1 \tau^{n+m/2} \tilde{G}_1 \quad , \quad (6.49)$$

$$\tilde{G}_1 = \int_0^{\xi_1} \sqrt{-\tilde{H}_1 \tilde{H}_{1,\xi_1}} d\xi^* \quad . \quad (6.50)$$

Substituting equation (6.46) and (6.49) into the evolution equation (6.40) yields

$$m = \frac{5}{4} \quad , \quad n = \frac{1}{2} \quad , \quad \alpha = \frac{7}{4} \quad ,$$

$$\begin{aligned} & \left( \left( \tilde{H}_1 - \eta_S (1 - e^{-C_{ms} \xi_1}) \left( \frac{3Fr}{(\epsilon Re)^2 Pr} \frac{(C_0 \eta_{N,1})^2}{C_1^5} \frac{\tilde{G}_1}{(-\tilde{H}_1 \tilde{H}_{1,\xi_1})^{3/2}} \right)^{1/3} \right)^3 \tilde{H}_{1,\xi_1} \right)_{\xi_1} \\ & + \frac{3Fr}{\epsilon Re} \frac{(C_0 \eta_{N,1})^2}{C_1^3} \left( \frac{5}{4} \xi_1 \tilde{H}_{1,\xi_1} - \frac{1}{2} \tilde{H}_1 \right) = 0 \quad , \\ & \tilde{G}_{1,\xi} = \sqrt{-\tilde{H}_1 \tilde{H}_{1,\xi_1}} \quad . \end{aligned}$$

Furthermore, we introduce the similarity transformation (6.46, 6.47) into the boundary conditions and obtain from the inflow condition (6.42)

$$\tilde{H}_1^3 \tilde{H}_{1,\xi_1} = -\alpha C_V \frac{3Fr}{\epsilon Re} \frac{C_0}{C_1^4} \eta_{N,1} \quad ,$$

and from the integral condition (6.45)

$$\int_0^1 \tilde{H}_1 d\xi_1 = \frac{C_V}{C_0 C_1 \eta_{N,1}} \quad .$$

Similar to section 6.4.1 we find similarity transformations only for  $\alpha = 7/4$ , for which both, the thermal layer and the height of the fluid grow with the same power law in time.

We intend to compare the shape functions  $\tilde{H}_1(\xi_1)$  and  $\tilde{H}_0(\xi_0)$  for spreading with and without solidification. Thus, we use identical length scales (3.32, 3.33). Substituting  $C_0$  and  $C_1$  into the differential equations and the boundary conditions yields

$$\left( \left( \tilde{H}_1 - \frac{P}{\eta_{N,1}^{4/9}} (1 - e^{-C_{ms}\xi_1}) \frac{\tilde{G}_1^{1/3}}{\sqrt{-\tilde{H}_1\tilde{H}_{1,\xi_1}}} \right)^3 \tilde{H}_{1,\xi_1} \right)_{\xi_1} + \frac{5}{4}\xi_1\tilde{H}_{1,\xi_1} - \frac{1}{2}\tilde{H}_1 = 0 \quad , \quad (6.51)$$

$$\tilde{G}_{1,\xi} = \sqrt{-\tilde{H}_1\tilde{H}_{1,\xi_1}} \quad , \quad (6.52)$$

with

$$P = \eta_S \left( 9C_V^4 Fr^2 (\epsilon Re)^3 Pr^5 \right)^{-1/15} \quad , \quad (6.53)$$

$$\xi_1 = 0 : \quad \tilde{H}_1^3 \tilde{H}_{1,\xi_1} = -\frac{7}{4}\eta_{N,1}^{-5/3} \quad , \quad (6.54)$$

$$\tilde{G}_1 = 0 \quad , \quad (6.55)$$

$$\xi_1 = 1 : \quad \tilde{H}_1 = 0 \quad , \quad (6.56)$$

$$\text{integral constraint :} \quad \int_0^1 \tilde{H}_1 d\xi_1 = \eta_{N,1}^{-5/3} \quad . \quad (6.57)$$

### 6.5.1.1 Numerical solution for the shape functions $\tilde{H}_1$ and $\tilde{G}_1$

For the numerical integration we use the same algorithm as described in section 3.2.2.2 and section 6.4.1.1. To transform equations (6.51-6.57) into an initial value problem, we additionally employ a new boundary condition for  $\tilde{G}_1$ , i.e

$$\xi_1 = \xi_{1,max} : \quad \tilde{G}_1 = d \quad ,$$

with  $d$  as a additional shooting parameter.

For the complete two-point boundary value problem we have the initial value problem

$$\left( \left( \tilde{H}_1 - \frac{P}{\eta_{N,1}^{4/9}} (1 - e^{-C_{ms}\xi_1}) \frac{\tilde{G}_1^{1/3}}{\sqrt{-\tilde{H}_1\tilde{H}_{1,\xi_1}}} \right)^3 \tilde{H}_{1,\xi_1} \right)_{\xi_1} + \frac{5}{4}\xi_1\tilde{H}_{1,\xi_1} - \frac{1}{2}\tilde{H}_1 = 0 \quad , \quad (6.58)$$

$$\tilde{G}_{1,\xi} = \sqrt{-\tilde{H}_1\tilde{H}_{1,\xi_1}} \quad , \quad (6.59)$$

with

$$P = \eta_S \left( 9C_V^4 Fr^2 (\epsilon Re)^3 Pr^5 \right)^{-1/15} , \quad (6.60)$$

$$\xi_1 = \xi_{1,max} : \quad \tilde{H}_1 = c(1 - \xi_1)^{1/3} , \quad (6.61)$$

$$\tilde{H}_{1,\xi_1} = -\frac{c}{3}(1 - \xi_1)^{-2/3} , \quad (6.62)$$

$$\tilde{G}_1 = d . \quad (6.63)$$

The conditions to determine the shooting parameters  $c$ ,  $d$ ,  $\eta_N$  are

$$c : \quad \tilde{H}_1(0)^3 \tilde{H}_{1,\xi_1}(0) = -\frac{7}{4} \int_0^{\xi_{1,max}} \tilde{H}_1 d\xi_1 , \quad (6.64)$$

$$d : \quad \tilde{G}_1(0) = 0 , \quad (6.65)$$

$$\eta_{N,1} : \quad \eta_{N,1}^{-5/3} = \int_0^{\xi_{1,max}} \tilde{H}_1 d\xi_1 . \quad (6.66)$$

## 6.5.2 Numerical solution of the nondimensional evolution equation for $H_1(X, \tau)$

For the numerical solution of equation (6.40) we use the same algorithm as discussed for the evolution equation (3.5). After introducing the transformation (3.52), i.e.

$$\xi_1 = \frac{X}{A_1(\tau)} , \quad (6.67)$$

we find solutions for  $H_1$  with a basal crust on a fixed domain  $0 \leq \xi_1 \leq 1$ . Contrary to the previous section, where we solved two coupled differential equations for  $\tilde{H}_1$  and  $\tilde{G}_1$ , we solve only one equation, using a discretized form of equation (6.39).

### 6.5.2.1 Transformation $(X, \tau) \rightarrow (\xi_1, \tau)$

Introducing the transformation (6.67) into equations (6.39, 6.40) and boundary conditions (6.42-6.45) results in

$$H_{1,\tau} - \xi_1 \frac{A_{1,\tau}}{A_1} H_{1,\xi_1} - \quad (6.68)$$

$$\frac{\epsilon Re}{3Fr} \frac{1}{A_1^2} \left( \left( H_1 - \eta_S (1 - e^{-C_{ms}\xi_1}) \left( \frac{3Fr}{(\epsilon Re)^2 Pr} \frac{G_1 A_1^{3/2}}{(-H_1 H_{1,\xi_1})^{3/2}} \right)^{1/3} \right)^3 H_{1,\xi_1} \right)_{\xi_1} = 0,$$

$$G_1 = \sqrt{A_1} \int_0^{\xi_1} \sqrt{-H_1 H_{1,\xi_1}} d\xi_1 , \quad (6.69)$$

with

$$\xi_1 = 0 : -\frac{1}{3} \frac{\epsilon Re}{Fr} \frac{1}{A_1} H_1^3 H_{1,\xi_1} = \alpha C_V \tau^{\alpha-1} \quad , \quad (6.70)$$

$$\xi_1 = 1 : H_1 = 0 \quad , \quad (6.71)$$

$$\text{integral constraint : } \int_0^1 H_1 d\xi_1 = \frac{C_V \tau^\alpha}{A_1} \quad . \quad (6.72)$$

Equations (6.69-6.72) represent, similar to section 3.2.3.1, the transformed problem on a rectangular domain as illustrated in figure 3.3.

### 6.5.2.2 Modified algorithm for numerical integration

For the numerical integration of equation (6.69) we have to approximate the function  $G_1$  at discrete values  $\xi = \xi_i$ . Using a trapezoidal rule for the integral in equation (6.69) yields

$$G_1(\xi_i, \tau) = \sqrt{A} \sum_{i^*=0}^i \frac{1}{2} (\xi_{i^*} - \xi_{i^*-1}) \left( \sqrt{-HH_\xi} \Big|_{\xi=\xi_i^*} + \sqrt{-HH_\xi} \Big|_{\xi=\xi_{i^*-1}} \right) \quad . \quad (6.73)$$

We introduce approximation (6.73) into the evolution equation (6.69). This allows to use the same algorithm as for the isothermal spreading problem. Again, we use the method of lines for numerical integration (cf. section 3.2.3.2) and a shooting method to calculate the position of the contact line (cf. section 3.2.3.3).

## 6.6 Results

### 6.6.1 Position of the l/g-interface, $H_1(X, \tau)$

#### 6.6.1.1 Similarity solution for $H_1(X, \tau)$

As inferred in section 6.4.1 and 6.5.1, it is only possible to find a similarity solution for the specific time behavior  $V \propto \tau^{7/4}$  of the volume. The solution is influenced by the solidified crust at the bottom, which depends on the parameter  $P$  (cf. equations (6.22, 6.53)). We will specifically focus onto the influence of the solidification temperature. Therefore, we fix the other parameters to

$$\begin{aligned} Re &= 1 \quad , \quad \epsilon = 0.01 \quad , \\ Fr &= 0.01 \quad , \quad C_V = 1 \quad , \\ Pr &= 1000 \quad , \quad C_{mS} = 500 \quad . \end{aligned}$$

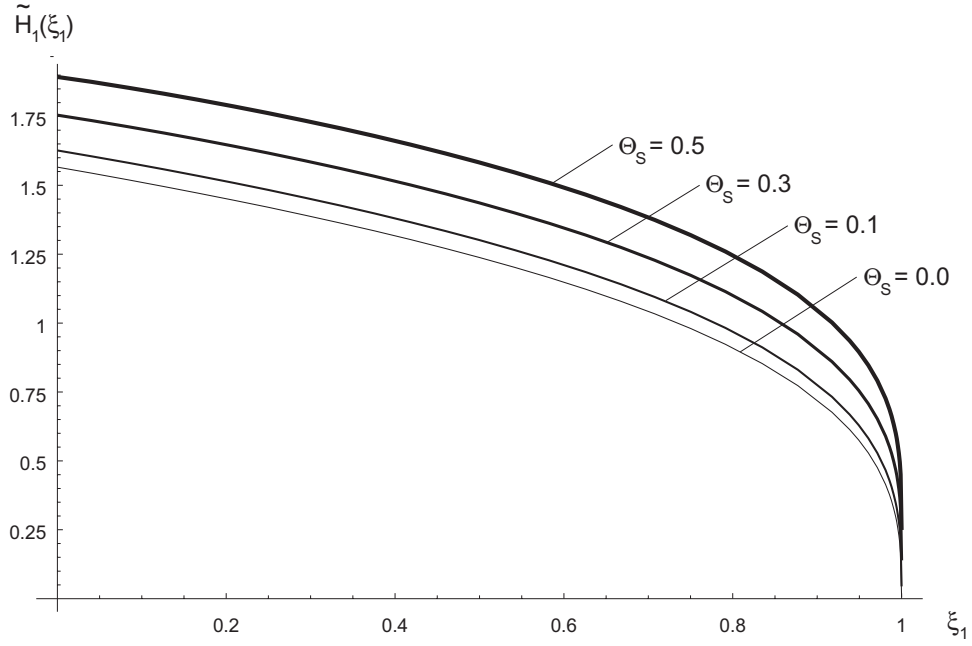


Figure 6.2: Shape function  $\tilde{H}_1(\xi)$  for different nondimensional solidification temperatures  $\Theta_S$  - weakly-coupled problem.

**Solution for  $\tilde{H}_1(\xi)$**  Figures 6.2 and 6.3 show the solution  $\tilde{H}_1(\xi)$  (and  $\tilde{G}_1(\xi)$ ) for different solidification temperatures  $\Theta_S$ . Due to the influence of the solidified crust,  $\tilde{H}_1$  (and  $\tilde{G}_1$ ) are increasing with increasing solidification temperatures. Increasing solidification temperatures  $\Theta_S$  lead to an increase of the crust thickness. As a consequence the value of  $\eta_{N,1}$  decreases with increasing  $\Theta_S$ . Hereby,  $\eta_{N,1}$  represents a horizontal length scale of the spreading. Thus, from decreasing values  $\eta_{N,1}$  we immediately recognize a slower spreading in comparison to the isothermal case (cf. figure 6.4).

Figures 6.5 and 6.6 show the influence of the constant  $C_{mS}$  on  $\eta_{N,1}$  for  $\Theta_S = 0.5$ .  $C_{mS}$  has been introduced in equation (5.4) to smooth out the singularity of  $S(X, \tau)$  and to allow for a numerical treatment. For  $C_{mS} \rightarrow \infty$  in equation (5.4) the influence should be negligible. For  $C_{mS} > 300$  the relative changes of  $\eta_{N,1}$  are less than  $2 \cdot 10^{-6}$ . Thus, for  $C_{mS} > 300$  the influence of this modification has almost no effect on the spreading process but allows for a reasonable mathematical treatment.

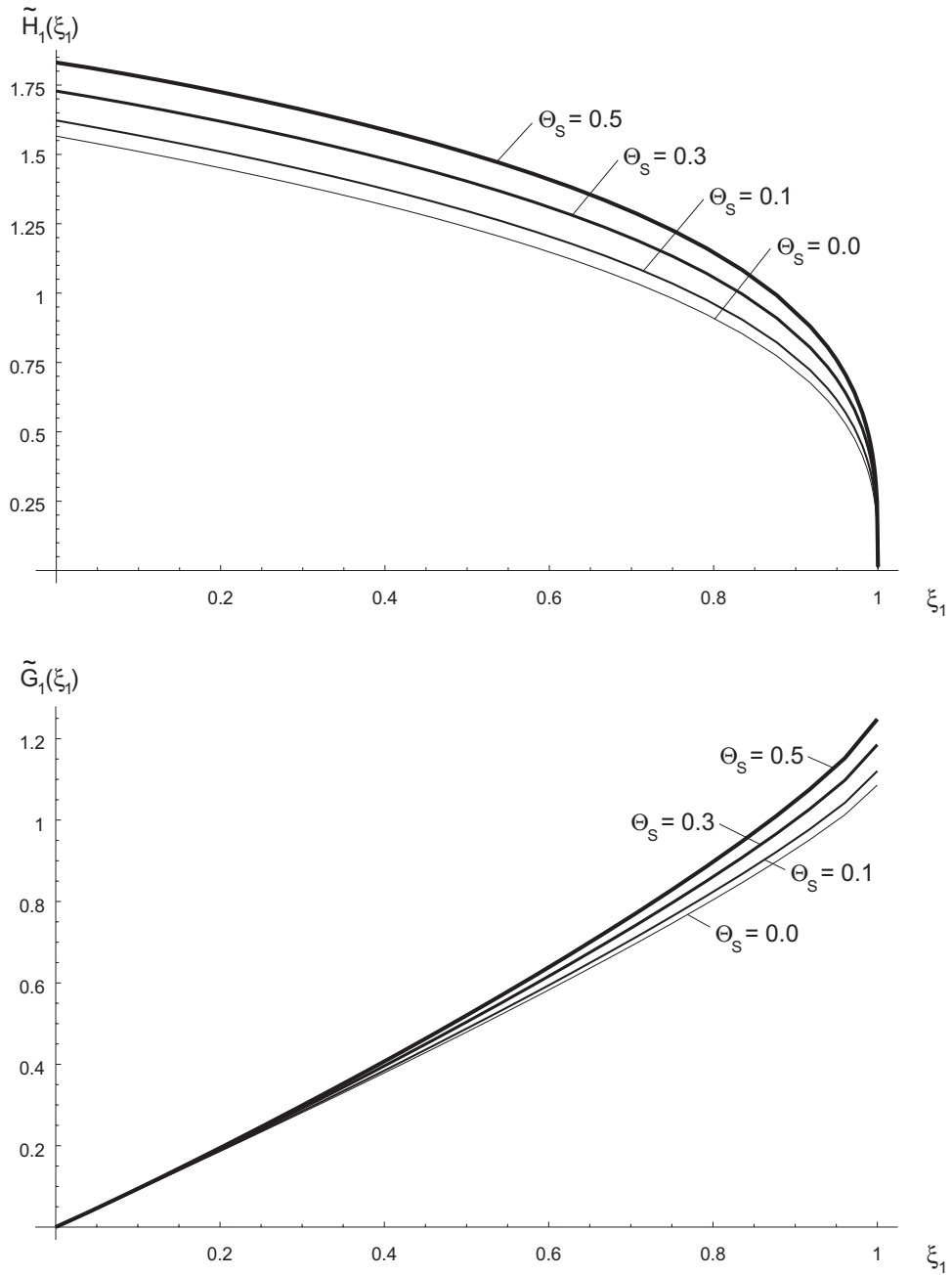


Figure 6.3: Shape functions  $\tilde{H}_1(\xi)$  and  $\tilde{G}_1(\xi)$  for different nondimensional solidification temperatures  $\Theta_S$  - fully-coupled problem.

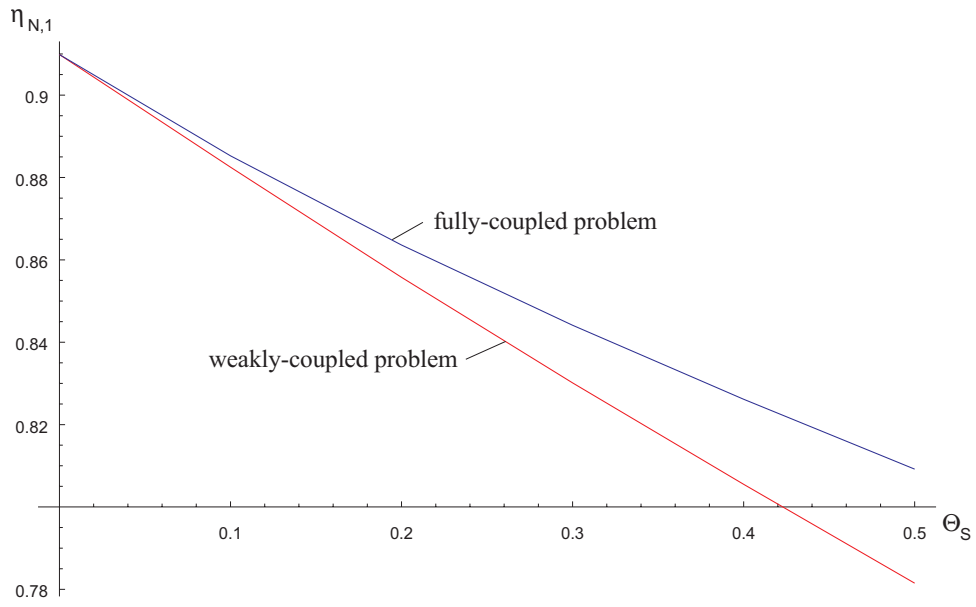


Figure 6.4: Values of  $\eta_{N,1}$  for different nondimensional solidification temperatures  $\Theta_S$ .

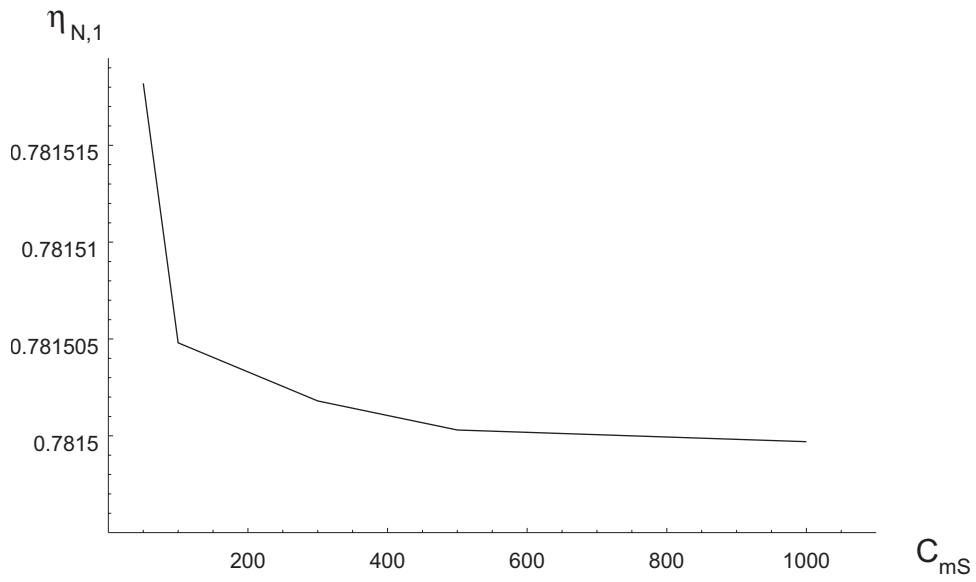


Figure 6.5: Sensitivity of  $\eta_{N,1}$  on the smoothing parameter  $C_{mS}$ ,  $\Theta_S = 0.5$  - weakly-coupled problem.

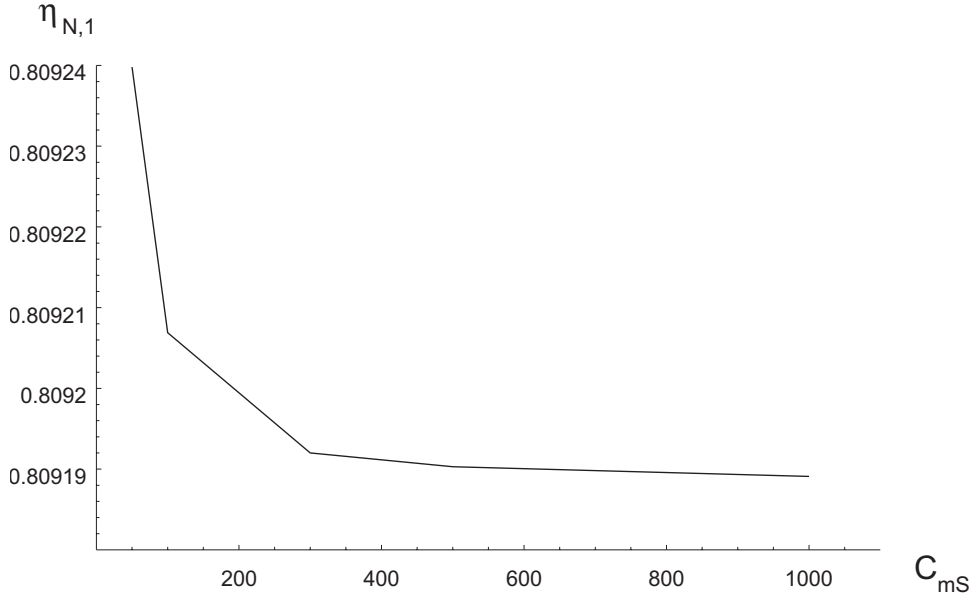


Figure 6.6: Sensitivity of  $\eta_{N,1}$  on the smoothing parameter  $C_{mS}$ ,  $\Theta_S = 0.5$  - fully-coupled problem.

**Solution for  $H(X, \tau)$**  For the backward transformation from the similarity variable  $\eta$  to  $X, \tau$ -coordinates solidification has no influence. All the effects of the solidified crust at the bottom plate are encoded in the shape function  $\tilde{H}_1$  and the value of  $\eta_{N,1}$ .

In agreement with section 3.3.1.1, we obtain from equations (6.18, 6.46) and equations (6.19, 6.47) for the similarity variable and equations (3.32, 3.33) for the scales  $C_0$  and  $C_1$  the expression

$$H(X, \tau) = \left(\frac{3Fr}{\epsilon Re}\right)^{1/5} C_V^{2/5} \eta_N^{2/3} \tau^{1/2} \tilde{H} \left( \left(\frac{3Fr}{\epsilon Re}\right)^{1/5} \frac{X}{\tau^{5/4} C_V^{3/5} \eta_N} \right) . \quad (6.74)$$

The contact line is at

$$A(\tau) = \left(\frac{\epsilon Re}{3Fr}\right)^{1/5} C_V^{3/5} \eta_N \tau^{5/4} . \quad (6.75)$$

### 6.6.1.2 Numerical solution for $H_1(X, \tau)$

For a more general time behavior of the volume  $V(\tau)$ , i.e. for arbitrary values of  $\alpha$ , we have to find a numerical solution for  $H_1(X, \tau)$ . In contrast to the similarity solution, we need to specify an initial condition for  $H_1$ . Based on the previous results in section 3.3, we use in

normalized  $\xi, \tau$ -coordinates the approximation

$$H_1(\xi_1, \tau_0) = c(1 - \xi_1)^{1/3} + S(1, \tau_0) \quad . \quad (6.76)$$

Substituting (6.76) into the boundary conditions (6.36, 6.70) and the integral constraints (6.38, 6.72) gives two conditions which allow to calculate  $c$  and  $A_1(\tau_0)$ .

The following results show the height profile  $H_1(X, \tau)$  for different nondimensional solidification temperatures  $\Theta_S$  using the fixed parameters

$$\begin{aligned} Re &= 1 \quad , \quad \epsilon = 0.01 \quad , \\ Fr &= 0.01 \quad , \quad C_V = 1 \quad , \\ Pr &= 1000 \quad , \quad C_{mS} = 500 \quad . \end{aligned}$$

Figures 6.7 and 6.8 show a comparison between the numerical solutions and the similarity solutions for  $A_1(\tau)$  and  $H_1(\xi, \tau = 20)$ . The agreement is good, proving that both the similarity solution and the numerical solution give identical results for  $\alpha = 7/4$ . We can view this as a verification of the numerical procedure and, thus, can apply the numerical method with confidence for arbitrary values of  $\alpha$ . In general we have an identical type of evolution equation and boundary conditions for all values  $\alpha$ .

Figures 6.9-6.14 show the front progression  $A_1(\tau)$  and height profiles for different values of  $\alpha = 1, 7/4, 2$  and varied solidification temperature  $\Theta_S = 0, 0.1, 0.3, 0.5$ . All height profiles show a significant influence of the solidified bottom crust. With increasing solidification temperature  $\Theta_S$ , we find an increasing crust thickness. Subsequently, the front propagation slows down for increasing solidification temperatures  $\Theta_S$ . Physically, this can be viewed as an uphill spreading whereas the crust represents the locally inclined substrate. If we compare figures 6.9-6.14 we, moreover, recognize that the influence of the crust is weak for large  $\alpha$  and strong for  $\alpha = 1$ . This is physically expected, as strong feeding of melt into the spreading allows only for a limited crust effect.

Furthermore, the characteristics of the specific value  $\alpha = 7/4$  can be shown in figures 6.9-6.14. For spreading flows with  $\alpha < 7/4$  the crust thickness  $S_1$  is growing faster in time than the height  $H_1$ . For  $\alpha > 7/4$ , in contrast,  $H_1$  is growing faster in time than  $S_1$ . As a consequence, we can expect complete freezing for  $\alpha < 7/4$ .

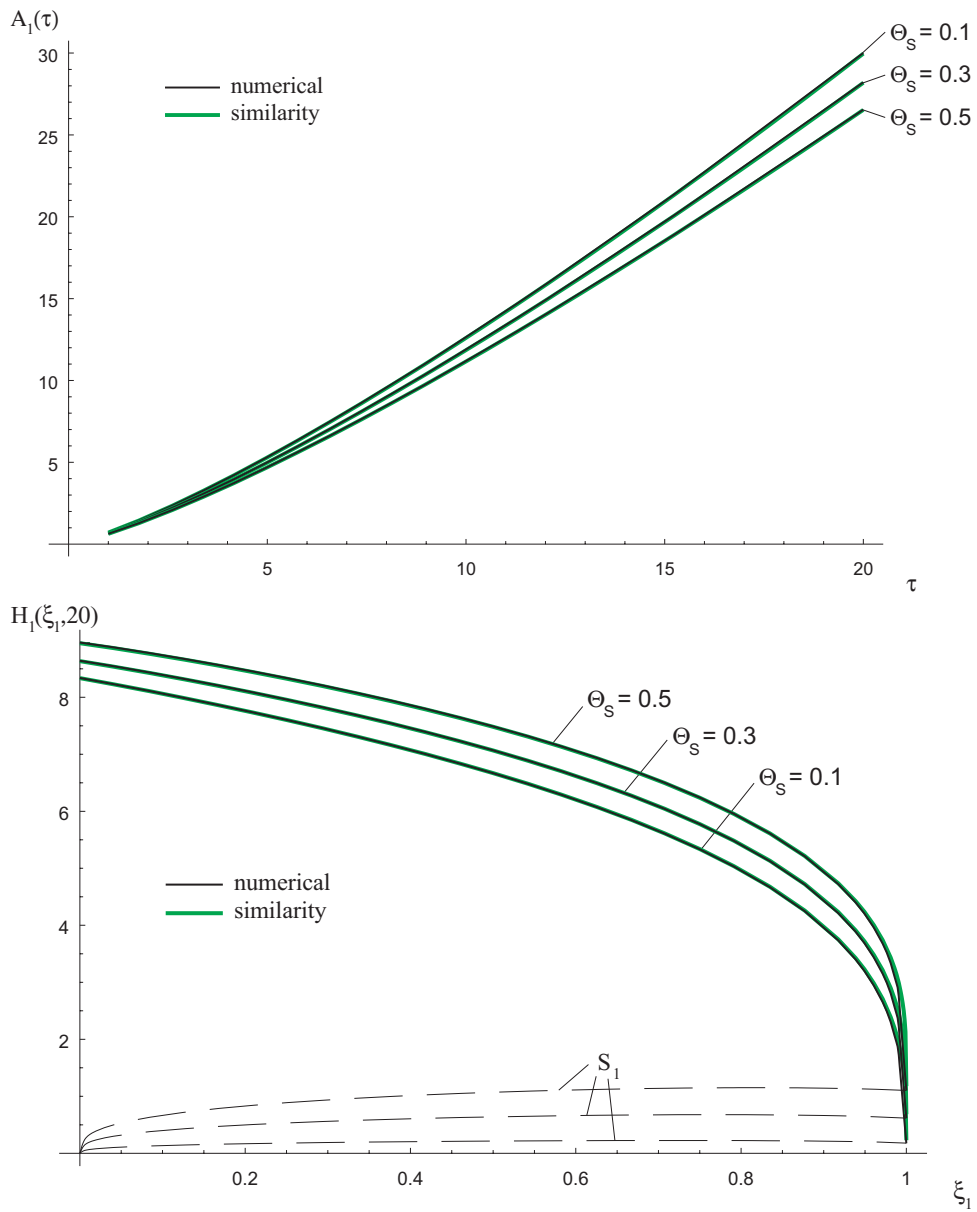


Figure 6.7: Comparison of the similarity solution and the numerical solution for  $A_1(\tau)$  and  $H_1(\xi_1, \tau = 20)$  for different nondimensional solidification temperatures  $\Theta_S = 0.1, 0.3, 0.5$ , and for  $\alpha = 7/4$  - weakly-coupled problem.

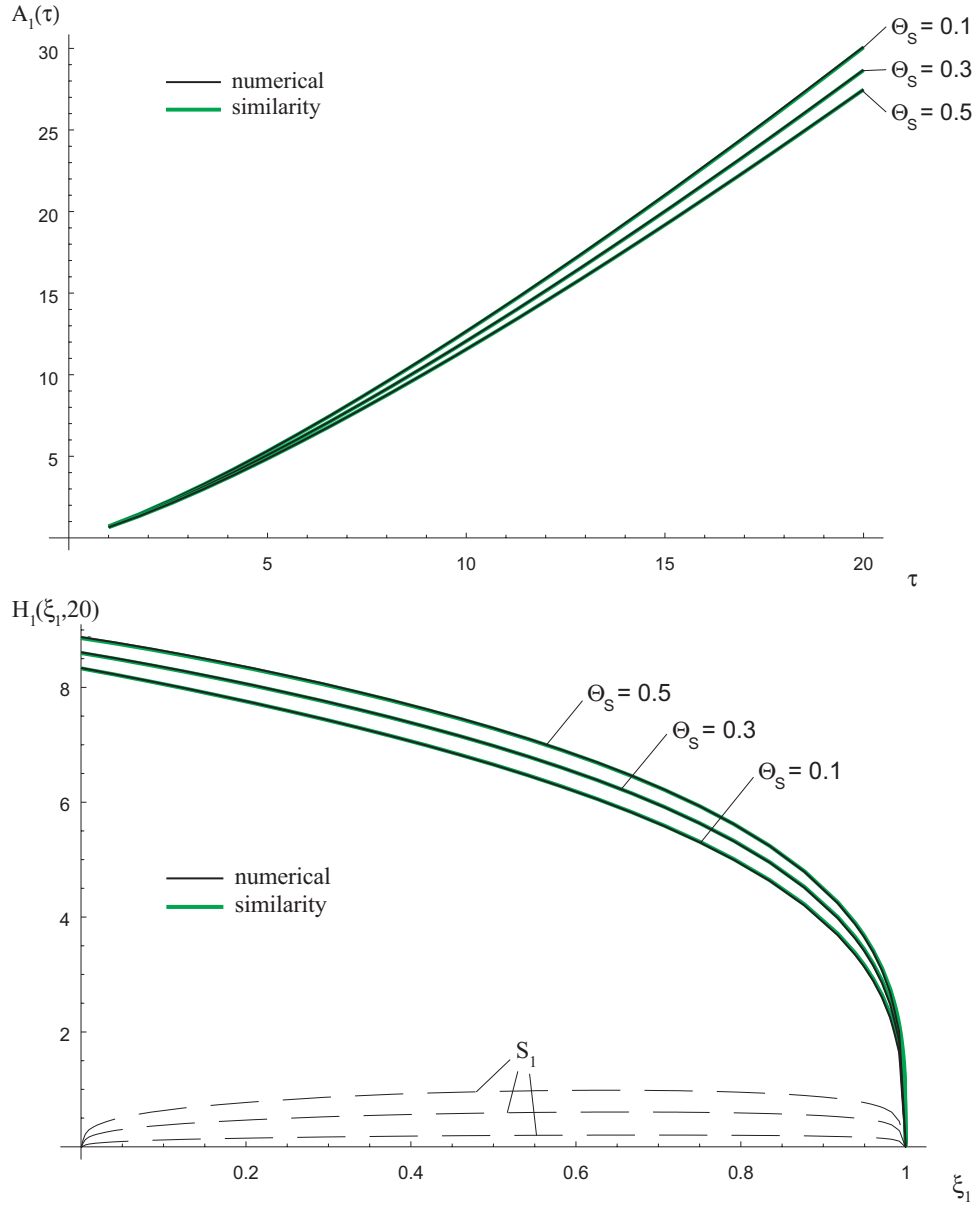


Figure 6.8: Comparison of the similarity solution and the numerical solution for  $A_1(\tau)$  and  $H_1(\xi_1, \tau = 20)$  for different nondimensional solidification temperatures  $\Theta_S = 0.1, 0.3, 0.5$ , and for  $\alpha = 7/4$  - fully-coupled problem.

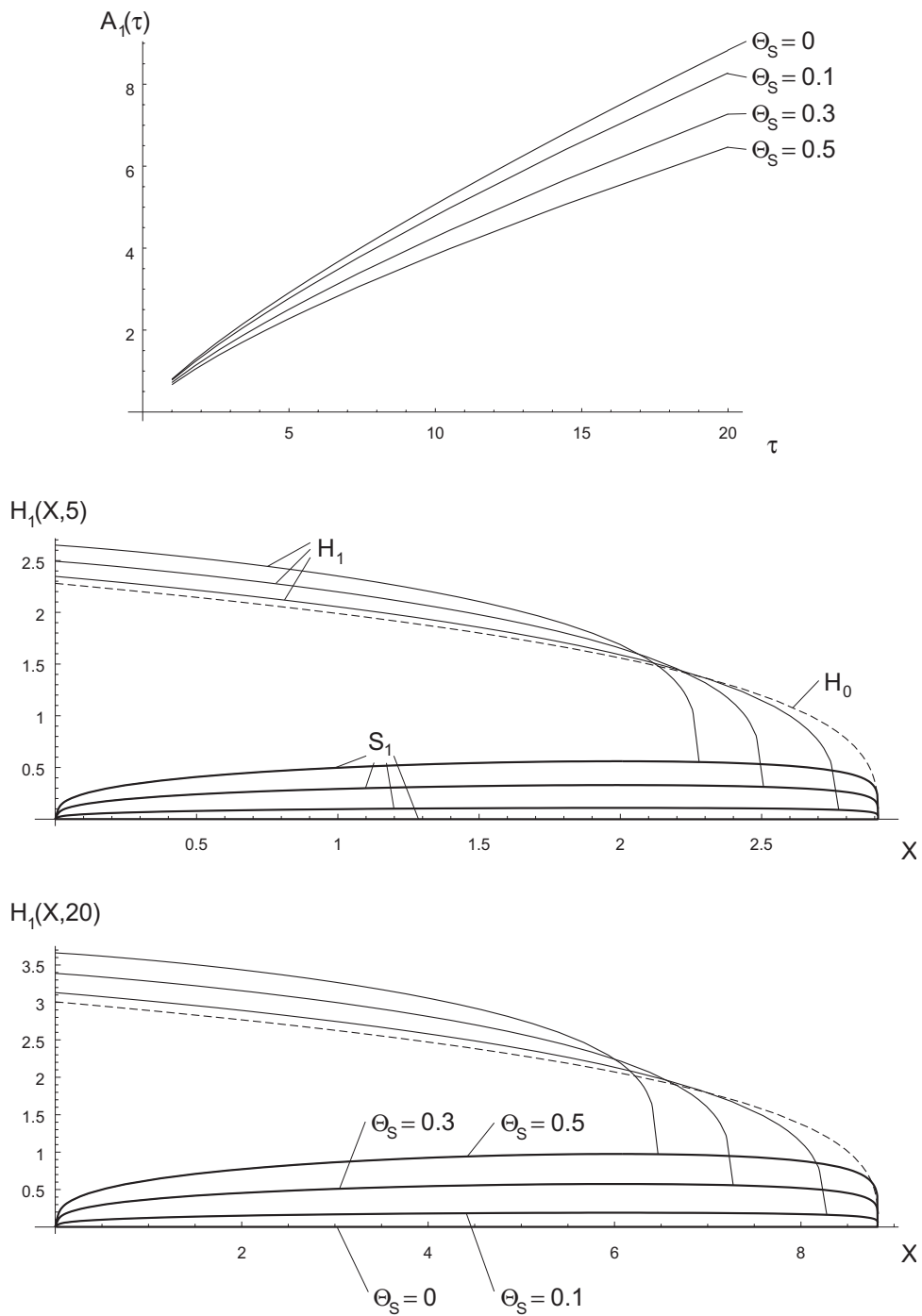


Figure 6.9: Numerical results for  $A_1(\tau)$ ,  $H_1(X, 5)$  and  $H_1(X, 20)$  for different nondimensional solidification temperatures  $\Theta_S$ ,  $\alpha = 1$  - weakly-coupled problem.

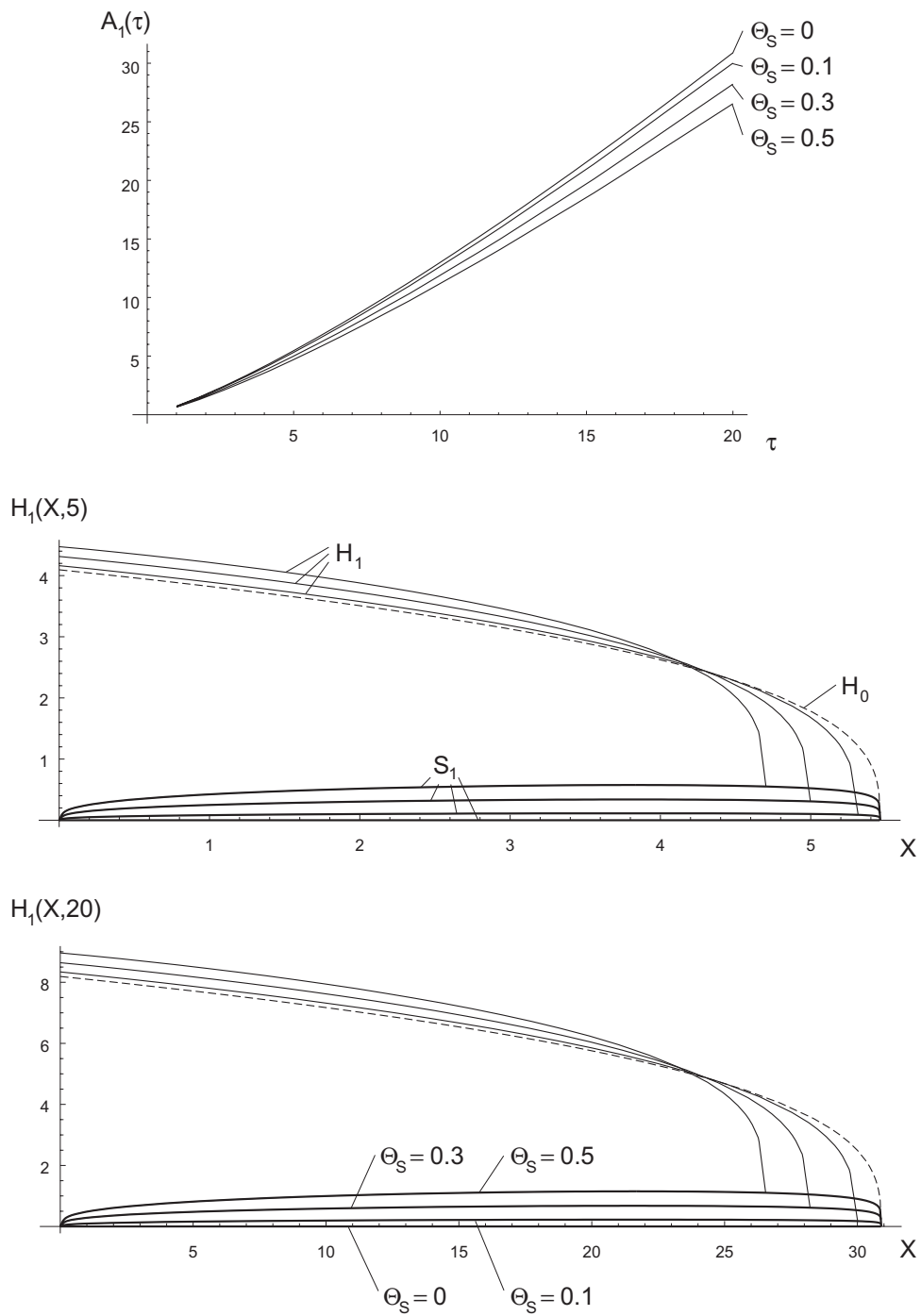


Figure 6.10: Numerical results for  $A_1(\tau)$ ,  $H_1(X, 5)$  and  $H_1(X, 20)$  for different nondimensional solidification temperatures  $\Theta_s$ ,  $\alpha = 7/4$  - weakly-coupled problem.

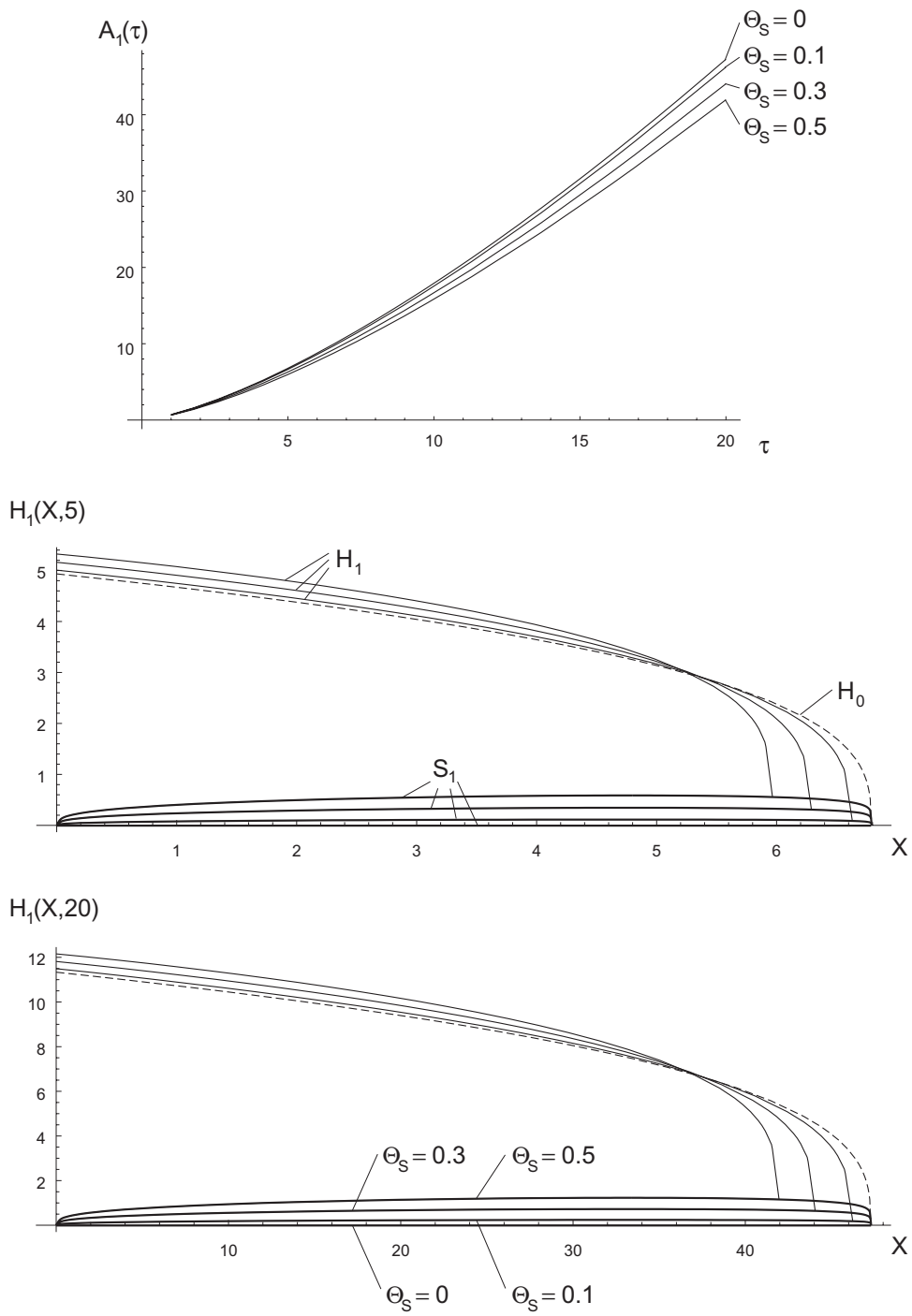


Figure 6.11: Numerical results for  $A_1(\tau)$ ,  $H_1(X, 5)$  and  $H_1(X, 20)$  for different nondimensional solidification temperatures  $\Theta_S$ ,  $\alpha = 2$  - weakly-coupled problem.

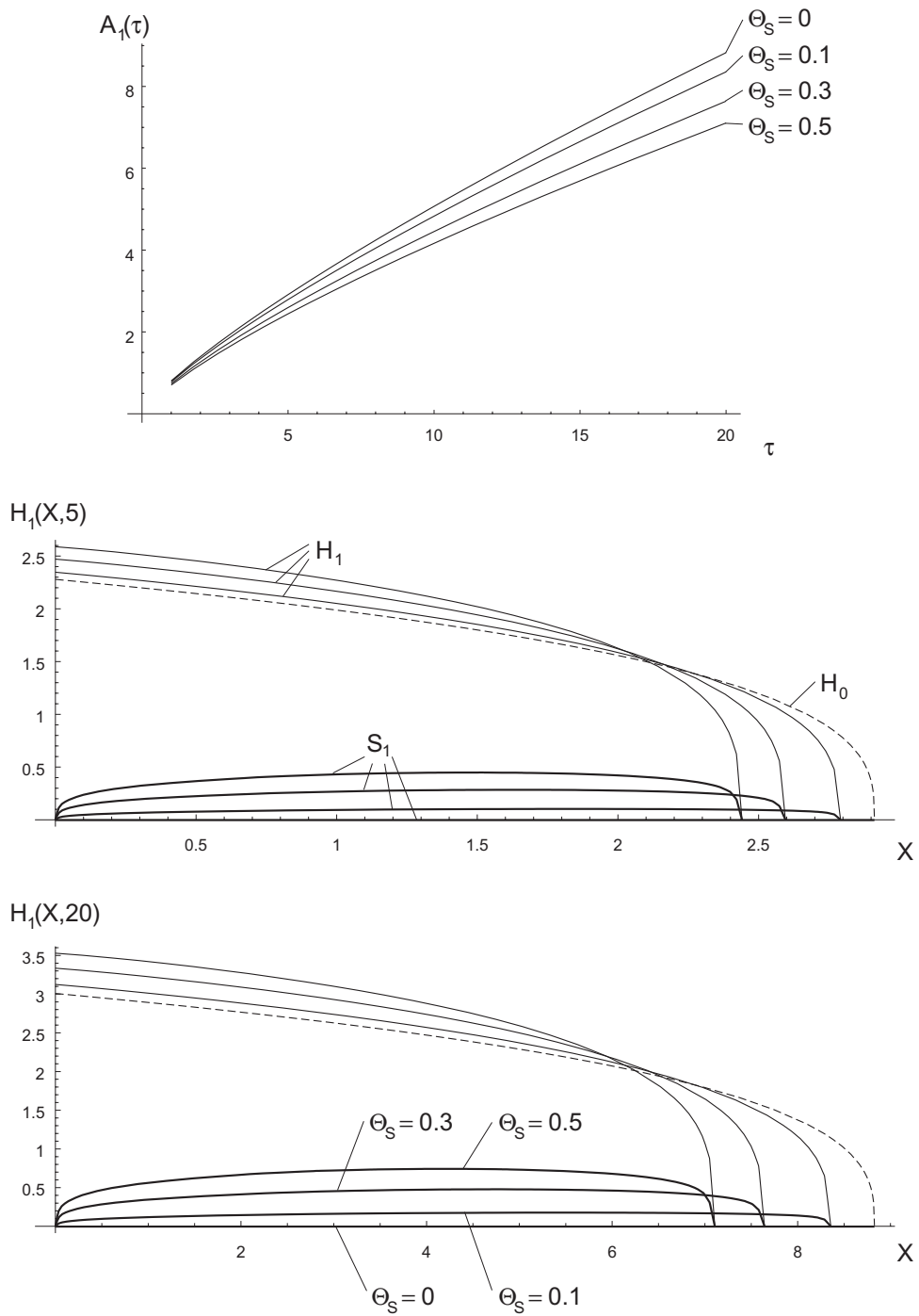


Figure 6.12: Numerical results for  $A_1(\tau)$ ,  $H_1(X, 5)$  and  $H_1(X, 20)$  for different nondimensional solidification temperatures  $\Theta_S$ ,  $\alpha = 1$  - fully-coupled problem.

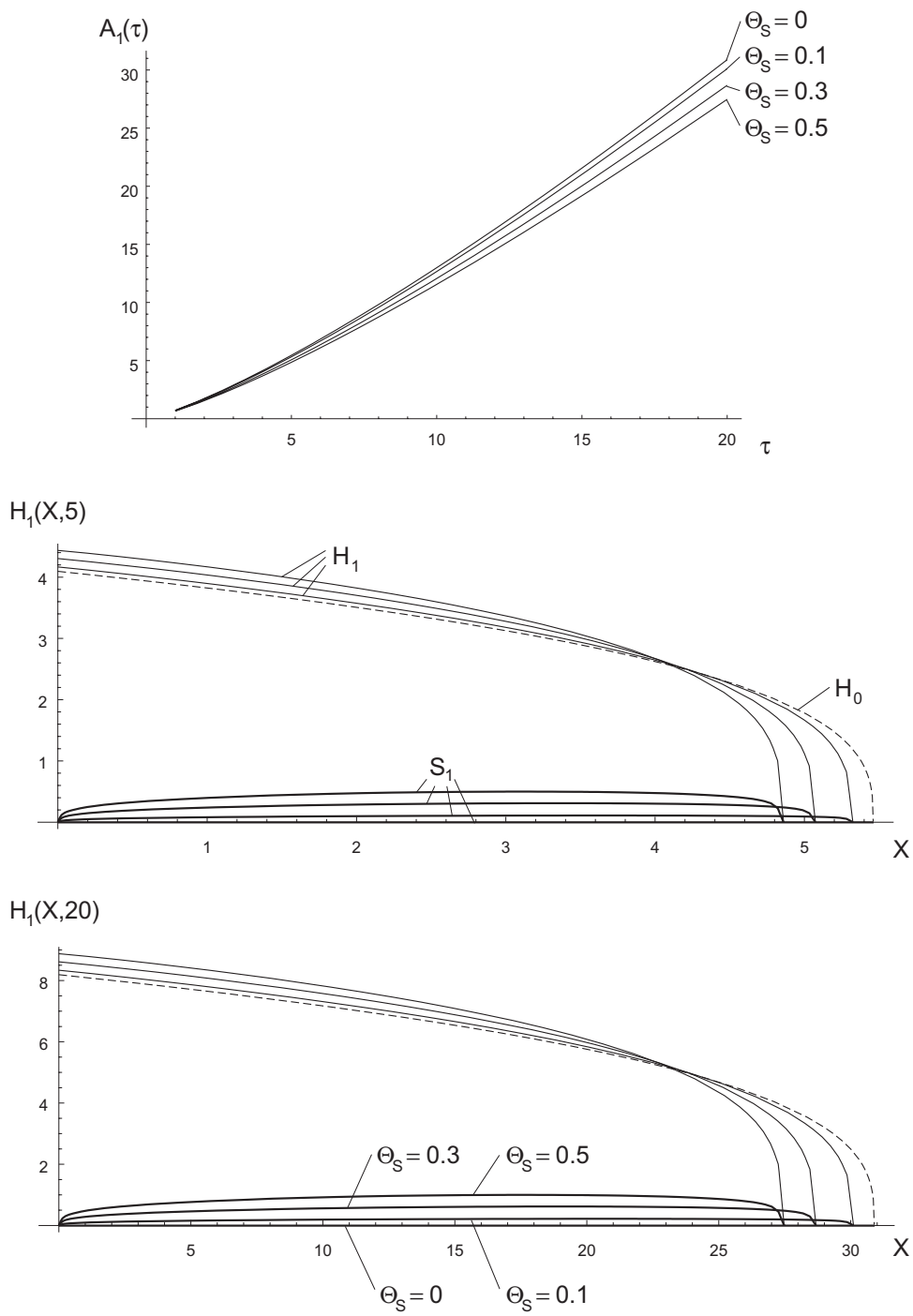


Figure 6.13: Numerical results for  $A_1(\tau)$ ,  $H_1(X, 5)$  and  $H_1(X, 20)$  for different nondimensional solidification temperatures  $\Theta_S$ ,  $\alpha = 7/4$  - fully-coupled problem.

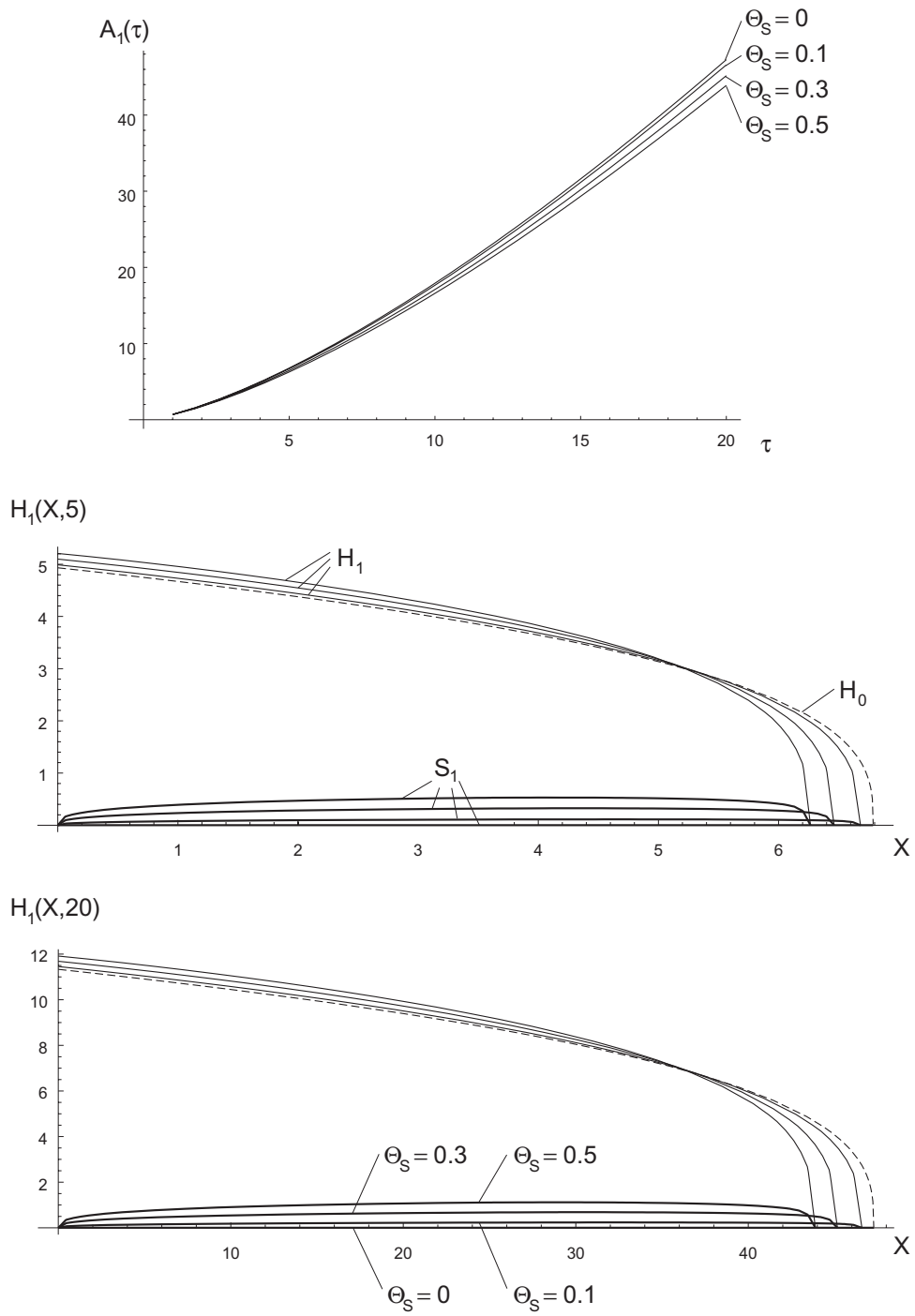


Figure 6.14: Numerical results for  $A_1(\tau)$ ,  $H_1(X, 5)$  and  $H_1(X, 20)$  for different nondimensional solidification temperatures  $\Theta_S$ ,  $\alpha = 2$  - fully-coupled problem.

## 6.6.2 Velocity fields

For a more detailed analysis of the phenomena of spreading with bottom crusting, we have plotted the interfaces and streamlines for different nondimensional solidification temperatures  $\Theta_S$  for both the weakly- and the fully-coupled problem in figures 6.15 and 6.16. At the s/l-interface the streamlines are parallel to  $S_1(X, \tau)$  due to the no-slip condition (6.1). At the l/g-interface the streamlines are not parallel to  $H_1(X, \tau)$  due to the kinematic boundary condition (6.3) in conjunction with the time dependent interface  $H_1(X, \tau)$ . For comparison, we have given the isothermal l/g-interface as dashed lines.

Figures 6.17 and 6.18 show vertical profiles of the velocity components  $U$  and  $W$  for different nondimensional solidification temperatures  $\Theta_S$  at different positions  $X$ . The horizontal velocity  $U$  clearly shows the solidified region, which increases in thickness for increasing solidification temperatures  $\Theta_S$ . The crust thickness likewise increases if we move toward the contact line (compare  $X = 0.1A(\tau)$  and  $X = 0.9A(\tau)$ ). In parallel the amplitude of  $U$  at the l/g-interface increases with increasing  $X$ . The vertical velocity  $W$  is likewise influenced by the crust, as we see only downward ( $W < 0$ ) movement for pure liquid spreading ( $\Theta_S = 0$ ). The crust may induce an upward flow ( $W > 0$ ), particularly for small  $X$ .

To obtain an impression for the influence of bottom crusting on the mass transport, figures 6.19 and 6.20 show particle paths for four different nondimensional solidification temperature  $\Theta_S$ . At  $\tau = 5$  we introduce four particles into the spreading flow on a vertical line, i.e. the positions are

$$\begin{aligned} X &= 0 \quad , \\ Z &= i/5 H(0, 5) \quad , \quad i = 1 \dots 4 \quad . \end{aligned}$$

In time steps  $\Delta\tau = 1$  figures 6.19 and 6.20 show the position of each particle together with the actual l/g- and s/l-interfaces. Only particles, which are close to the l/g-interface at  $X = 0, \tau = 5$  have a chance to arrive at the s/l-interface. This is due to high velocities, present at the l/g-interface (cf. figures 6.17 and 6.18).

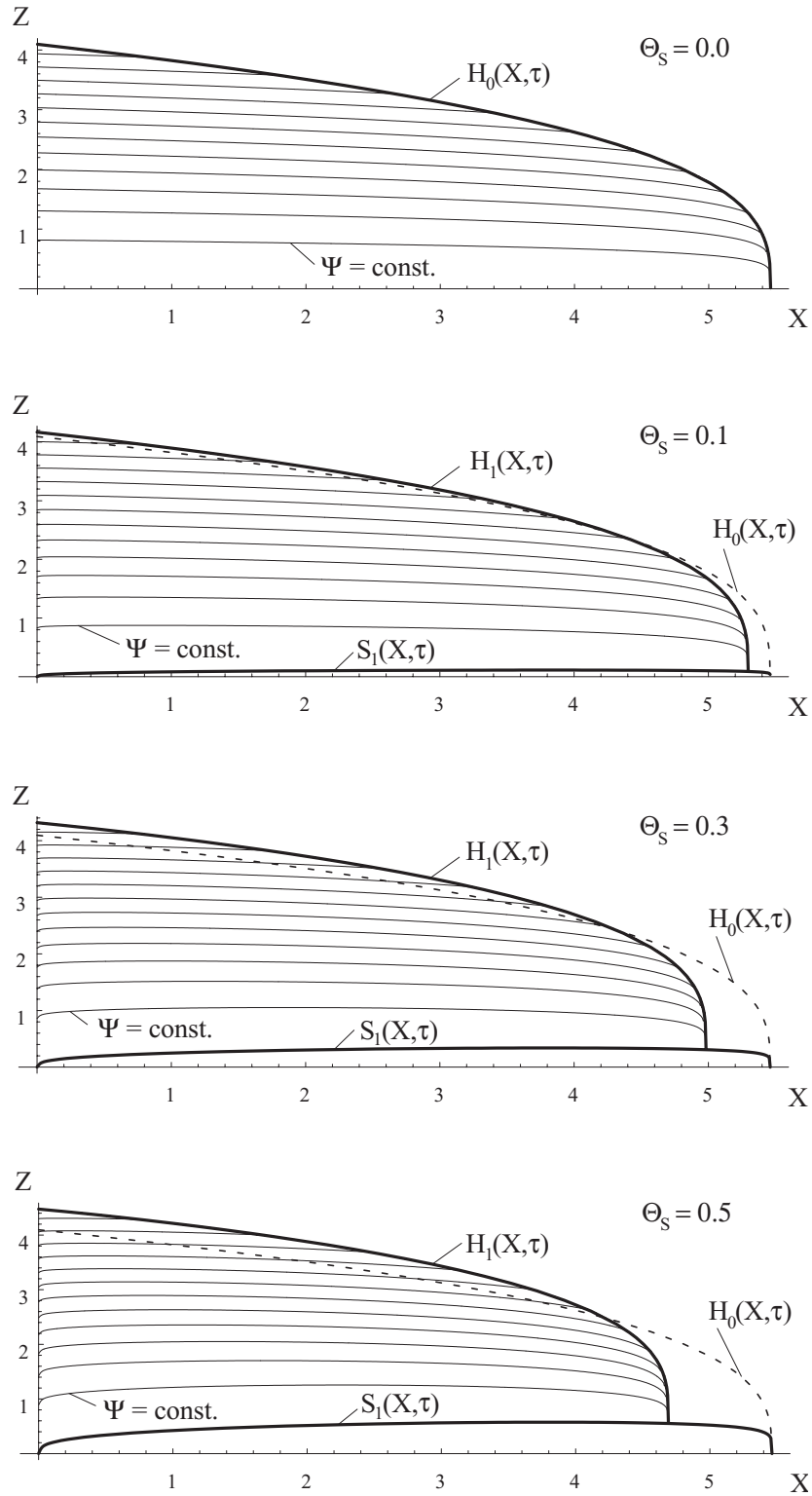


Figure 6.15: Interfaces and isolines of the streamfunction  $\Psi$  for different nondimensional solidification temperatures  $\Theta_s$ , and for  $\alpha = 7/4$ ,  $\tau = 5$  - weakly-coupled problem.

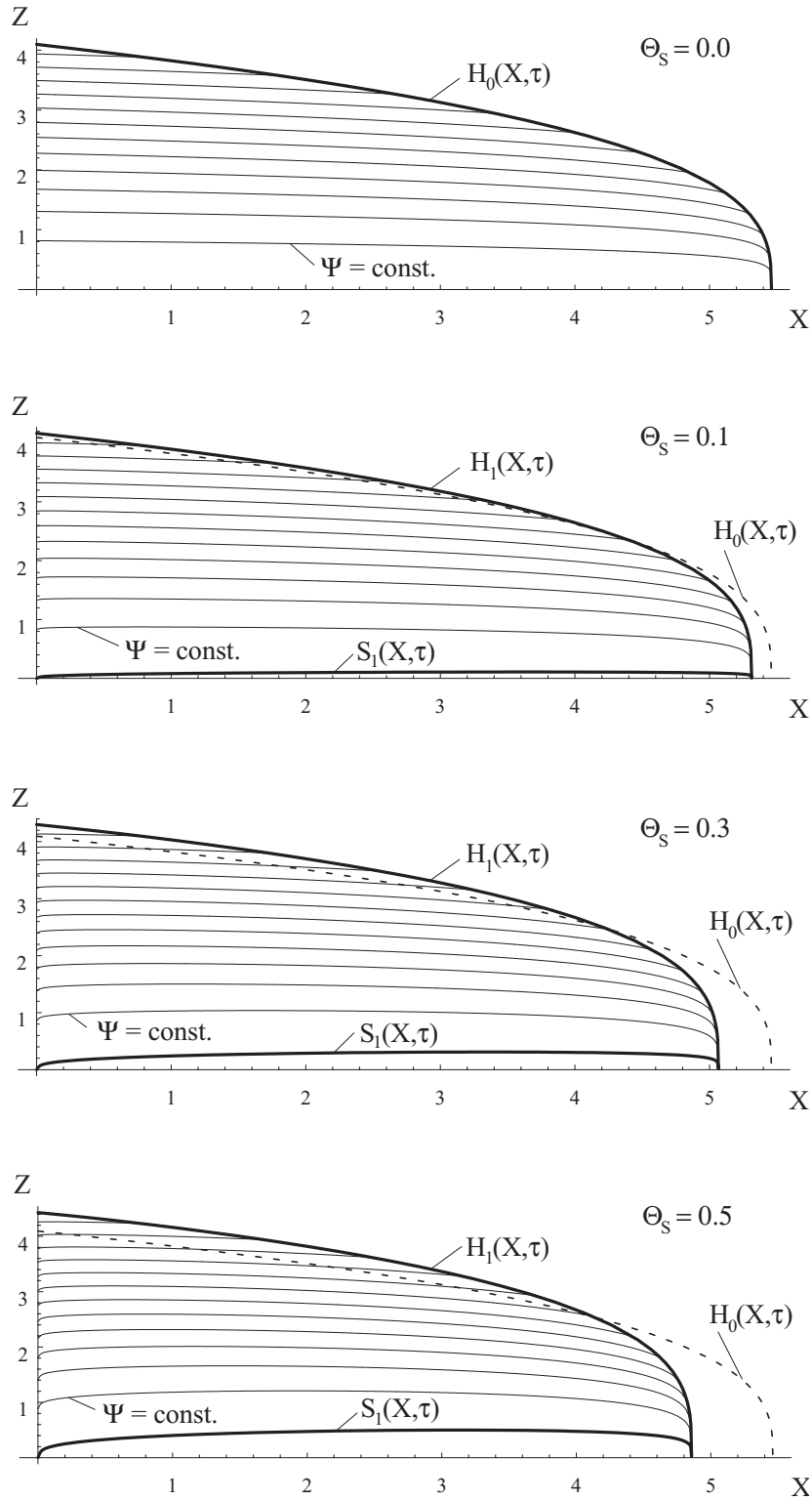
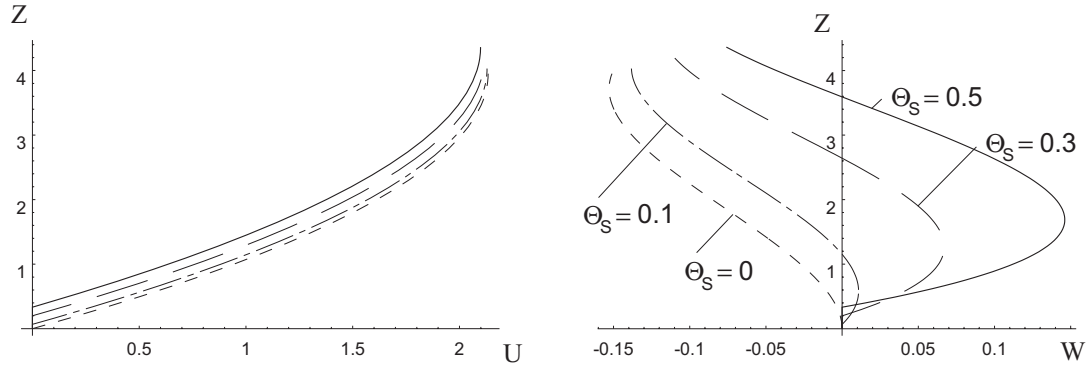
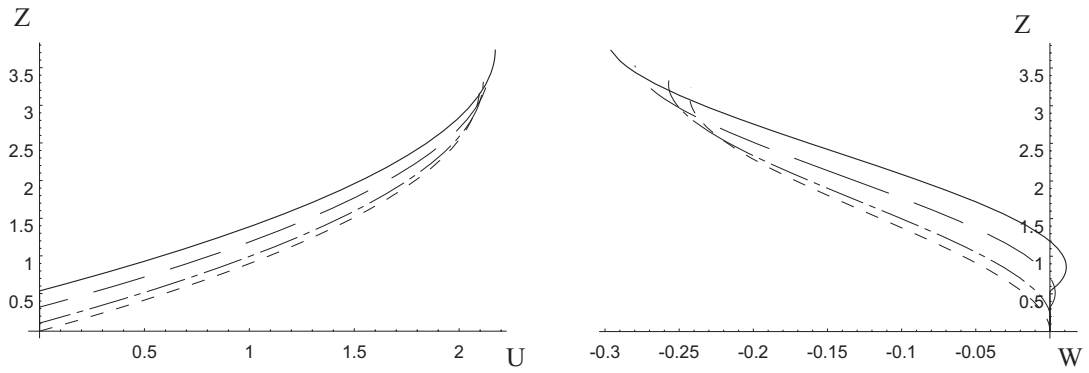


Figure 6.16: Interfaces and isolines of the streamfunction  $\Psi$  for different nondimensional solidification temperatures  $\Theta_S$ , and for  $\alpha = 7/4$ ,  $\tau = 5$  - fully-coupled problem.

$X = 0.1 A(\tau)$ :



$X = 0.5 A(\tau)$ :



$X = 0.9 A(\tau)$ :

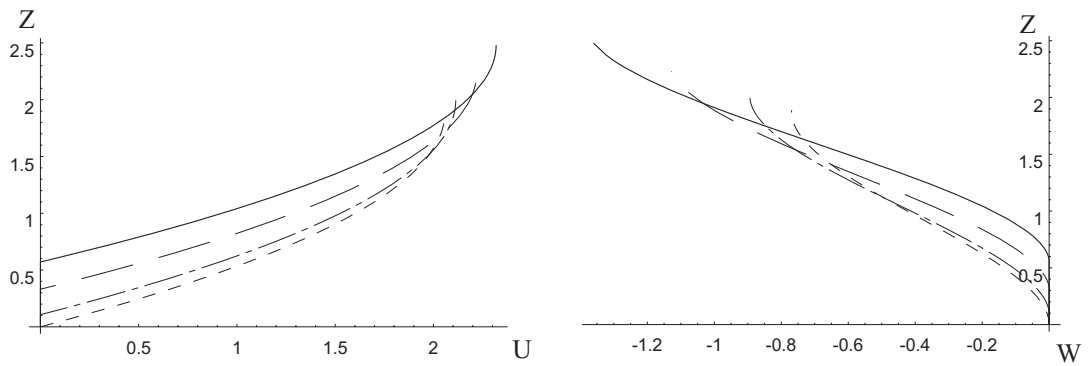
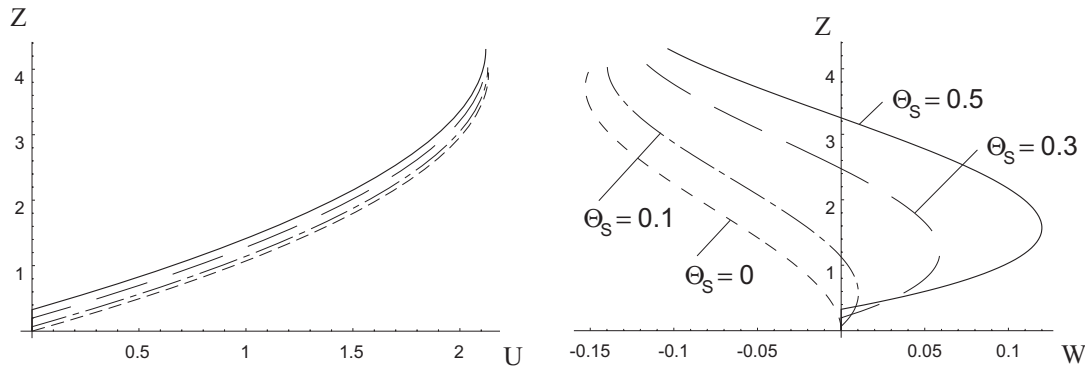
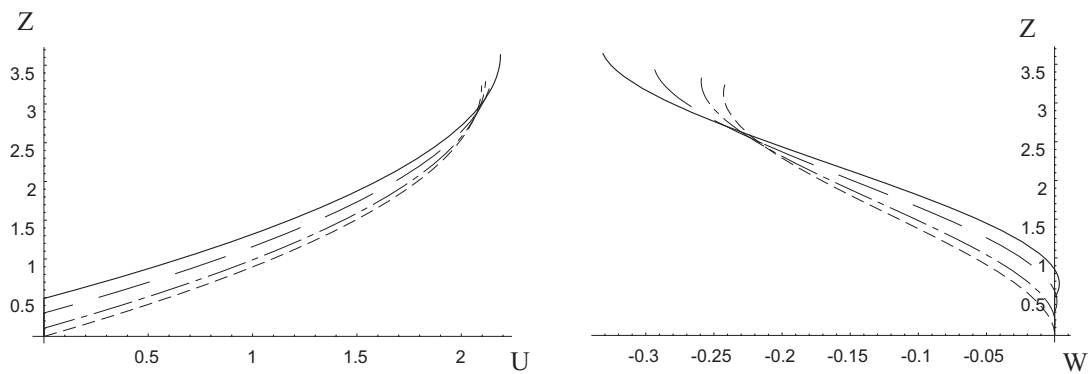


Figure 6.17: Vertical profiles of  $U$  and  $W$  for different nondimensional solidification temperatures  $\Theta_S$  at different positions  $X$  and  $\alpha = 7/4$  - weakly-coupled problem.

$X = 0.1 A(\tau)$ :



$X = 0.5 A(\tau)$ :



$X = 0.9 A(\tau)$ :

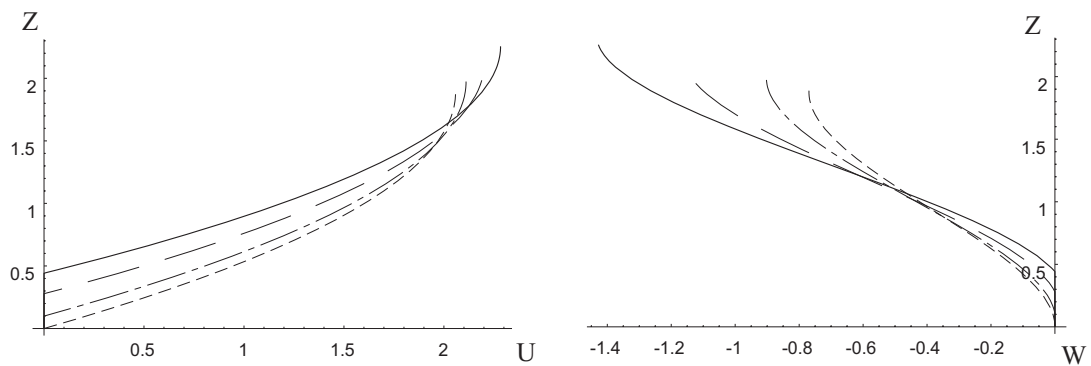


Figure 6.18: Vertical profiles of  $U$  and  $W$  for different nondimensional solidification temperatures  $\Theta_S$  at different positions  $X$  and  $\alpha = 7/4$  - fully-coupled problem.

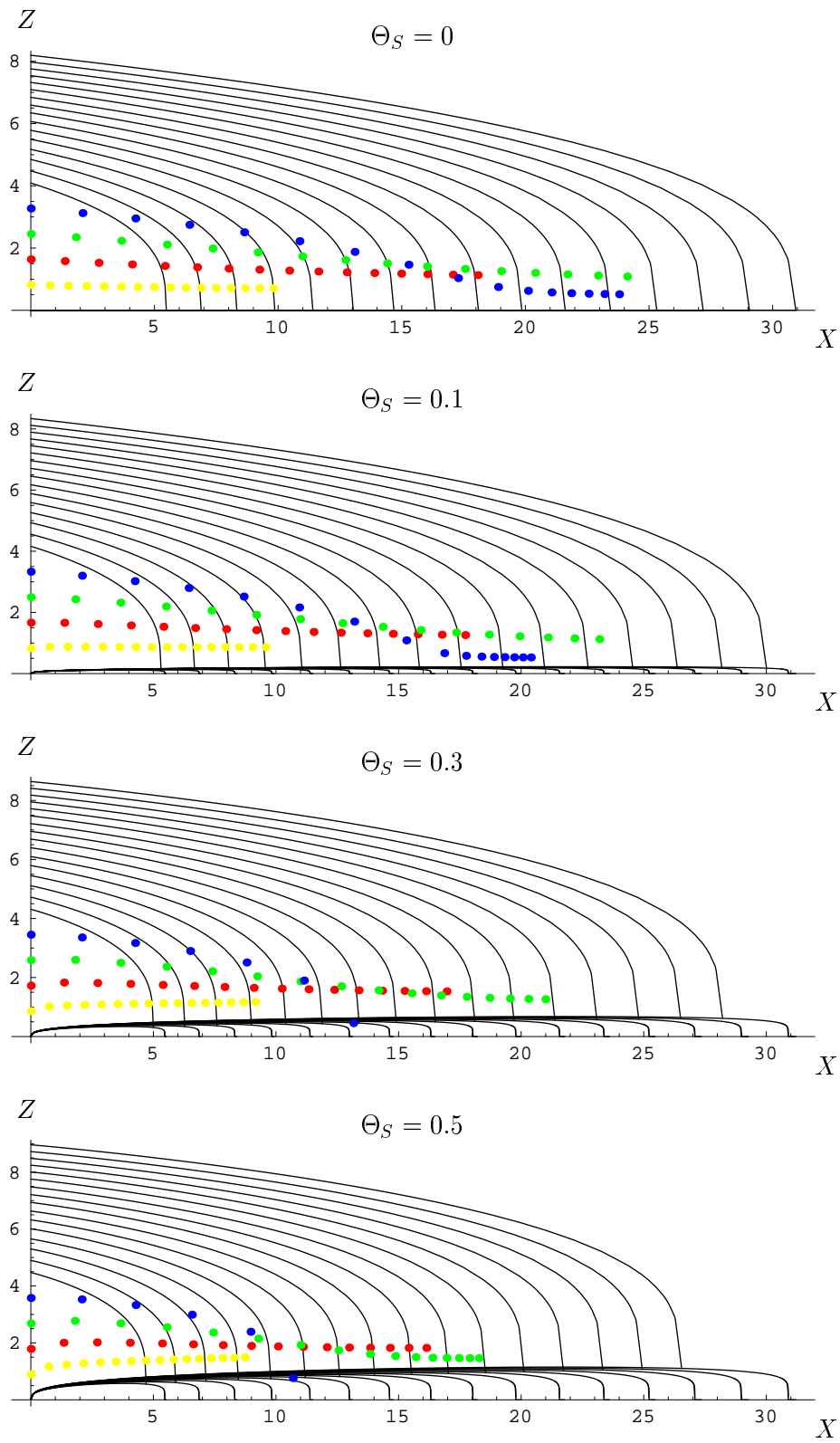


Figure 6.19: Particle paths for different nondimensional solidification temperatures  $\Theta_S$  and  $\alpha = 7/4$  - weakly-coupled problem.

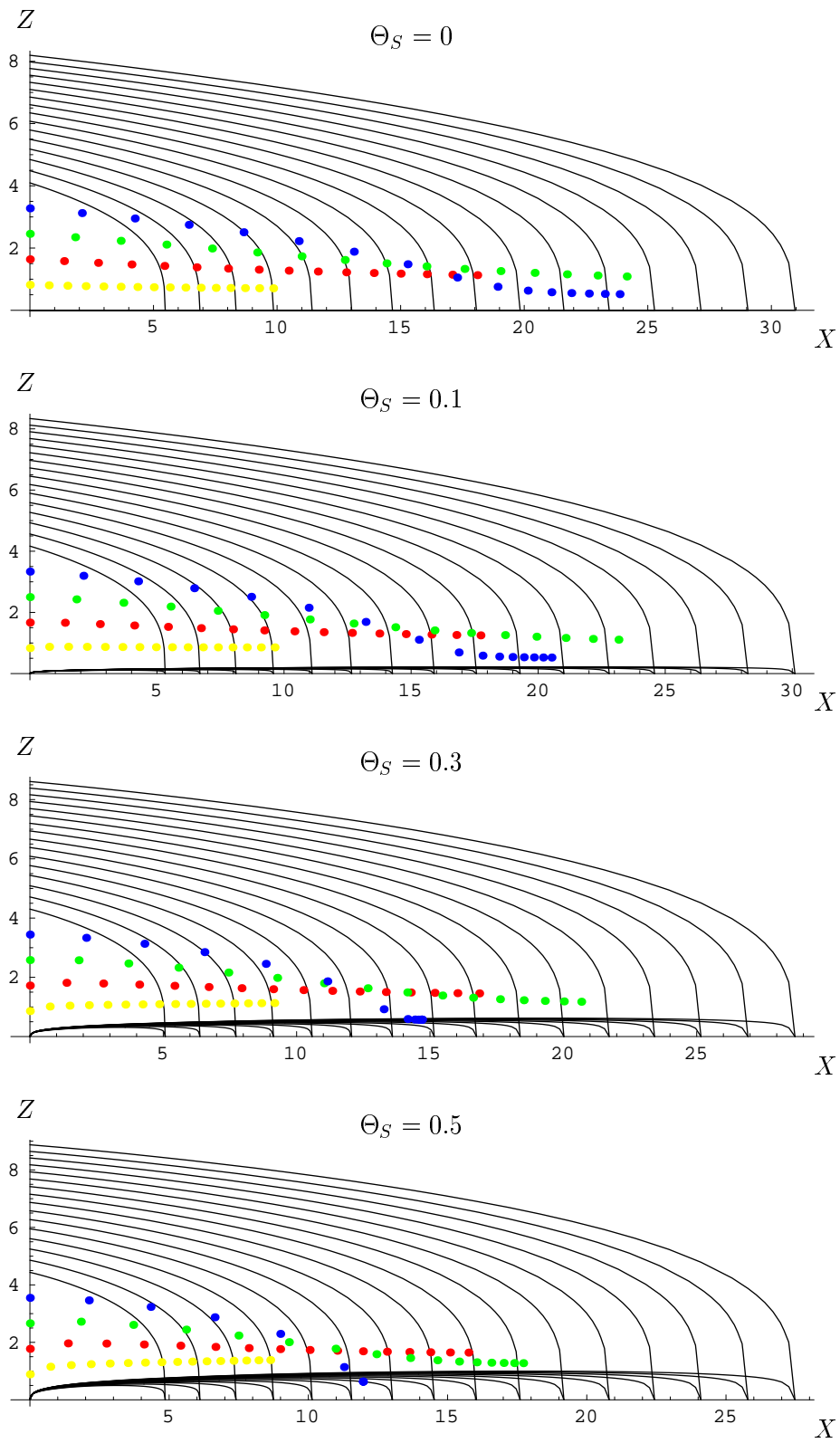


Figure 6.20: Particle paths for different nondimensional solidification temperatures  $\Theta_S$  and  $\alpha = 7/4$  - fully-coupled problem.

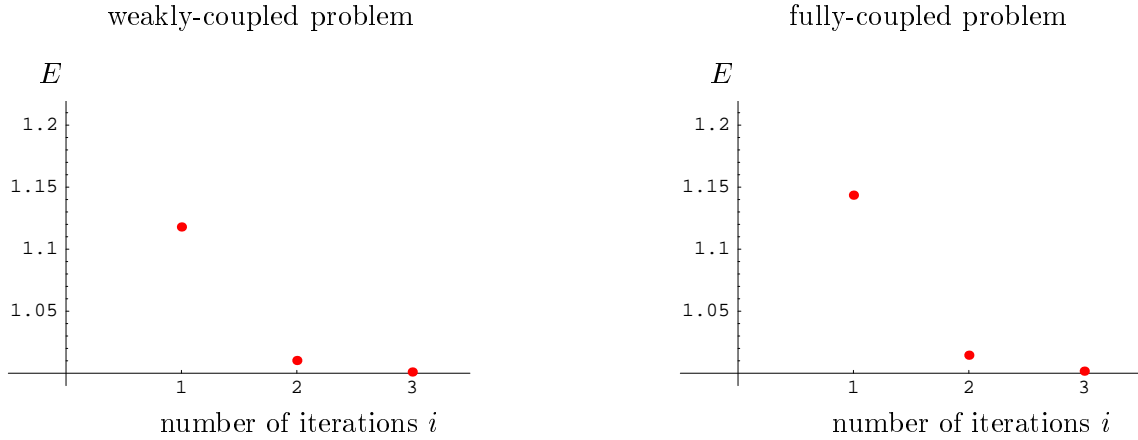


Figure 6.21: Convergence of the iterative scheme. The data are obtained for  $\Theta_S = 0.1$ ,  $\alpha = 1$ ,  $Pr = 10000$ ,  $X = 1/2 A(\tau)$  and averaged for three different times  $\tau = 5, 12.5, 20$ .

### 6.6.3 Convergence of the iterative scheme

To judge the quality of the iterative scheme on the position of the s/l-interface  $S(X, \tau)$  we introduce the ratio

$$E = \frac{S_i(X, \tau)}{S_{i-1}(X, \tau)} \quad ,$$

(cf. section 5.1). A perfect iteration is obtained if  $E \rightarrow 1$ . The evaluation of  $E$  is performed at  $X = 1/2 A(\tau)$  for three typical times  $\tau$ . The result is given in figure 6.21.  $E$  shows only a weak dependence on time, such that a time average can be used. As expected, only a slightly disturbance of the crust  $S(X, \tau)$  onto the temperature field for melts with high Prandtl numbers ( $Pr \gg 1$ ) is present. Thus, in both the weakly-coupled and the fully-coupled problem the error of the first iteration is less than 15% for this set of parameters. Further, in both cases the second and third iteration rapidly converge.

# Chapter 7

## Summary

We have derived a model to describe the influence of basal solidification onto the spreading for a melt with a large Prandtl number. Based on an iterative scheme it occurs possible to describe the influence of bottom crusting in an mostly analytical fashion.

Starting with the isothermal spreading problem, which has been solved kinematically by Huppert [3], we obtain an approximation for the temperature field and, thus, for the position of the s/l-interface. In the next step we capture the influence of the solidified crust at the substrate by solving a new spreading problem on top of the solidified crust. A comparison of similarity solutions and numerical solutions shows good agreement for both, the flow field and the temperature field.

For the spreading we find only a weak influence of solidification onto the spreading flow due to  $\delta_{th} \ll h_0$ . In all cases the spreading flow slows down for increasing crust thickness. For the specific case  $V \propto \tau^{7/4}$  we find, that the crust thickness and the melt height grow with identical power laws in time. This leads to the characterization of two regimes. For  $\alpha < 7/4$  the crust thickness grows faster than the melt height. This should lead to a complete stop of the spreading process for  $t \rightarrow \infty$ . For  $\alpha > 7/4$ , the melt height grows faster than the crust thickness, which means that solidification cannot stop the spreading. Finally, an evaluation of the iterative scheme shows, that only a few iterations are needed to obtain a perfect approximation of the kinematic influence of the crust onto the spreading flow.

# Bibliography

- [1] H. Carslaw and J. Jaeger. *Conduction of heat in solids*. Oxford at the clarendon press, 1959.
- [2] J. H. Fink and R. W. Griffiths. Radial spreading of viscous-gravity currents with solidifying crust. *Journal of Fluid Mechanics*, 221:485–509, 1990.
- [3] H. E. Huppert. The propagation of two-dimensional and axisymmetric visous gravity currents over a rigid horizontal surface. *Journal of Fluid Mechanics*, 121:43–58, 1982.
- [4] G. Pert. A class of similar solutions of the non-linear diffusion equation. *J. Phys. A: Math. Gen.*, 10(4):583–593, 1977.
- [5] H. Schlichting and K. Gersten. *Grenzschicht-Theorie*. Springer, 1997.
- [6] N. Smyth and J. Hill. High-order nonlinear diffusion. *IMA Journal of Applied Mathematics*, 40:73–86, 1988.
- [7] S. Wolfram. *The MATHEMATICA Book*. Wolfram Media, Inc.; Cambridge University Press, 1996.